

LIBRARY & INFORMATICS
NIST(CSIR) TRIVANDRUM



G1906

**ORGANIC MATERIALS FOR NONLINEAR OPTICS :
SYNTHESIS AND PHOTOPHYSICAL STUDIES OF SOME
DONOR-ACCEPTOR SUBSTITUTED MOLECULES**

THESIS SUBMITTED TO
MAHATMA GANDHI UNIVERSITY
IN PARTIAL FULFILMENT OF THE REQUIREMENTS
FOR THE DEGREE OF
DOCTOR OF PHILOSOPHY
IN CHEMISTRY
UNDER THE FACULTY OF SCIENCE

BY

MATHEW GEORGE

PHOTOCHEMISTRY RESEARCH UNIT
REGIONAL RESEARCH LABORATORY (CSIR)
TRIVANDRUM, +695 019, KERALA, INDIA

SEPTEMBER, 1997

**ORGANIC MATERIALS FOR NONLINEAR OPTICS :
SYNTHESIS AND PHOTOPHYSICAL STUDIES OF SOME
DONOR-ACCEPTOR SUBSTITUTED MOLECULES**

THESIS SUBMITTED TO
MAHATMA GANDHI UNIVERSITY
IN PARTIAL FULFILMENT OF THE REQUIREMENTS
FOR THE DEGREE OF
DOCTOR OF PHILOSOPHY
IN CHEMISTRY
UNDER THE FACULTY OF SCIENCE

BY
MATHEW GEORGE

PHOTOCHEMISTRY RESEARCH UNIT
REGIONAL RESEARCH LABORATORY (CSIR)
TRIVANDRUM - 695 019, KERALA, INDIA

SEPTEMBER, 1997

STATEMENT

I hereby declare that the matter embodied in this thesis is the result of investigations carried out by me at the Photochemistry Research Unit of the Regional Research Laboratory, Trivandrum, under the guidance of Dr. Suresh Das of RRL, Trivandrum and Dr. C. V. Asokan of the School of Chemical Sciences, Mahatma Gandhi University, Kottayam, and the same has not been submitted elsewhere for a degree.

In keeping with the general practice of reporting scientific observations, due acknowledgement has been made wherever the work described is based on the findings of other investigators.

Mathew George



PHOTOCHEMISTRY RESEARCH UNIT
REGIONAL RESEARCH LABORATORY (CSIR)
TRIVANDRUM-695 019, INDIA

Dr. SURESH DAS
SCIENTIST

Telephone: 91-471-490392 Fax: 91-471-490186
E. mail: das@csrrltd.ren.nic.in

CERTIFICATE

Certified that the work embodied in this thesis entitled: "**Organic Materials for Nonlinear Optics: Synthesis and Photophysical Studies of Some Donor-Acceptor Substituted Molecules**" has been carried out by Mr. Mathew George under the combined guidance of myself and Dr. C. V. Asokan, School of Chemical Sciences, Mahatma Gandhi University, Kottayam-686 560, Kerala, India (co-guide) and the same has not been submitted elsewhere for a degree.

Suresh Das
(Principal Guide)

C. V. Asokan
(Co-guide)

ACKNOWLEDGEMENTS

It is with great pleasure that I place on record my deep sense of gratitude to my research supervisors, Dr. Suresh Das and Dr. C. V. Asokan, for suggesting the research problem and encouraging me for a successful completion of the work.

I would like to express my sincere thanks to Professor M. V. George for his constant encouragement and help throughout the tenure of my research work. Also, I wish to thank Dr. A. D. Damodaran, former Director, RRL, Trivandrum and Dr. G. Vijay Nair, Director, RRL, Trivandrum for their support and permission to utilize the facilities of the laboratory. My sincere thanks are also due to Professor V. N. Rajasekharan Pillai, Vice Chancellor, Mahatma Gandhi University, Kottayam and Dr. M. Padmanabhan, Director in Charge, Mahatma Gandhi University, Kottayam for their help and encouragement.

I wish to express my sincere thanks to Dr. Pius Kuruvila, Mahatma Gandhi University, Kottayam for his valuable suggestions at various stages of my work. Also, I wish to thank Dr. P. K. Das and Dr. P. C. Ray, of the Inorganic and Physical Chemistry Division, Indian Institute of Science, Bangalore for the NLO measurements, and Dr. M. Swaminathan of the Polymer Division, RRL, Trivandrum for the POM and DSC measurements reported in this thesis.

Thanks are also due to all the members of the Photochemistry Research Unit, RRL, Trivandrum for their help and support. Also, I would like to thank the members of the Organic Chemistry Division, Professor C. P. Joshua of the University of Kerala, and Dr. S. Ajayakumar and Dr. Thomas Mathew, former members of the Photochemistry Research Unit for their help and cooperation. I

wish to express my appreciation and thanks to Mrs. Sarada Nair for typing a major portion of the thesis.

Financial assistance from CSIR is gratefully acknowledged.

Finally, I am deeply indebted to my teachers and all the members of my family for their invaluable support and encouragement.

Trivandrum

September, 1997

Mathew George

CONTENTS

	Page
Statement	ii
Certificate	iii
Acknowledgements	iv
Preface	ix
 CHAPTER 1. Introduction	
1.1. Theoretical principles of nonlinear optics	1
1.2. Organic materials for second harmonic generation	5
1.2.1. Early studies	6
1.3. Molecular engineering of NLO materials	6
1.3.1. Effect of chirality on SHG	15
1.3.2. Role of hydrogen bonding for SHG materials	19
1.3.3. Metallic complexes	21
1.3.4. Polymeric systems	24
1.3.5. Supramolecular systems	28
1.3.6. Molecular recognition induced self-organization and NLO effects	34
1.3.7. Liquid crystals	35
1.4. Summary	39
1.5. References	40
 CHAPTER 2: Synthesis and Studies of Photophysical and Second Harmonic Generation Properties of Some Butadiene Derivatives	
2.1. Abstract	48
2.2. Introduction	48
2.3. Results and discussion	50

2.3.1.	Synthesis of butadiene derivatives	50
2.3.2.	Synthesis of bicyclic compounds	54
2.3.3.	Absorption and emission spectra	59
2.3.3.1.	Solvent effects on fluorescence spectra	61
2.3.3.2.	Effect of temperature on dual fluorescence	67
2.3.3.3.	Substitution effects on dual fluorescence	72
2.3.3.4.	Discussion on the mechanism of dual fluorescence	75
2.3.4.	Second harmonic generation measurements	77
2.4.	Experimental section	78
2.4.1.	Measurement of second harmonic generation efficiency	79
2.4.2.	Materials	79
2.5.	References	94

CHAPTER 3. Studies of Substituent Effects on the NLO Properties of Some Donor-Acceptor Systems

3.1.	Abstract	97
3.2.	Introduction	98
3.3.	Results and discussion	100
3.3.1.	Synthesis	100
3.3.2.	Absorption properties	101
3.3.3.	Nonlinear optical studies	102
3.3.3.1.	Determination of d_{33} values by the electric field poling method	102
3.3.3.2.	Determination of β by hyper-Rayleigh scattering method	105
3.3.3.3.	Theoretical calculations	107
3.3.3.4.	Determination of SHG efficiency by Kurtz and Perry powder method	110
3.4.	Experimental section	110
3.4.1.	Second harmonic generation measurements	111

3.4.1.1. Electric field poling method	111
3.4.1.2. Hyper-Rayleigh scattering (HRS) measurements	113
3.4.1.3. Kurtz and Perry powder method	114
3.4.2. Materials	114
3.5. References	121

**CHAPTER 4. Synthesis and Studies of Nonlinear Optical and
Photoswitching Properties of Some
Cholesterol-linked Azobenzene Derivatives**

4.1. Abstract	124
4.2. Introduction	125
4.3. Results and discussion	135
4.3.1. Liquid crystalline properties	136
4.3.2. Nonlinear optical studies	143
4.3.3. Photoinduced pitch change of liquid crystalline films	145
4.4. Experimental section	153
4.4.1. Materials	154
4.5. References	159

APPENDIX

5.1. Appendix I	164
-----------------	-----

PREFACE

The thesis entitled: "Organic Materials for Nonlinear Optics: Synthesis and Photophysical Studies of Some Donor-Acceptor Substituted Molecules" deals mainly with efforts on designing new molecules capable of second harmonic generation (SHG).

The first Chapter of the thesis contains a brief discussion on the origins of optical nonlinearity in organic molecules and a survey of organic materials capable of SHG.

The second Chapter describes the synthesis and photophysical studies of some donor-acceptor substituted butadiene derivatives. Two of these compounds, 1H-indene-1,3(2*H*)-dione-2-[3-pyrrolidino(2-methanol)-3-phenylpropylidene] (6a) and 1H-indene-1,3(2*H*)-dione-2-[3-pyrrolidino(2-methanol)-3-anisylpropylidene] (6b) showed dual fluorescence. The anomalous red-shifted fluorescence band which appears in polar solvents was attributed to formation of intramolecular charge transfer excited states. The dependence of dual emitting properties of these compounds on solvent polarity as well as temperature has been studied in detail. SHG efficiencies of these compounds were measured by the Kurtz and Perry powder technique, using the 1064 nm fundamental wave from a Nd:YAG laser. Compounds containing chiral groups showed the best efficiencies for SHG. For example compounds 6a and 2,4,6(1*H*, 3*H*, 5*H*)-pyrimidinetrione-5-[3-pyrrolidino(2-methanol)-3-phenylpropylidene] (7a) showed efficiencies ranging up to 50 % of that of urea. The presence of chiral groups ensures that the molecules crystallize in a non-centrosymmetric fashion.

The synthesis and studies of some butadiene derivatives containing a bicyclic donor moiety are also described in this Chapter. These compounds were formed by the replacement of one methylthio- group of 4,4-bismethylthio-1,1-dicyano-2-aryl-1,3-butadienes (13a-c) with 2-hydroxymethylpyrrolidine to give an unstable intermediate, which undergoes cyclization. Rearranged products (15a-c) were also formed along with the expected bicyclic derivatives (14a-c). Formation of these rearranged products was found to be favoured under basic conditions. The structures of these compounds were confirmed on the basis of analytical data and X-ray crystallographic analysis. SHG efficiencies of these compounds were also investigated.

Our studies on the effect of electron withdrawing and donating substituents on the donor side on SHG efficiencies of some butadiene derivatives are described in Chapter 3. The acceptor moiety in these systems is Meldrum's acid. The second order coefficient (d_{33}) of these compounds were obtained after aligning them in a polymer matrix using an electric field. The β values were measured by hyper-Rayleigh scattering technique. A good correlation was obtained between the β values of these compounds experimentally determined by hyper-Rayleigh scattering method and obtained from finite field calculations.

Chapter 4 of the thesis describes the synthesis and studies of some cholesterol derivatives, covalently linked to azobenzene. All these compounds show liquid crystallinity over a wide range of temperatures. Their second order coefficients (d_{33}) measured in poled polymer films are in the range of 1.3 - 7.7 pm/V. The β values of these cholesterol derivatives were measured by hyper-Rayleigh scattering technique. Thin films of cholesteric liquid crystals made from eutectic mixtures of cholesterol derivatives containing the azobenzene-linked cholesterols, which show a reflectance band in the visible region were prepared.

Photoinduced *trans-cis* isomerization of the azobenzene chromophore in these films leads to a large shift in the reflectance band, resulting in visual changes in the colour of the films. These processes have been examined in detail.

CHAPTER 1

INTRODUCTION

1.1. Theoretical Principles of Nonlinear Optics

Before the advent of lasers, transparent optical materials were assumed to be essentially passive, unaffected by light travelling through them. The high powers of laser beams made it possible for the first time to observe that the presence of light can indeed affect the optical properties of the medium.¹

The interaction of the electric field of an electromagnetic radiation with any material polarizes that material.²⁻⁴ This induced polarization results in charge separation i.e., positive and negative charges in the constituent molecules are moved in opposite directions; inducing an oscillating dipole in the medium. An oscillating dipole emits electromagnetic radiation. The secondary radiation combines with the original incident radiation to produce the characteristic optical properties.

The induced dipole per unit volume is called polarization, P , and to a very good approximation, it is linearly proportional to the strength of the applied field E ,

$$P = \chi E \quad 1.1$$

where the constant, χ is the linear susceptibility of a collection of molecules and is related to the dielectric constant and refractive index of the material.

When the electronic charge in the optical material is displaced by the electric field of the applied electromagnetic radiation and polarization takes place, the total electric field, D , which is the sum of the electric fields due to

the electromagnetic radiation and that generated due to polarization of the material, becomes ⁵

$$D = E + 4\pi P = (1 + 4\pi\chi)E \quad 1.2$$

where, $4\pi\chi E$ is the internal electric field created by induced polarization.

The dielectric constant, ϵ in a given direction is defined as the ratio of the total internal field to the applied field in that direction,

$$\epsilon = D/E = 1 + 4\pi\chi \quad 1.3$$

The frequency dependence of dielectric constant provides insight into the mechanism of charge polarization. At optical frequencies, in the absence of absorption or dispersion of electromagnetic radiation by the material, the square of the refractive index equals the dielectric constant.

$$n^2(\omega) = \epsilon(\omega) \quad 1.4$$

Consequently, we can relate the refractive index to the bulk susceptibility of the material as,

$$n^2(\omega) = 1 + 4\pi\chi(\omega) \quad 1.5$$

In general, equation 1.5 relates the property of light to the property of electron density distribution (polarizability). From this equation, it is clear that the optical properties of a material depend on electron density distribution, which is dictated by the chemical structure of the material.

When the material is subjected to laser light of high intensity, the polarizability can change and be driven beyond the linear limit. The polarizability can now be expressed as a power series (equation 1.6), ^{2-4, 6}

$$P = P_0 + \chi^{(1)} E + \chi^{(2)} E^2 + \chi^{(3)} E^3 + \dots \quad 1.6$$

where, P_0 is the static dipole of the sample, $\chi^{(n)}$ is the n^{th} order susceptibility of the material. The $\chi^{(1)}$ term is responsible for linear optical properties such as light reflection and refraction. The terms beyond $\chi^{(1)}E$ are not linear in E . They are referred to as nonlinear polarization and give rise to nonlinear optical (NLO) effects. At low field strengths, the polarization will approximately show a linear response, since the higher order terms become negligible and can be ignored. With increasing field strength however, nonlinear effects become more important.

The odd terms ($\chi^{(1)}$, $\chi^{(3)}$ etc.) in equation 1.6 contribute to the polarization of all materials, but the values of the even coefficients ($\chi^{(2)}$, $\chi^{(4)}$ etc.) are restricted by a symmetry requirement. These terms are non-zero only if the material lacks a center of symmetry, i.e., non-zero even order coefficients will be found only in crystals having a noncentrosymmetric space group. In amorphous solids, in liquids and gases and in solids in which the molecules are related by a center of symmetry, the even terms are always zero. The coefficient $\chi^{(2)}$ is used below to illustrate the nature of induced nonlinear polarization. The coefficient is often written as,⁷

$$\chi_{ijk}^{(2)}(-2\omega; \omega, \omega) \quad 1.7$$

where, i, j, k refer to the principal axes of the medium and indicate tensorial characteristics of $\chi^{(2)}$. 2ω represents the frequency of the resultant field for the input frequencies ω . The minus sign is a convention indicating momentum conservation given by the vector sum,⁷

$$k_1 + k_2 + k_3 = 0 \quad 1.8$$

where, k_1 , k_2 and k_3 are the wave vectors (2ω , ω and ω in this case) given by $k_i = 2\pi/\lambda$ and points in the direction of propagation of the wave.

A variety of nonlinear optical effects can occur through $\chi^{(2)}$ and $\chi^{(3)}$ depending on the exact nature of the input frequencies, the proximity of molecular vibration or resonance to the input frequencies or frequency combinations and phase matching conditions. Some of the observable optical effects and applications are listed in Table 1.1 for $\chi^{(2)}$ and $\chi^{(3)}$.⁷

Table 1.1. Various NLO effects and possible applications

Susceptibility	Effect	Applications
$\chi^{(2)}(0; \omega, -\omega)$	optical rectification	hybrid bistable device
$\chi^{(2)}(-\omega; \omega, 0)$	electro-optic (Pockels) effect	modulators, variable phase retarders
$\chi^{(2)}(-2\omega; \omega, \omega)$	frequency doubling	second harmonic generation (SHG)
$\chi^{(3)}(-\omega; \omega, \omega, -\omega)$	AC-Kerr effect degenerate four-wave mixing	optical bistability, phase conjugation, real-time holography
$\chi^{(3)}(-3\omega; \omega, \omega, \omega)$	frequency tripling	deep UV conversion

The coefficient $\chi^{(2)}$ leading to frequency doubling consists of a new component, 2ω . This is called a “three-wave mixing” process, since two photons with frequency ω have combined to generate a single photon with frequency 2ω . This analysis can be extended to third and higher order terms, thus, third-order processes involve “four-wave mixing.”

Our ability to optimise the NLO properties of organic materials relies on a fundamental understanding of the interrelationship between chemical structure and molecular nonlinearities. At a molecular level, the induced dipole

generated by the interaction of electric field of electromagnetic wave with molecule can be represented by equation 1.9 which is analogous to equation 1.6,⁸

$$\mu = \mu^0 + \alpha E + \beta E^2 + \gamma E^3 + \dots \quad 1.9$$

where, μ^0 is the static dipole of the molecule in the absence of any external field, α is the linear polarizability and β and γ are the first and second hyperpolarizabilities of the molecule, respectively. The molecular coefficients, α , β etc. are analogous to the susceptibility of the material ($\chi^{(n)}$) except that for the χ terms, local field factors arising from the surrounding medium are taken into account.

Design of materials possessing second order NLO effects relies on the relationship between molecular structures and property. The basic strategies accepted for designing SHG materials should take into account factors such as (i) the material should be polarizable, (ii) there should be asymmetric charge distribution, (iii) contain a π -conjugated electron pathway and (iv) possibility of acentric crystal packaging.⁹

1.2. Organic Materials for Second Harmonic Generation

Second-order effects are associated with the third term in the polarization equation (equations 1.6 and 1.9). Molecules containing a conjugated π -electronic system with charge asymmetry exhibit extremely large values of β . To induce charge asymmetry, donor and acceptor groups are substituted on opposite ends of a conjugated molecule which lead to low-lying charge transfer resonance states. The common donor groups are characterised by predominant p character (sp^3 bonding) and often have available electron pairs on a p orbital and the common acceptor groups are characterised by the possession of more s character (sp^2 or sp bonding), or vacant orbitals (as in certain boron compounds).

1.2.1. Early Studies

The first generation of materials used for SHG, were inorganics such as ammonium dihydrogen phosphate (ADP),¹⁰ potassium dihydrogen phosphate (KDP),¹⁰ and β -barium borate (BBO).¹¹ These materials possess only moderate nonlinear coefficients. However, they have relatively large transparency ranges from UV to IR and high optical damage thresholds. Organic materials were initially assumed to be fragile, less easily processed and also less physically and chemically stable. However, the unique electronic properties of organic materials impart them with much higher second order nonlinearities and shorter switching times than the known inorganic materials.¹²⁻¹⁷

In the early 1960s very little was known about the requisite structural features to be present in organic molecules to have NLO properties and hence compounds were examined on the basis of their ready availability. Some of these compounds are listed in Table 1.2.

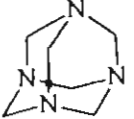
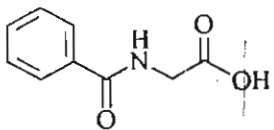
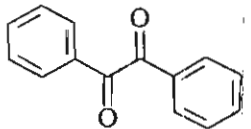
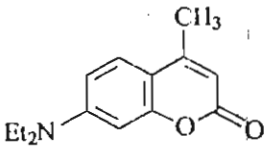
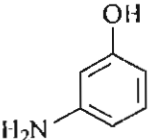
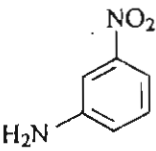
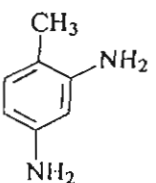
An interesting aspect of all these compounds is that although they are nonchiral they crystallise in noncentrosymmetric space groups.

The SHG properties of urea were first reported by Kurtz and Perry.²⁵ Urea is considered as the first potentially useful organic nonlinear material although it has only a moderate nonlinear coefficient ($\chi^{(2)} = 3 \times \text{KDP}$). It is however transparent down to 200 nm and has fairly large birefringence.

1.3. Molecular Engineering of NLO Materials

Molecular engineering is "the planned synthesis of materials possessing desired bulk properties."²⁶ In the present context, it is the synthesis of organic materials which possess efficient SHG properties at both the molecular and material level. The observed nonlinear response of a material is governed by the optical characteristic of constituent molecular chromophores, the frequencies of the input radiation and the overall spatial orientation that can be imposed

Table 1.2. Structure and NLO efficiency of some organic molecules

Compound	Structure	Space group	NLO efficiency	Reference
1		$I\bar{4}3m$	10 x KDP	18
2		$P2_12_12_1$	6 x KDP	19
3		$P32$	9 x KDP	20
4		$P2_1$	10 x KDP	21
5		Pca	3 x KDP	22
6		$Pbc2_1$	51 x KDP	23
7		$Pna2_1$	29 x KDP	24

upon large ensembles of these constituents. The spatial organization is important for second order NLO properties, because in order for β (or $\chi^{(2)}$) to be non-zero, the molecules (or material) used have to be noncentrosymmetric.⁷ Regrettably, as one modifies the molecular properties it becomes more difficult

to simultaneously obtain the desirable absorption and optical properties such as transparency in the near UV to visible range and low scattering. Furthermore, they must be orientationally, environmentally, and photochemically stable.

A typical SHG material consists of an electron accepting group, a conjugated bridge, and an electron donating group. The conjugated bridge allows for good communication between the donor and acceptor groups. Changing a donor (D) or an acceptor (A) group alone on the π system will perturb the electron density of the molecule. The most dramatic effect is found when both D and A groups interact in a mesomeric fashion (Figure 1.1).

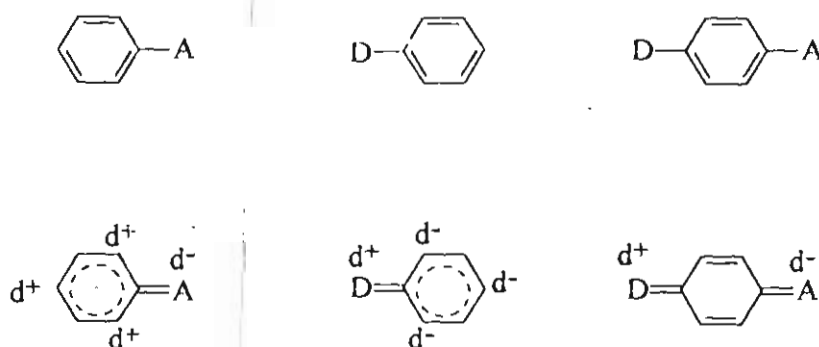
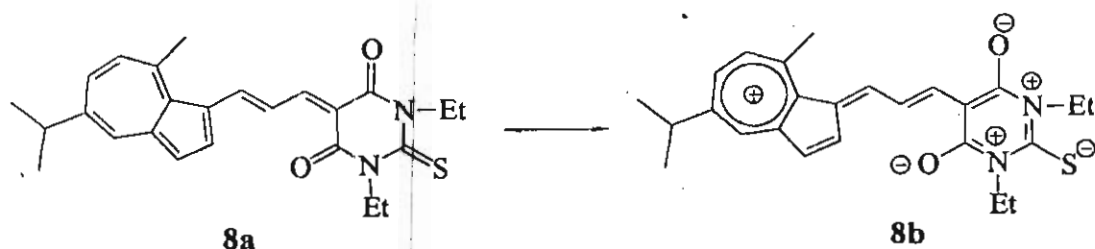


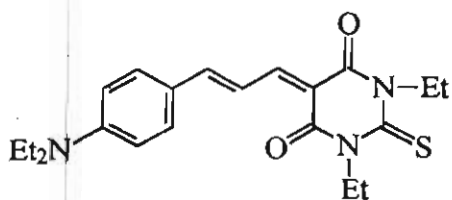
Figure 1.1. Substituent-induced electronic perturbations. Substitution of benzene by a donor-acceptor pair results in ground-state mesomeric charge redistribution

This analogy is illustrated by Asato *et al.* by synthesizing a series of compounds that contain substituted azulenes as donor.²⁷ A representative example (8) is shown in Scheme 1.1.



Scheme 1.1

The disruption of aromaticity of azulene on going to the zwitterionic state is more than compensated by the gain of resonance energy upon formation of the aromatic azulenylium carbocation.²⁸ The $\mu\beta$ value of compound **8** is 1323×10^{-48} esu at 1907 nm, which is comparable to that of the diethylaniline derivative **9** ($\mu\beta = 1400 \times 10^{-48}$ esu),¹³ shown in Chart 1.1.



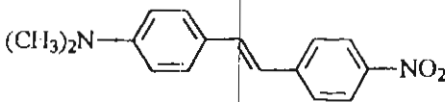
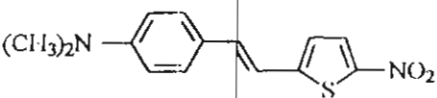
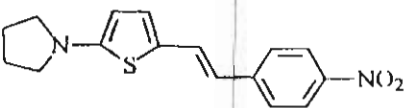
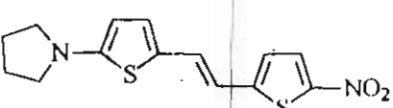
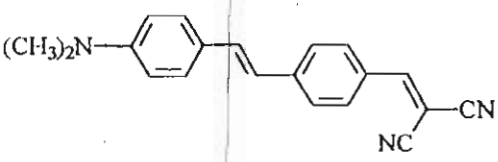
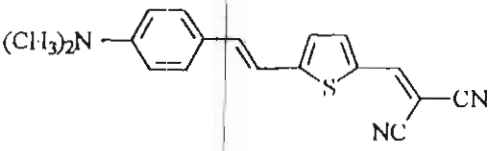
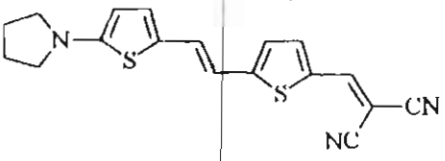
9

Chart 1.1

Drost *et al.* have reported that the introduction of electron rich five membered heteroaromatics such as thiophene as part or all of the π -conjugation between the donor and acceptor increases the hyperpolarizability of the molecule (Table 1.3).²⁹ These results were supported by molecular orbital calculations.³⁰ From Table 1.3 it is clear that substituting a phenyl group by thiophene brings about a significant enhancement of the $\mu\beta$ value. The enhancement in $\mu\beta$ values on thiophene substitution has been attributed to the

lower resonance energy (117 kJ/mol) compared to that of benzene (151 kJ/mol).

Table 1.3. Thiophene-based donor-acceptor compounds

Compound	Structure	λ_{\max} (nm) in dioxane	$\beta\mu$, 10^{-48} esu, at $\lambda = 1907$ nm
10		424	580
11		478	600
12		460	660
13		516	1040
14		468	1100
15		513	1300
16		584	2600

A number of new organic compounds have been synthesized in order to find the optimum features of donor and acceptor groups for generating new materials with efficient SHG properties. The relationship between donor and acceptor strengths and $\mu\beta$ value are not straightforward. For example, a recent study has shown that increasing acceptor strength does not necessarily lead to increase in the values of $\mu\beta$ (Table 1.4).³¹

Table 1.4. Nonlinear optical coefficient of donor-acceptor substituted chromophores of the form D(CH=CH)_nA

Compound	D	A	n	No. of conjd. atoms	λ_{max} (nm)	$\mu\beta \times 10^{-48}$ esu
17	Me ₂ N	CHO	0	3	<240	1.8
18	Me ₂ N	CHO	1	5	284	21
19	Et ₂ N	CHO	2	7	363	130
20	Me ₂ N	CHO	3	9	422	366
21	Me ₂ N	CH=C(CN) ₂	0	5	352	7.6
22	Me ₂ N	CH=C(CN) ₂	1	7	374	54
23	Et ₂ N	CH=C(CN) ₂	2	9	476	482
24	Me ₂ NC ₆ H ₄	CH=C(CN) ₂	3	11	550	2089
25	Me ₂ NC ₆ H ₄	CHO	0	7	326	32
26	Me ₂ NC ₆ H ₄	CHO	1	9	384	1.58
27	Me ₂ NC ₆ H ₄	CH=C(CN) ₂	0	9	420	250
28	Me ₂ NC ₆ H ₄	CH=C(CN) ₂	1	11	486	689

The contribution to the molecular hyperpolarizability, β can be resolved into two components, an additive term and a charge transfer term.^{32,33}

$$\beta = \beta_{add} + \beta_{CT} \quad 1.10$$

Of these β_{add} is the additive part due to substituent-induced asymmetry in the charge distribution and β_{CT} is the charge transfer term.

The charge transfer term, β_{CT} can be described in terms of ground and first excited states having charge transfer character and is related to the energy of the optical transition W , its oscillator strength f , and the difference between excited and ground state dipole moments, $\Delta\mu_{\text{c,g}}$ by equation 1.11,³⁴

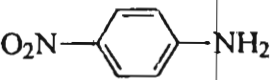
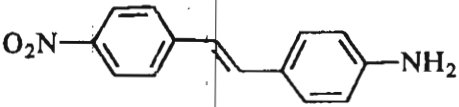
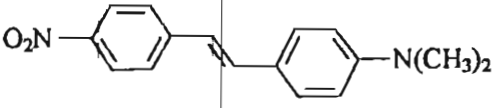
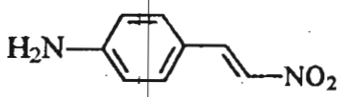
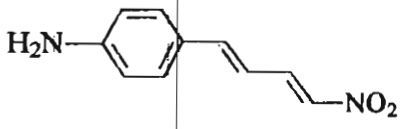
$$\beta_{\text{CT}} = \frac{3e^2\hbar^2}{2m} F(\omega) f \Delta\mu_{\text{c,g}} \quad 1.11$$

$$F(\omega) = \frac{W}{[W + (2\hbar\omega)^2][W^2 - (\hbar\omega)^2]} \quad 1.12$$

$$\Delta\mu_{\text{c,g}} = \mu_{\text{c}} - \mu_{\text{g}} \quad 1.13$$

Clearly, to maximise β , it is favourable to seek molecules that have an electronic transition with a small energy gap near 2ω accompanied by a large oscillator strength and dipole moment change. The spectroscopic energy gap W is related to the frequency (or wavelength, λ) of absorptions found in the UV-Vis spectra of the molecules and the oscillator strength is related to the extinction coefficient ϵ of the absorption. From equation 1.11, it is clear that β will be maximum when the value of W is moderate and $\Delta\mu$, the difference in dipole moment between the excited and ground state is maximum. Good agreement was obtained between the value of β_{CT} predicted by this expression and β_{exp} (assuming that $\beta_{\text{exp}} = \beta_{\text{CT}}$) for a series of disubstituted benzene and stilbene derivatives. Table 1.5 lists experimentally determined values of β for various nitroanilines and monosubstituted compounds.³⁴

Table 1.5. Charge-transfer contribution, β_{CT} , calculated from the two level model, and experimental values β_{exp} for a series of benzene and stilbene derivatives

Compound	Structure	$\beta_{CT} \times 10^{-30}$ (esu)	$\beta_{exp} \times 10^{-30}$ (esu)
29		19	34.5
30		227	260
31		383	450
32		217	220
33		715	650

A significant enhancement of polarizability has been demonstrated by extending the conjugation length between donor and acceptor. This generally results from decreasing the energy gap and increasing the transition dipole moment between the relevant states. The quantitative relationship between hyperpolarizability and chain length of a conjugated system has been derived by various groups³⁵⁻³⁷ (equations 1.14 – 1.16).

$$\alpha = 8e^2 b^2 (2m + 1)^3 / \pi^5 \gamma \propto L^3 \quad 1.14$$

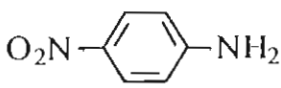
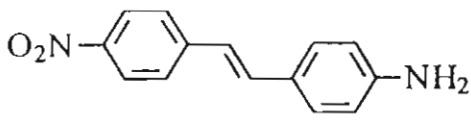
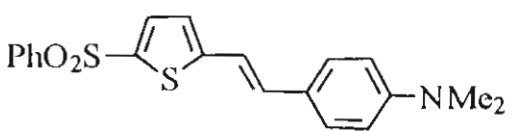
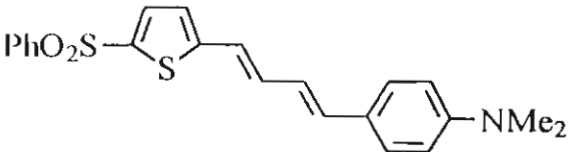
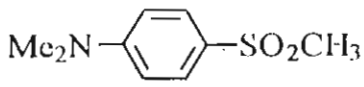
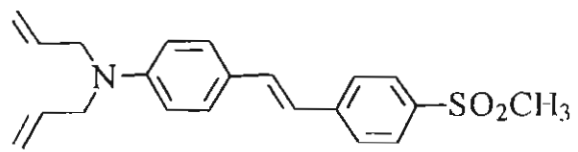
$$\beta = 3\Delta\mu\gamma_0/\alpha \propto L^3 \quad 1.15$$

$$\gamma = I^5 / a_0^3 e^2 \propto L^5 \quad 1.16$$

This strategy is applicable to conjugated systems, except for molecules with strong aromatic bridges, such as stilbenes. This is due to the loss of aromaticity on going from the ground state to charge-separated excited state in the case of systems with aromatic bridges. Table 1.6 illustrates the effect of chain length on the first hyperpolarizability of some conjugated systems.^{38,39}

However, even if a molecule has a large β value, it might fail to exhibit SHG activity. Crystallization in a noncentrosymmetric fashion is also required, and since about 70% of all nonchiral molecules crystallise in centrosymmetric space groups, this is a major problem. To counter this, many strategies for forming accentric crystals capable of showing SHG activity have been employed and some of these include (i) incorporation of chiral groups,^{40,41} (ii) hydrogen bonding,^{40,42-44} (iii) ionic chromophores,^{45,46} (iv) steric hindrance,⁴⁷ (v) inclusion phenomena,⁴⁸⁻⁵¹ (vi) Langmuir-Blodgett techniques,⁵² (vii) cocrystallization,⁵³ and (viii) reduction of dipole-dipole interaction.⁵⁴ These methods have met with varying degrees of success in ensuring a dipolar alignment favourable for SHG. The influence of some of these effects on NLO properties of materials are described in following sections.

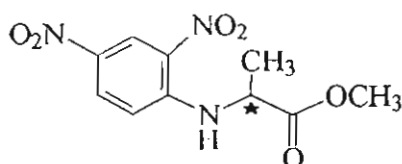
Table 1.6. Second-order hyperpolarizabilities of some conjugated chromophores

Compound	Structure	$\beta \times 10^{-30}$ esu
34		34.5
35		260
36		59
37		145
38		26
39		573

1.3.1. Effect of Chirality on SHG

Enhancement of the SHG properties of materials by introducing chiral moieties such as amino acids and sugars has been studied extensively.⁵⁵ Several naturally occurring amino acids and sugars which contain chiral centers were found to be SHG active. Recognising the role of chirality in

enhancing the SHG properties of molecules, several polarizable donor-acceptor systems attached to chiral groups have been examined. For example, the 2,4-dinitroaniline derivative, MAP (40),⁵⁶ containing the methyl ester of the active amino acid (S)-(+)-alanine showed SHG efficiency 14 times that of urea (Chart 1.2).



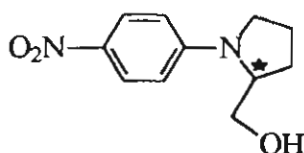
40

Chart 1.2

To date, only the chirality of the tetrahedral carbon has been utilized in this fashion. The five other general chirality types (asymmetric heteroatom, asymmetric octahedral center, restricted rotation of dissymmetric planes, helical dissymmetry, and dissymmetric knots and braids) remain to be exploited.

Although chirality guarantees a noncentrosymmetric molecular structure, this may not ensure noncentrosymmetric packing of the molecules in the crystal. Dipolar forces will tend to favour the head-to-tail antiparallel dimerization of molecules, and chirality may not significantly modify this tendency. The dipolar interactions can however be surpassed by the effect of intermolecular hydrogen bonds, since these bonds are one or two orders of magnitude more energetic than van der Waals and dipole-dipole interactions. Furthermore, hydrogen bonds, as opposed to dipolar potentials, are not predisposed towards generating centro- or noncentrosymmetric crystal structures. The combination of chirality and hydrogen bonding potential can thus promote a greater number of interesting structures.

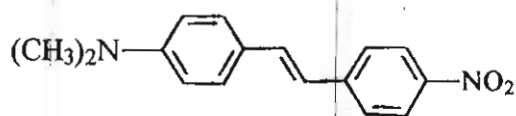
Zyss *et al.* have demonstrated the effect of chirality and hydrogen bonding in N-(4-nitrophenyl)-(L)-prolinol (NPP, 41).⁵⁷ This compound is 10 times more active than MAP (40).



41

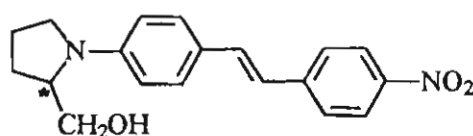
Chart 1.3

The simultaneous chiral and hydrogen-bonding character of electron donating prolinol group enhances the nonlinear response of this molecule. In another example, replacement of dimethylamino group by prolinol in the stilbene derivative increases the β value by about two times (Chart 1.4).⁴³



42

$$\mu\beta = 580 \times 10^{-48} \text{ esu}$$

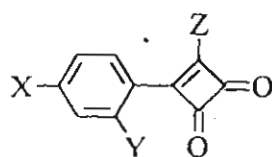


43

$$\mu\beta = 1130 \times 10^{-48} \text{ esu}$$

Chart 1.4

Molecules containing cyclobutandione acceptor moiety substituted by chiral groups have been reported.⁴⁶ The presence of both chirality and hydrogen bonding properties leads to materials with large SHG efficiencies (Table 1.7).



44 - 50

Chart 1.5

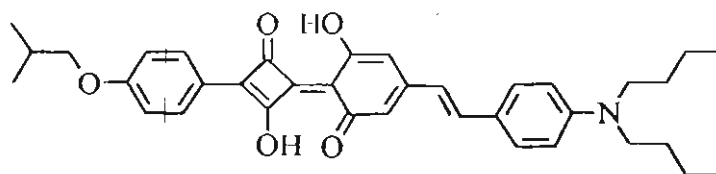
Table 1.7. SHG efficiencies (relative to urea) of cyclobutanedione derivatives

Compound	X	Y	Z	SHG
44	Me	H	OH	2.5
45	Me ₂ N	H	OH	0.0
46	Me ₂ N	H	NHCH ₂ CH(OH)Me	64.0
47	Me ₂ N	H	NHCH(Et)CH ₂ OH	6.0
48	Me ₂ N	H	NHCH(CH ₂ Ph)CH ₂ OH	8.0
49	Me ₂ N	Et	NHCH(Et)CH ₂ OH	26.0
50	MeO(CH ₂) ₂ (Me) ₂ N	H	NHCH ₂ CH(OH)Me	58.0

The high SHG efficiencies of these compounds is due to several factors such as (i) the strong electron accepting property of cyclobutanedione, (ii) their high molecular absorption coefficient, (iii) hydrogen bonding properties, and (iv) chirality. Powder SHG measurements indicate that compound 45 is inactive (Table 1.7) probably due to electrostatic interactions between the adjacent molecules predominating over hydrogen bonding interactions in this case.

A squaraine dye with extended conjugation possessing a large molecular hyperpolarizability ($\mu\beta = 481 \times 10^{-30}$ esu) has been reported by Chen *et al.* (Chart 1.6).⁵⁸ Although it has a strong absorption in the near IR

region (732 nm) it possess a large transparency window in the range of 260 to 680 nm, making it highly suited for SHG applications.



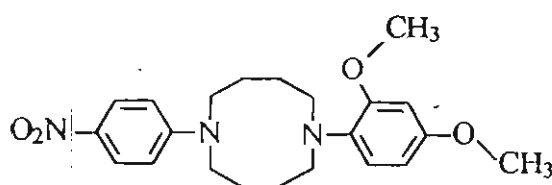
51

Chart 1.6

1.3.2. Role of Hydrogen Bonding for SHG Materials

Hydrogen bonds most often found in SHG materials involve interaction between a hydrogen bound to sp^3 nitrogen or oxygen and an oxygen atom with more s character.

Hosseini *et al.* have synthesized 1,6-diazacyclodecane derivative 52 in which the donor and acceptor moieties are attached to the nitrogen atoms on either side of the diaza compound (Chart 1.7).⁵⁹ The electronic communication between donor and acceptor groups is achieved by transannular hydrogen bond as shown in Scheme 1.2.



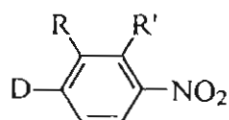
52

Chart 1.7



Scheme 1.2

Intermolecular hydrogen bonding induced by attaching a highly polar group to the conjugated backbone of the nonchiral molecule can make the crystal noncentrosymmetric resulting in high SHG coefficients (Table 1.8).⁶⁰



53 - 56

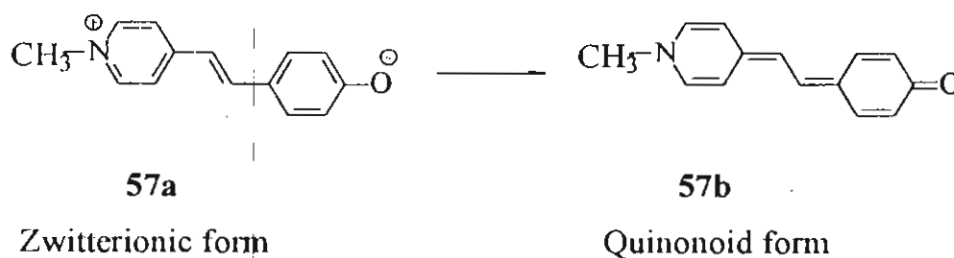
Chart 1.8

Table 1.8. SHG efficiency of nonchiral 4-nitroaniline derivatives

Compound	D	R	R'	SHG (\times SHG _{urea})
53	HO-CH ₂ -CH ₂ -CH ₂ -NH-	H	H	80
		CF ₃	H	30
54	HO ₂ C-CH ₂ -CH ₂ -CH ₂ -NH-	H	CF ₃	80
		CF ₃	H	115
55	NC-CH ₂ -N(CH ₃) ₂ -	H	H	140
56	NC-CH ₂ -N(CH ₃) ₂ -	H	H	85

Intermolecular hydrogen bonding can also help in bringing about cocrystallization of two different chromophores. Pan *et al.* have reported the cocrystallization of a merocyanine dye 57 with nitrophenol derivatives 58 and

59,⁶¹ which involve short hydrogen bonding (R-OH...O ca. 2.46 Å) between the phenolic groups, whereas they could not get cocrystals of 57 and nitroaniline derivatives.



Scheme 1.3

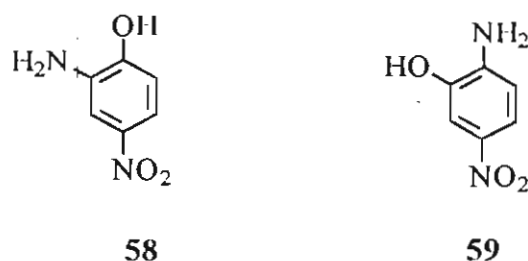


Chart 1.9

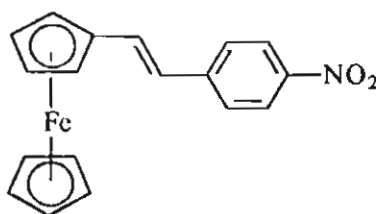
Short hydrogen bonds have several advantages in that they are characterized by high bonding strengths and higher degree of flexibility which can adapt their bonding directions to fit the three dimensional packing for stabilization of the crystal.

1.3.3. Metallic Complexes

In addition to conventional organic end groups, transition metal moieties have been examined as donors and acceptors. Incorporation of metals into SHG systems introduces a new dimension with possibilities of many new

variables. The metals can have a large diversity of oxidation states and ligand environments, and due to their polarizable *d* electrons are likely to possess greater nonlinear activity.

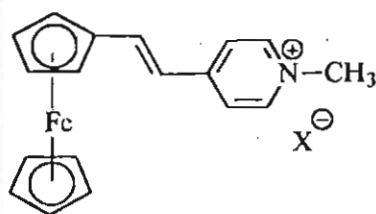
The first report on organometallic compounds for SHG came in 1987 by Green *et al.*⁶² The *cis*-ferrocene derivative, **60** (Chart 1.10) was analyzed, since it crystallizes in noncentrosymmetric space group. The *trans*-isomer shows no SHG signal, because of its center of symmetry. Kurtz powder measurements at 1064 nm for the compound gave SHG efficiency 62 times larger than that of urea. The facile redox ability exhibited by the metallocene derivatives leads to large value of β by charge transfer through the π -conjugation system.



60

Chart 1.10

Other than ferrocene derivatives, metal carbonyls,⁶³ octahedral metal complexes,⁶⁴ square-planar metal complexes,⁶⁵ and silicon complexes⁶⁶ were extensively studied by different groups. The largest SHG values for organometallic compounds, reported to date, are for a series of salts of the type shown in Chart 1.11 and the results are summarised in Table 1.9.



61 - 69

Chart 1.11

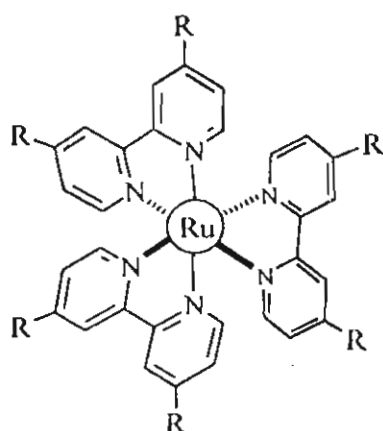
Table 1.9. Powder SHG efficiencies of a series of salts of the type shown in Chart 1.11

Compound	X	SHG efficiency (x Urea)
61	I	220
62	Br	165
63	Cl	0
64	BF ₄	50
65	NO ₃	120
66	B(C ₆ H ₅) ₄	13
67	PF ₆	0.05
68	CF ₃ SO ₃	0
69	<i>p</i> -CH ₃ C ₆ H ₄ SO ₃	13

The values of the powder SHG signals depend on the counter ions. Compound 61, which possess I⁻ as the counter ion, for example showed SHG efficiency 220 times than that of urea, whereas 63 and 68 possessing Cl⁻ and CF₃SO₃⁻ as the counter ions were inactive.⁶⁷

Large $\mu\beta$ values can also be obtained for molecules that do not possess a dipole moment. Trisubstituted ruthenium complexes in spite of having zero

dipole moments, show SHG efficiency due to multidirectional metal-to-ligand charge transfer.⁶⁸ Ruthenium complexes also exhibit excellent thermal and photochemical stability.⁶⁹ An example is the tris-bipyridine ruthenium complex **70**, which has a β value of 2200×10^{-30} esu. This value is comparable to those of long dipolar donor-acceptor conjugated molecules.^{69,70}

**70****Chart 1.12**

1.3.4. Polymeric Systems

Polymers embedded or chemically bonded with a nonlinear chromophore comprise a very promising class of NLO materials due to their processibility, which can give large-area high-quality films for integrated optical applications. As mentioned earlier, for even-order NLO interactions, materials possessing centrosymmetries result in vanishing macroscopic nonlinear response. Different poling techniques have been invented for the removal of the centrosymmetry in polymers. These techniques consist of the use of an

external force to align the NLO chromophore by means of a mechanical stress, a magnetic field, an electric field, or polarized laser beam.

Electric field poling techniques are most often used for second-order NLO applications. This technique allows the alignment of polar components of a thin film of a polymeric material. The different steps involved are indicated in the following sequence.⁷¹

Poling steps

1. Heat thin film of the polymeric material above its glass transition temperature (T_g)
2. Switch on the electric field
3. Cool
4. Switch off the electric field

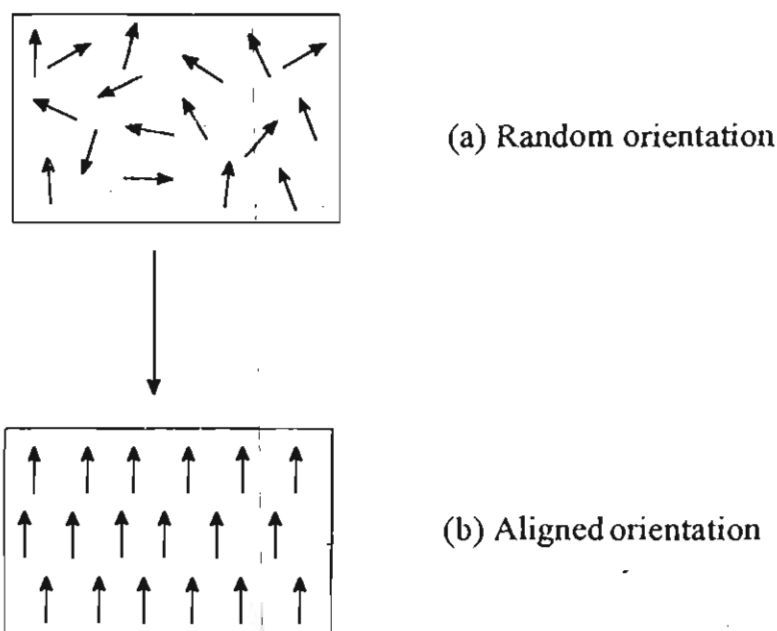
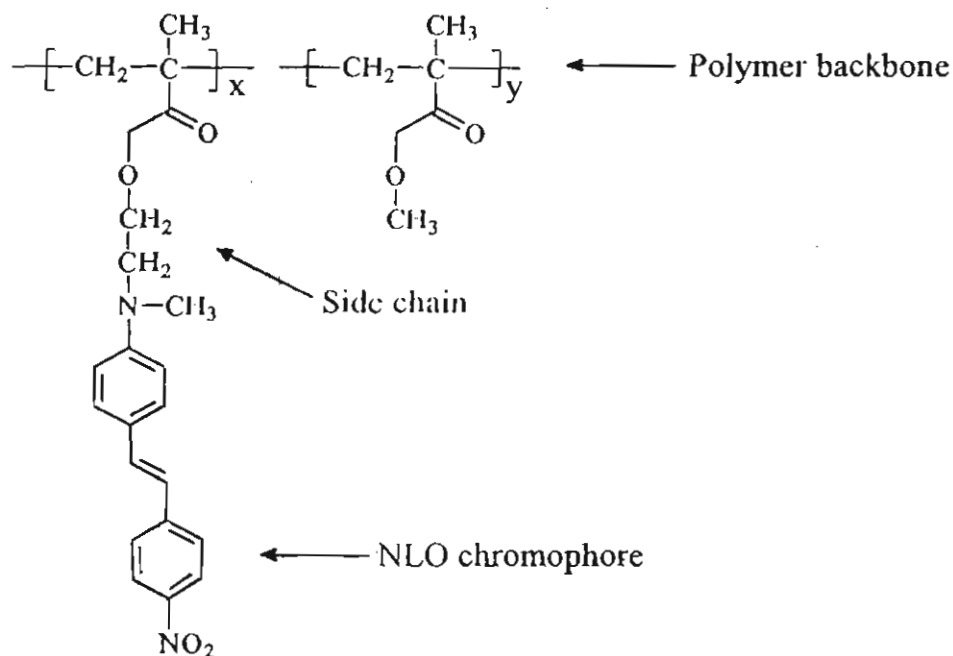


Figure 1.2. Schematic representation of alignment of chromophore moieties (a) before and (b) after poling

There are two types of electric field poling, namely electrode poling and corona discharge.⁷² In the case of electrode poling a strong DC electric field (permanent or pulsed, of the order of 10^6 V/cm) is applied to a pair of electrodes sandwiching a NLO material composing a host material and chromophore to be oriented, above the glass-transition temperature (T_g) of the host material. The orientation is then frozen by cooling while keeping the electric field on. Corona discharge is carried out by charging the surface of a film under a strong potential. This method is more flexible with fewer limitations on the geometry of the electrodes.

The major drawback of polymer films is that $\chi^{(2)}$ is perpendicular to the film surface. For bulk electro-optic applications it is desirable to have a film with $\chi^{(2)}$ parallel to the film surface to achieve electro-optic modulation for two-dimensional device applications. This drawback is yet to be overcome. One of the main problems with polymers loaded with NLO active molecules⁷³ is that chromophores cannot be introduced into the polymer at high concentrations. With increasing concentration of the guest molecules, the polymer tends to crystallize causing problems of light scattering. The other major problem is the loss of alignment of the chromophores on removal of the poling field even in the frozen state of the molecule. One method of overcoming these problems is to covalently link optically active chromophores as pendent groups on to the polymer backbone.⁷⁴ In this manner quite high chromophore concentrations can be obtained and the alignment in such systems also tends to be retained for much longer times. In this context methacrylate copolymers with side chains containing aminonitrostilbene moieties, **71** (Chart 1.13) have been studied.⁷⁵ Such polymers typically have refractive indices in the range of 1.5-1.7 and dielectric constant of about 3

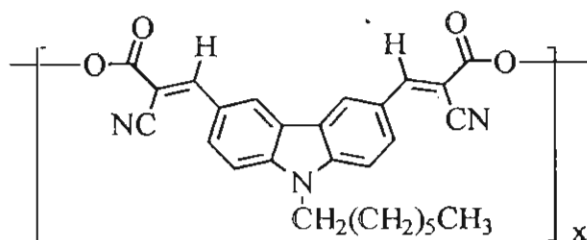
Debye units which is constant over a very wide frequency range. Better orientational stability was also observed.



71

Chart 1.13

Another type of NLO polymers are those that contain active chromophores in the main-chain.⁷⁶ Most of the reported main chain polymers are head-to-tail polymers in which all the chromophore dipole moments point in the same direction along the polymeric main chain.^{76,77} Zhang *et al.* have reported the synthesis and SHG properties of a main-chain diaceptor substituted carbazole derivative 72 in which the chromophores are aligned in a shoulder-to-shoulder arrangement (Chart 1.14).⁷⁸



72

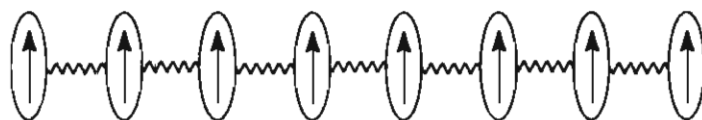


Chart 1.14

The use of polymers which are simultaneously liquid crystals enhances the net guest alignment achievable with an applied field by the inherent axial alignment properties of the liquid crystals through intermolecular interactions between the host and the guest.⁵¹ However, the scattering texture found in liquid crystals is problematic and limits the use of such liquid crystalline polymers as host materials.

1.3.5. Supramolecular Systems

Supramolecular chemistry,⁵² the chemistry of the intermolecular bond, involves both organization and function, depending, in particular, on molecular recognition events. It extends towards the design of molecular devices that operate on photon, electron or ion control modes and which can be formed through self-assembling of their components.^{52,53} It has been pointed out by Lehn that by molecular recognition or complex formation various types of molecular systems can be organized to a high degree, to generate materials possessing NLO properties.⁵⁴ This may be achieved by introducing the

molecules into organized phases such as molecular films, liquid crystals or solid state structures, by suitable derivatization or mixing with host substances.

In the Langmuir-Blodgett film technique,⁷⁹ for example, monolayers of molecules containing a hydrophilic group at one end and hydrophobic tail on the other are spread over the surface of water in an appropriate fixture. By controlling the surface pressure the molecules can be made to organize into highly oriented structures at the air water interface. It is also possible to transfer the monolayers on to a substrate of appropriate polarity. Subsequent deposition cycles can be employed to fabricate multilayer films of macroscopic dimensions. With appropriate choices of head and tail units noncentrosymmetric films with polar cylindrical symmetry can be fabricated (Figure 1.3).

LB film formation and SHG studies of three polysiloxanes (Chart 1.15) were reported by Kalita *et al.* in 1992.⁸⁰ All these compounds form Z-type layers on a variety of substrates. Monolayers of **74** were found to possess a nonlinear optical susceptibility, $\chi^{(2)}$ ($-\omega; \omega, \omega$) of 10.6 pm/V. For multilayer films, the SHG intensity was found to increase with the thickness of the LB structure.

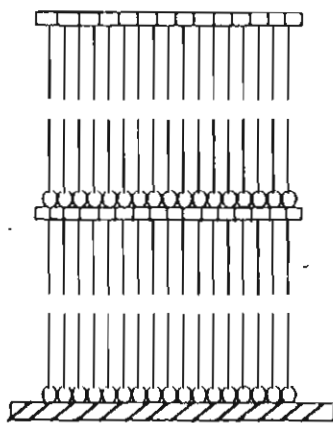


Figure 1.3. Schematic representation of a noncentrosymmetric LB film. The nonlinear chromophores represented by squares is incorporated into alternate layers

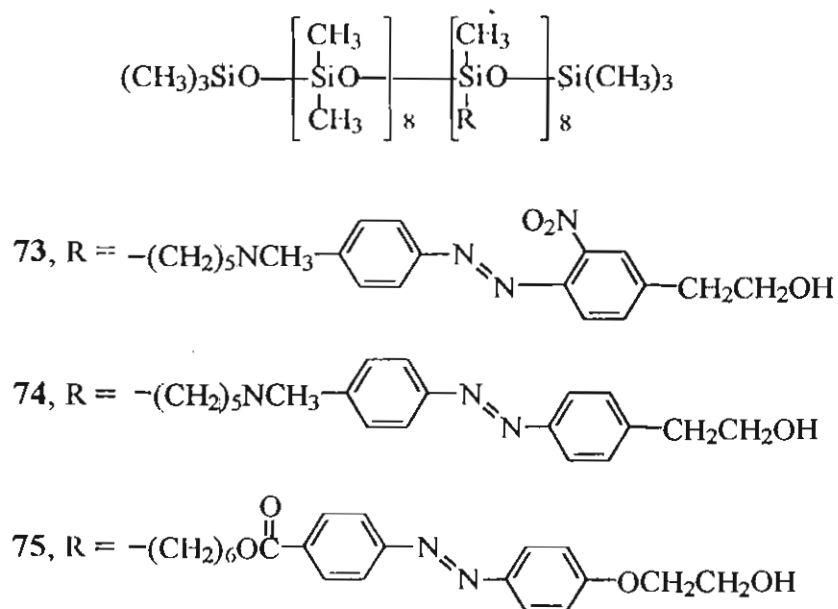
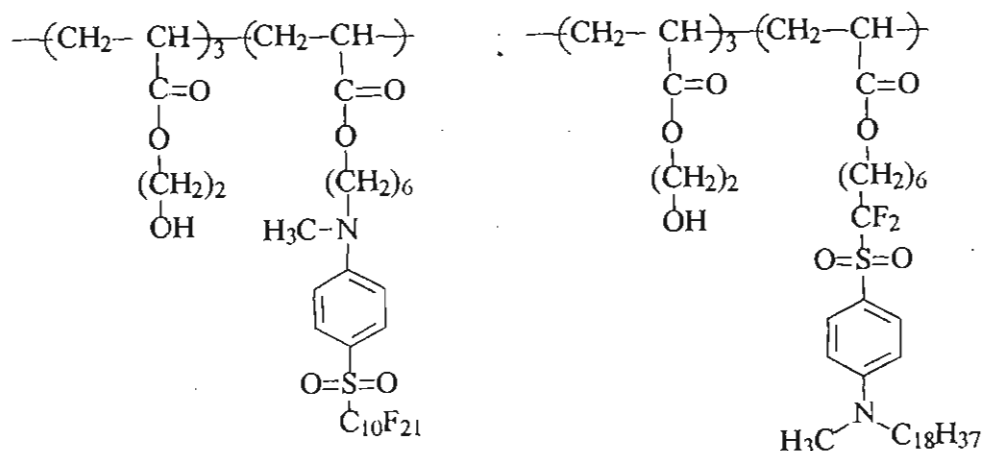


Chart 1.15

Prasad *et al.* have shown that the SHG intensity from multilayer LB films of polymers of the type shown in Chart 1.16 increases quadratically, with increasing number of bilayers, indicating that $\chi^{(2)}$ of the bilayer is a linear sum of the macroscopic optical nonlinearities of the individual monolayers (Table 1.10).⁸¹ The multilayer LB film of each polymer was made by alternate deposition with a spacer polymer, poly(*tert*-butyl methacrylate).

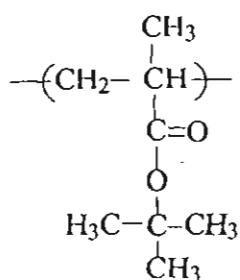


76

Normal polymer (N)

77

Reverse polymer (R)



78

Poly(*t*-butyl methacrylate) (P)

Chart 1.16

Table 1.10. SHG intensities of different bilayer samples measured at an incident angle of 45°

Type of bilayer	$I^{2\omega}$ (10 layers)	$I^{2\omega}$ (20 layers)
Polymers N and R	0.148 ± 0.024	0.425 ± 0.097
Polymers N and P	0.037 ± 0.006	0.112 ± 0.021
Polymers R and P	0.034 ± 0.007	0.128 ± 0.018

Ashwell *et al.* have made an interesting observation that centrosymmetric molecules can exhibit SHG if they aggregate in a noncentrosymmetric manner, and there is a contribution to the bulk susceptibility from intermolecular charge transfer.⁸² For example, monolayers of centrosymmetric squaraine dyes deposited by LB technique possess SHG properties. The X-ray crystal structure of a representative example of this series, 2,4-bis(4-(N,N-dibutylamino)phenyl) squaraine, **79**, has confirmed that the chromophore is planar and centrosymmetric. The bulk material does not exhibit SHG because of the centrosymmetry of the molecule, whereas the LB films of this compound are SHG active.

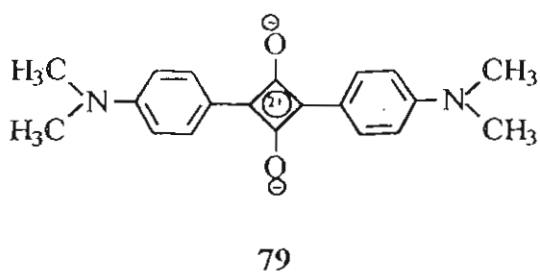
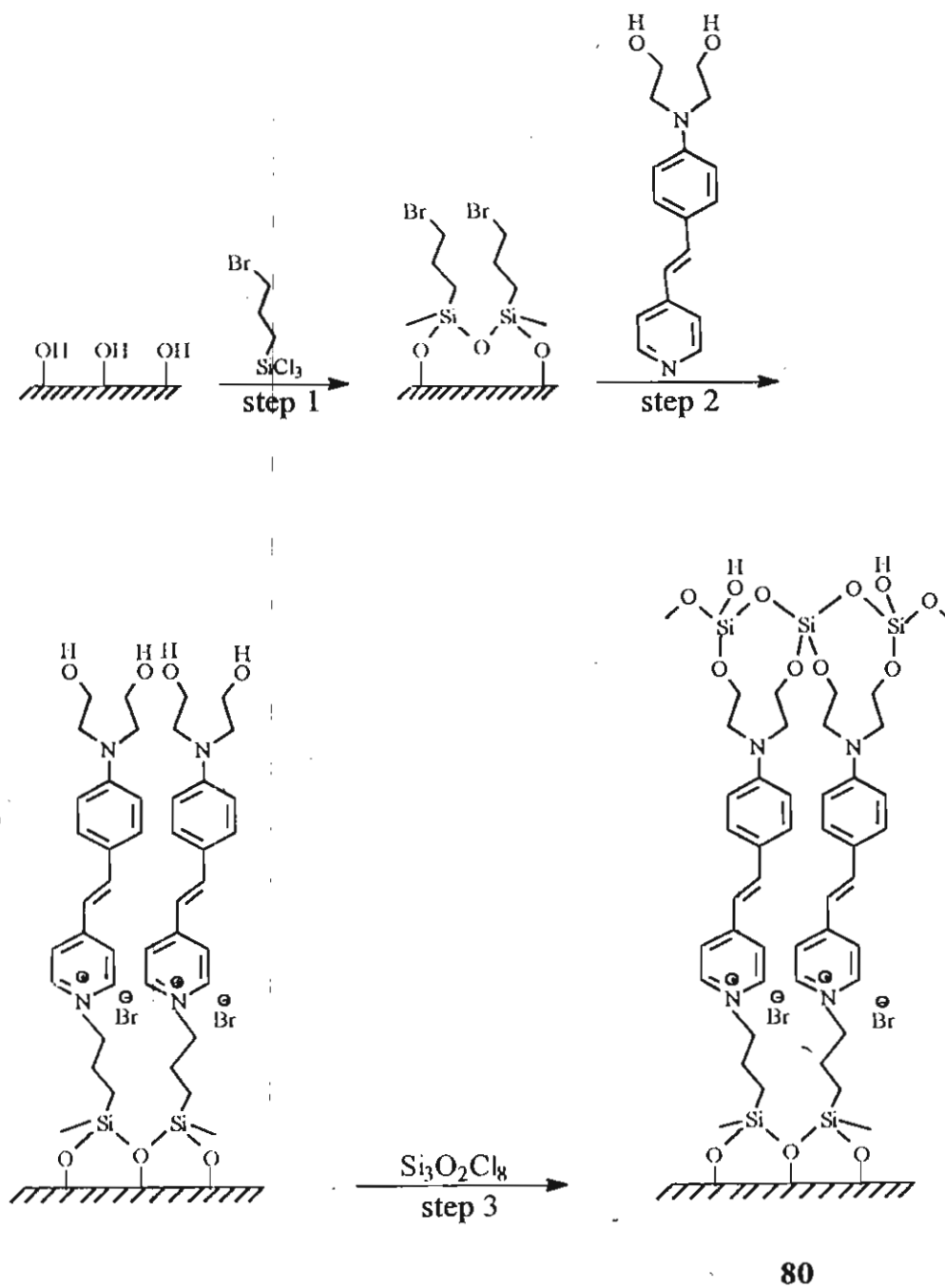


Chart 1.17

An alternative to LB film techniques would be the construction of covalently linked molecular layer structures. The key assembly step is effected in either a solvent-free solid state or chemical vapour deposition mode, which allows the assembly of chromophoric groups with high structural regularity and large NLO responses. An illustrative example of such a system is shown in Scheme 1.4.⁸³

Construction of such superlattices involves the basic siloxane technology developed by Sagiv *et al.*,^{84,85} and refined by Ulman and others.^{86, 87} These steps can be repeated to get multilayers with net chromophore alignment. These materials offer greater number densities than poled films and



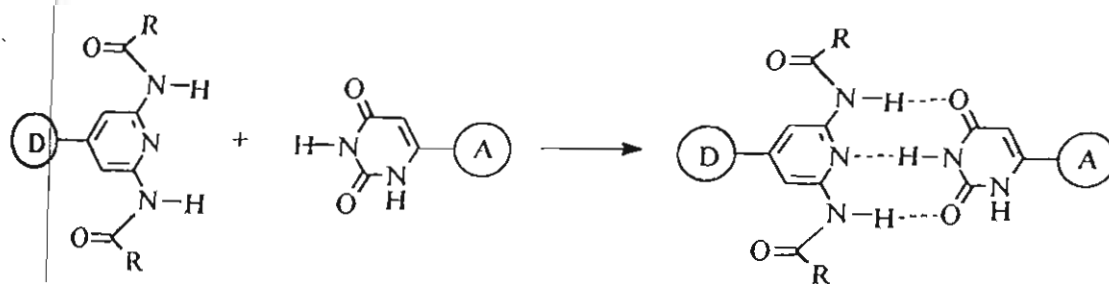
Scheme 1.4

far greater structural control and stability than LB films. The course of multilayer evolution can be monitored by following the growth of absorption of the chromophore (in this case at 510 nm), XPS spectroscopy, contact angle measurements and NLO characteristics. These films adhere strongly to glass, and are insoluble in common organic solvents and strong acids. The SHG efficiency of the monolayer film of **80** with 22 Å thickness was found to be $\sim 700 \times 10^9$ esu, which is considerably higher than that of typical poled polymers and compares well with the best LB films.^{88, 89}

1.3.6. Molecular Recognition Induced Self-Organization and NLO Effects

Molecular recognition process is based on selective intermolecular interactions between complementary components. They may affect the properties of the system at the molecular, supramolecular and material levels by (i) perturbing the electronic and optical properties of the component, (ii) generating supramolecular species, and (iii) inducing organization in condensed phase, respectively. All these effects are of importance with respect to the NLO properties of the material and its constituents.⁹⁰

The binding of two complementary components of donor D and acceptor A type yields a push-pull supramolecular species in which the interaction may be expected to modify the initial donor and acceptor features of the isolated species (Scheme 1.5).



Scheme 1.5

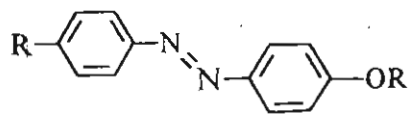
Molecular recognition directed self-assembling of organized phases has been described in the formation of mesophases by association of complementary molecular components,⁹¹ supramolecular liquid crystalline polymers,⁹² and ordered solid state structures.⁹³ In all these cases, the incorporation of NLO active groups may be expected to produce materials whose SHG properties would depend on molecular recognition induced self-organization.

1.3.7. Liquid Crystals

Another class of orientationally ordered assembly is liquid crystalline systems. They are often inhomogeneous, a property which arises from the phase of the liquid crystal such as helical structure of cholesteric liquid crystals and chiral phase in smectic liquid crystals.

The bulk susceptibilities of liquid crystals are related to the orientational order of the molecules in the material. Due to this orientational anisotropy, liquid crystals experience body torque in the presence of applied fields, which may give rise to director (unit vector describing the average direction of the molecular long axis) reorientation. This leads to large changes in dielectric tensor. Therefore directional reorientation is responsible for extremely large nonlinear susceptibilities in liquid crystals. NLO effects can also exist without director reorientation. In these cases the nonlinearities originate from changes in the degree of orientational order, changes in density due to the action of the optical field, and may involve laser heating or other mediating mechanisms.

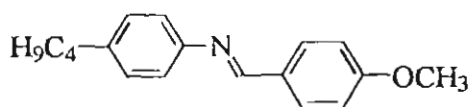
Liquid crystals may be obtained from suitably modified molecules having NLO properties. Various liquid crystalline azobenzene derivatives of the general structure shown in Chart 1.18 have found applications in image storage and optical switching.⁹⁴



81

Chart 1.18

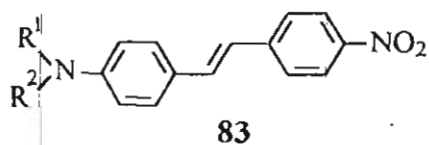
Although SHG was observed in aligned samples of MBBA⁹⁵ (Chart 1.19), these types of compounds were assumed to possess center of symmetry.



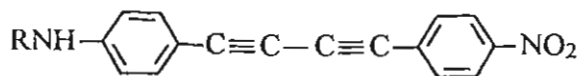
82

Chart 1.19

Various push-pull stilbene and diacetylene derivatives bearing long alkyl chains have also been shown to display nematic and smectic mesophases (Chart 1.20).⁹⁶



83

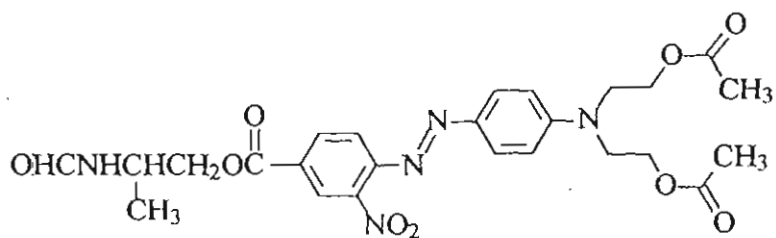


84

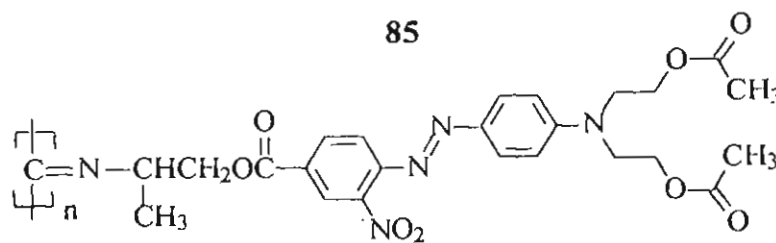
Chart 1.20

These compounds are highly polarizable and possess nonlinear optical properties.

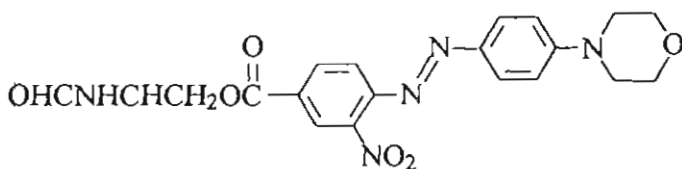
Kauranen *et al.* have reported the synthesis of orientationally ordered side chain polymers with a rigid back bone (85-88, Chart 1.21).⁹⁷ Here, poling of the chromophore is achieved by chemical synthesis, without applying any external field.



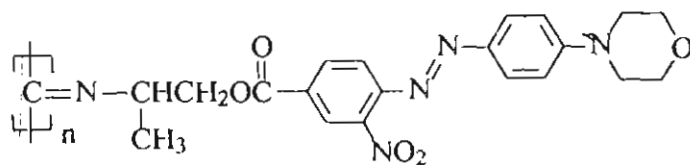
85



86



87



88

Chart 1.21

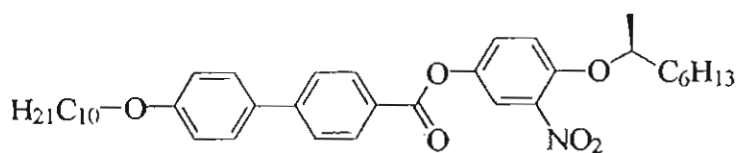
The very large permanent dipole moment observed for such systems can be due to two reasons: (i) addition of dipole moments of the chromophores, or (ii) dipole moment associated with the supramolecular structure itself.⁹⁸

The hyperpolarizabilities of the polymer compounds were much larger than those of the respective chromophores (Table 1.11). This shows that the chromophores are arranged in a noncentrosymmetric fashion in the polymer chain and each chromophore contributes coherently to the hyperpolarizability of the polymer.

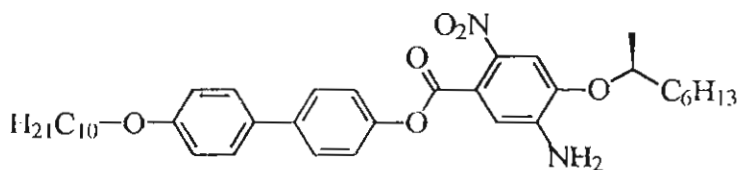
Table 1.11. Properties of individual chromophores 85-88

Compound	λ_{\max} (nm)	$\beta \times 10^{-30}$ esu
85	457	774
86	438	3020
87	448	564
88	435	5150

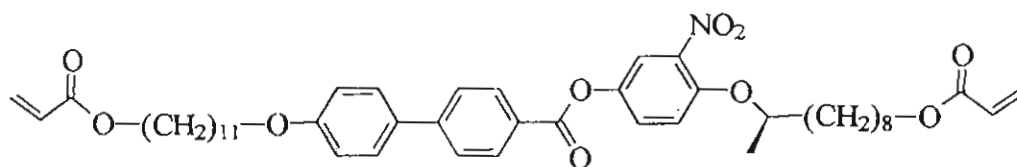
Ferroelectric liquid crystals (FLC) are distinguished by spontaneous polarization, and hence do not possess inversion symmetry. They are known to exhibit relatively low SHG coefficients. However in 1991, Walba *et al.* synthesized a low molar mass compound (89) specially designed for second order nonlinear optics, and this compound showed a second harmonic coefficient (d_{22}) of 0.6 ± 0.3 pm/V in the chiral smectic C (Sc*) phase.^{99, 100} The NLO chromophores aligned in the direction of the polarization, perpendicular to the long axis direction of the molecule, were later improved by Schmitt *et al.* by the addition of an electron donating amino group in the *para* position to the electron accepting nitro group (compound 90, Chart 1.22).¹⁰¹



89



90



91

Chart 1.22

Hult *et al.* in 1996 reported NLO studies of the polymer obtained by the photopolymerization of the ferroelectric monomer 91.¹⁰² The monomer was poled and subsequently cross-linked by *in-situ* photopolymerization. The cross-linked pyroelectric polymer exhibited an electro-optical coefficient of 15 - 35 pm/V.

1.4. Summary

This Chapter covers some of the salient aspects of NLO materials and their properties. However, we have not covered the entire spectrum of compounds synthesized for nonlinear optics. Excellent reviews and texts¹⁰³⁻¹⁰⁴ are available in

the literature on organic,¹⁰⁵⁻¹¹⁰ organometallic,⁹ polymeric,^{111, 112} and liquid crystalline materials.¹¹³⁻¹¹⁶

1.5. References

1. Franken, P. A.; Hill, A. E.; Peters, C. W.; Weinrich, G. *Phys. Rev. Lett.* **1961**, *7*, 118.
2. *Nonlinear Optics*, Ed. Boyd, R. W. Academic Press, New York, **1992**.
3. *The Principles of Nonlinear Optics*, Ed. Shen, Y. R. Wiley, New York, **1984**.
4. *Nonlinear Optics*, Ed. Bloembergen, N. W. A. Benjamin, New York, **1965**.
5. Bredas, J. L.; Adant, C.; Tackx, P.; Persoons, A. *Chem. Rev.* **1994**, *94*, 243.
6. *Quantum Electronics*, Ed. Yariv, A. Wiley, New York, **1975**, p419.
7. Williams, D. J. *Angew. Chem. Int. Ed. Engl.* **1984**, *23*, 690.
8. *An Introduction to Electrooptic Devices*, Ed. Kaminow, I. Academic Press, New York, **1974**, p56.
9. Long, N. J. *Angew. Chem. Int. Ed. Engl.* **1995**, *34*, 21.
10. Reintes, J. F. in *Laser Handbook*, Eds. Bass, M.; Stitch, M. I. North Holland, Amsterdam, **1985**.
11. Chen, C.; Wu, B.; Jiang, A.; You, G. *Sci. Sin. B.* **1985**, *28*, 235.
12. Williams, D. J. *Thin Solid Films* **1992**, *216*, 117.
13. Eaton, D. F.; Meredith, G. R.; Miller, J. S. *Adv. Mater. (Weinheim Fed. Repub. Ger.)* **1992**, *4*, 45.
14. *Introduction to Nonlinear Optical Effects in Molecules and Polymers*, Eds. Prasad, P. N.; Williams, D. J. Wiley, New York, **1991**.
15. Eaton, D. F. *Science* **1991**, *253*, 281.

16. Williams, D. J. Ed. *Proc. SPIE-Int. Soc. Opt. Engl.* **1992**, 1775 (*Nonlinear Optical Properties of Organic Molecules V*).
17. *Conjugated Polymers: The Novel Science and Technology of Highly Conducting and Nonlinear Optically Active Materials*, Eds. Bredas, J. L.; Silbey, R. J. Kluwer, Dordrecht, Neth. **1991**.
18. Heilmeyer, G. H.; Ockman, N.; Braunstein, R.; Kramer, D. A. *Appl. Phys. Lett.* **1964**, *5*, 229.
19. Orlov, R. V. *Sov. Phys.-Crystallogr. (Engl. Trans.)* **1966**, *11*, 410.
20. Jerphagnon, J. *IEEE J. Quantum Electron.* **1971**, *QE-7*, 42.
21. Southgate, P. D.; Hall, D. S. *Appl. Phys. Lett.* **1971**, *18*, 456.
22. Southgate, P. D.; Hall, D. S. *J. Appl. Phys.* **1972**, *43*, 2765.
23. Kato, K. *IEEE J. Quantum Electron.* **1980**, *QE-16*, 1288.
24. Shigorin, V. D.; Shipulo, G. P.; Grazhulene, S. S.; Musikhin, L. A.; Shekhtman, V. Sh. *Sov. J. Quantum Electron. (Engl. Trans.)* **1976**, *5*, 1393.
25. Kurtz, S. K.; Perry, T. T. *J. Appl. Phys.* **1968**, *39*, 3798.
26. Le Fevre, R. J. W. *Rev. Pure Appl. Chem.* **1970**, *20*, 67.
27. Asato, A. E.; Liu, R. S. H.; Rao, V. P.; Cai, Y. M. *Tetrahedron Lett.* **1996**, *37*, 419.
28. Herndo, W. C. *J. Phys. Chem.* **1981**, *85*, 3040. The resonance energy of azulene is 33 kcal/mol. The azulenylium carbocation is estimated to be ~10 kcal/mol more stable than azulene itself.
29. Drost, K. J.; Jen, A. K.-Y.; Rao, V. P. *Chemtech.* **1995**, *25*, 16 and references cited therein.
30. Morley, J. O. *J. Chem. Soc. Faraday Trans.* **1991**, *87*, 3009.
31. Marder, S. R.; Gorman, C. B.; Tiemann, B. G.; Cheng, L.-T. *J. Am. Chem. Soc.* **1993**, *115*, 3006.
32. Levine, B. F. *Chem. Phys. Lett.* **1976**, *37*, 516.

33. Oudar, J. L.; Chemla, D. S. *J. Chem. Phys.* **1977**, *66*, 2664.
34. Oudar, J. L. *J. Chem. Phys.* **1977**, *67*, 446.
35. Davies, P. L. *Trans. Faraday Soc.* **1952**, *48*, 789.
36. Oudar, J. L.; Chemla, D. S. *Opt. Commun.* **1975**, *13*, 164.
37. Rustagi, K. C.; Ducuing, J. *Opt. Commun.* **1974**, *10*, 258.
38. Chou, S.-S. P.; Sun, D.-J.; Haang, J.-Y.; Yang, P.-K.; Lin, H.-C. *Tetrahedron Lett.* **1996**, *37*, 7279.
39. Ulman, A.; Willand, C. S.; Kohler, W.; Robello, D. R.; Williams, D. J.; Handley, L. in *Nonlinear Optical Properties of Organic Molecules and Crystals*, Eds. Chemla, D. S.; Zyss, J. Academic Press, New York, **1987**, Vol. 1, 170.
40. Twieg, R. J.; Jain, K. in *Nonlinear Optical Properties of Organic and Polymeric Materials*, Ed. Williams, D. J. ACS Symposium Series, Vol. 233, Washington, DC, **1983**.
41. Rao, V. P.; Cai, Y. M.; Jen, A. K.-Y. *J. Chem. Soc. Chem. Commun.* **1994**, 1689.
42. Ikeda, H.; Kawabe, Y.; Sakai, T.; Kawasaki, K. *Chem. Lett.* **1989**, 1803.
43. Lequan, M.; Lequan, R. M.; Ching, K. C.; Barzoukas, M.; Fort, A.; Bravic, G.; Chasseau, D.; Barrans, Y.; Huche, M. *Chem. Phys. Lett.* **1993**, *213*, 71.
44. Kawamata, J.; Inoue, K. *Chem. Lett.* **1993**, 921.
45. Ulman, A.; Willand, C. S.; Kohler, W.; Robello, D. R.; Williams, D. J.; Handley, L. in *Materials for Nonlinear Optics: Chemical Perspectives*, Eds. Marder, S. R.; Sohn, J. E.; Stucky, G. D. ACS Symp. Ser. **1991**, Chapter 10.
46. Lyong Sun Pu *J. Chem. Soc. Chem. Commun.* **1991**, 429.
47. Levine, B. F.; Betha, C. G.; Thurmond, C. D.; Lynch, R. T.; Bernstein, J. L. *J. Appl. Phys.* **1979**, *50*, 2523.

48. Kohler, W.; Robello, D. R.; Dao, P. T.; Willand, C. S.; Williams, D. J. *J. Chem. Phys.* **1990**, *93*, 9157.
49. Kohler, W.; Robello, D. R.; Willand, C. S.; Williams, D. J. *Macromolecules*, **1991**, *24*, 4589.
50. Man, H. T.; Yoon, H. N. *Adv. Mater.* **1992**, *4*, 159.
51. Meredith, G. R.; Vandusen, J. G.; Williams, D. J. in *Nonlinear Optical Properties of Organic Molecules and Crystals*, Eds. Chemla, D. S.; Zyss, J. Academic Press, New York, **1987**, Vol.1, 109.
52. Lehn, J. M. *Angew. Chem. Int. Ed. Engl.* **1988**, *27*, 89.
53. Lehn, J. M. *Angew. Chem. Int. Ed. Engl.* **1990**, *29*, 1304.
54. Lehn, J. M. in *Nonlinear Optical Properties of Organic Molecules and Crystals*, Eds. Chemla, D. S.; Zyss, J. Academic Press, New York, **1987**, Vol.1, 215.
55. Rieckhoff, K.; Peticolas, W. F. *Science*, **1965**, *147*, 611.
56. Nicoud, J. F.; Twieg, R. J. in *Nonlinear Optical Properties of Organic Molecules and Crystals*, Eds. Chemla, D. S.; Zyss, J. Academic Press, New York, **1987**, Vol.1, 227.
57. Zyss, J.; Nicoud, J. F.; Coquilloy, M. *J. Chem. Phys.* **1984**, *81*, 4160.
58. Chen, C.-T.; Marder, S. R.; Chen, L.-T. *J. Am. Chem. Soc.* **1994**, *116*, 3117.
59. Schneider, R.; Hosseini, M. W.; Planeix, J.-M. *Tetrahedron Lett.* **1996**, *37*, 4721.
60. Nicoud, J. F. *Mol. Cryst. Liq. Cryst. Inc. Nonlin. Opt.* **1988**, *156*, 257.
61. Pan, F.; Wong, M. S.; Gramlich, V.; Bosshard, C.; Gunter, P. *J. Chem. Soc. Chem. Commun.* **1996**, 1557.
62. Green, M. L. H.; Marder, S. R.; Thompson, M. E.; Bandy, J. A.; Bloor, D.; Kolinsky, P. V.; Jones, R. J. *Nature*, **1987**, *330*, 360.

63. Frazier, C. C.; Harvey, M. A.; Cockerham, M. P.; Hand, H. M.; Chauchard, E. A.; Lee, C. H. *J. Phys. Chem.* **1986**, *90*, 5703.
64. Coe, B. J.; Jones, C. J.; McCleverty, J. A.; Bloor, D.; Kolinsky, P. V.; Jones, R. J. *J. Chem. Soc. Chem. Commun.* **1989**, 1485.
65. Tam, W.; Calabrese, J. C. *Chem. Phys. Lett.* **1988**, *144*, 79.
66. Mignani, G.; Barzoukas, M.; Zyss, J.; Soula, G.; Balegroune, F.; Grandjean, D.; Josse, D. *Organometallics* **1991**, *10*, 3660.
67. Marder, S. R.; Perry, J. W.; Tiemann, B. G.; Schaefer, W. P. *Organometallics* **1991**, *10*, 1896.
68. Dhenaut, C.; Ledoux, I.; Samuel, I. D. W.; Zyss, J.; Bourgault, M.; Bozec, H. L. *Nature*, **1995**, *374*, 339.
69. Barzoukas, M.; Blanchard, D.-M.; Josse, D.; Lehn, J.-M.; Zyss, J. *J. Chem. Phys.* **1989**, *133*, 323.
70. Blanchard, D.-M.; Lehn, J.-M.; Barzoukas, M.; Ledoux, I.; Zyss, J. *J. Chem. Phys.* **1994**, *181*, 281.
71. Sundararajan, G. *Proc. of the Fourth NOST Confer.* **1995**, 89.
72. US Patent No. 4365283, **1982**.
73. Singer, K. D.; Sohn, J. E.; Lalama, S. J. *Appl. Phys. Lett.* **1986**, *49*, 248.
74. Rondou, P.; Beylen, M. V.; Samyn, C.; Sheeren, G.; Peersoons, A. *Makromol. Chem.* **1992**, *193*, 3045.
75. de Martino, R. M.; Yoon, H. N.; US Patent No. 4808332.
76. Fuso, F.; Padias, A. B.; Hall, H. K. Jr. *Macromolecules* **1991**, *24*, 1710.
77. Mitchell, M. A.; Tomida, M.; Padias, A. B.; Hall, H. K. Jr. *Chem. Mater.* **1993**, *5*, 1044.
78. Zhang, Y.; Wang, L.; Wada, T.; Sasabe, H. *Macromolecules* **1996**, *29*, 1569.
79. Zadadzinski, J. A.; Viswanathan, R.; Madsen, L.; Garnæs, J.; Schwartz, D. K. *Science*, **1994**, *263*, 1726.

80. Kalita, N.; Cresswell, J. P.; Petty, M. C.; McRoberts, A.; Lacey, D.; Gray, G.; Goodwin, M. J.; Carr, N. *Opt. Mater.* **1992**, *1*, 259.
81. Wijekoon, W. M. K. P.; Wijaya, S. K.; Bhawalkar, J. D.; Prasad, P. N.; Penner, T. L.; Armstrong, N. J.; Ezenyilimba, M. C.; Williams, D. J. *J. Am. Chem. Soc.* **1996**, *118*, 4480.
82. Ashwell, G. J.; Jefferies, G.; Hamilton, D. G.; Lynch, D. E.; Roberts, M. P. S.; Bahra, G. S.; Brown, C. R. *Nature*, **1995**, *375*, 385.
83. Lin, W.; Yitzchaik, S.; Malik, A.; Durbin, M. K.; Richter, A. G.; Wong, G. K.; Dutta, P.; Marks, T. J. *Angew. Chem. Int. Ed. Engl.* **1995**, *34*, 1497.
84. Netzer, L.; Iscovici, R.; Sagiv, J. *Thin Solid Films* **1983**, *99*, 235.
85. Pomerantz, M.; Segmuller, A.; Netzer, L.; Sagiv, J. *Thin Solid Films* **1985**, *132*, 153.
86. Tillman, N.; Ulman, A.; Penner, T. L. *Langmuir*, **1989**, *5*, 101.
87. Ulman, A. *Adv. Mater.* **1990**, *2*, 573, and references therein.
88. Penner, T. -L.; Motschmann, H. R.; Armstrong, N. J.; Ezenyilimba, M. C.; Williams, D. J. *Nature*, **1993**, *367*, 49.
89. Williams D. J.; Penner, T. -L.; Schildkraut, J. S.; Tillman, N.; Ulman, A. *Adv. Mater.* **1993**, *5*, 195.
90. *Supramolecular chemistry. Concepts and Perspectives.* Lehn, J.-M. VCH, Verlagsgesellschaft, Germany, **1995**, Chapter 9.
91. Brienne, M.-J.; Gabard, J.; Lehn, J.-M.; Stibor, I. *J. Chem. Soc. Chem. Commun.* **1989**, 1868.
92. Fouquey, C.; Lehn, J.-M.; Levelut, A.-M. *Adv. Mater.* **1990**, *2*, 254.
93. Lehn, J.-M.; Mascal, M.; De Cian, A.; Fischer, J. *J. Chem. Soc. Chem. Commun.* **1990**, 479.
94. Ikeda, T.; Tsutsumi, O. *Science*, **1995**, *268*, 1873.
95. Arakelian, S. M.; Grigorian, G. L.; Nersisyan, S. Ts.; Nshayan, M. A.; Chilingaryan, Yu. S. *Sov. Phys. JETP Lett.* **1978**, *28*, 186.

96. Fouquey, C.; Lehn, J.-M.; Malthete, J. *J. Chem. Soc. Chem. Commun.* **1987**, 1424.
97. Kauranen, M.; Verbiest, T.; Boutton, C.; Teerenstra, M. N.; Clays, K.; Schouten, A. J.; Nolte, R. J. M.; Persoons, A. *Science*, **1995**, *270*, 966.
98. O'Konski, C. T.; Yoshioka, W. H.; Orttung, J. *J. Phys. Chem.* **1959**, *63*, 1558.
99. Walba, D. M.; Ros, M. B.; Clark, N. A.; Shao, R.; Johnson, K. M.; Robinson, M. G.; Liu, J. Y.; Doroski, D. *Mol. Cryst. Liq. Cryst.* **1991**, *198*, 51.
100. Liu, J. Y.; Robinson, M. G.; Johnson, K. M.; Walba, D. M.; Ros, M. B.; Clark, N. A.; Shao, R.; Doroski, D. *J. Appl. Phys.* **1991**, *70*, 3426.
101. Schmitt, K.; Herr, R. -P.; Schadt, M.; Funfschilling, J.; Buchecker, R.; Chen, X. H.; Benecke, C. *Liq. Cryst.* **1993**, *14*, 1735.
102. Trollsas, M.; Orrenius, C.; Sahlen, F.; Gedde, U. W.; Norin, T.; Hult, A.; Hermann, D.; Rudquist, P.; Komitov, L.; Lagerwall, S. T.; Landstrom, J. *J. Am. Chem. Soc.* **1996**, *118*, 8542.
103. *Materials for Nonlinear Optics: Chemical Perspectives*, Eds. Marder, S. R.; Sohn, J. E.; Stucky, G. D. ACS Symp. Ser. **1991**.
104. *Nonlinear Optical Properties of Organic Molecules and Crystals*, Eds. Chemla, D. S.; Zyss, J. Academic Press, New York, **1987**, Vol.1 and 2.
105. *Nonlinear Optical Properties of Organic and Polymeric Materials*, Ed. Williams, D. J. ACS Symposium Series, Vol. 233, Washington, DC **1983**.
106. *Nonlinear Optical and Electroactive Polymers*, Eds. Prasad, P. N.; Ulrich, D. R. Plenum Press, New York, **1988**.
107. Kaino, T.; Tomaru, S. *Adv. Mater.* **1993**, *5*, 172.
108. Nalwa, H. S. *Adv. Mater.* **1993**, *5*, 341.
109. Nie, W. *Adv. Mater.* **1993**, *5*, 520.
110. Marder, S. R.; Perry, J. W. *Adv. Mater.* **1993**, *5*, 804.

111. Buckley, A. *Adv. Mater.* 1992, 4, 153.
112. Marks, T. J.; Ratner, M. A. *Angew. Chem. Int. Ed. Engl.* 1995, 34, 155.
113. Palffy-Muhoray, P. in *Liquid Crystals*, Ed. Bahadur, B. World Scientific, Singapore, 1991, Vol. 1, 494-545.
114. Tabiryan, N. V.; Sukhov, A. V.; Zel'dovich, B. Y. *Mol. Cryst. Liq. Cryst.* Special topic XIX, 1986, 136, 1.
115. Khoo, I. C. in *Progress in Optics*, XXVI, Ed. Wolf, E. North Holland, New York, 1988.
116. Janossy, I. in *Perspectives in Condensed Matter Physics*, Ed. Miglio, L. Kluwer Academic Publishers, 1990.

CHAPTER 2

SYNTHESIS AND STUDIES OF PHOTOPHYSICAL AND SECOND HARMONIC GENERATION PROPERTIES OF SOME BUTADIENE DERIVATIVES

2.1. Abstract

The synthesis and photophysical properties of some donor-acceptor linked butadiene derivatives 6-10 as well as two bicyclic compounds 14a, b are described. The Kurtz and Perry powder measurements of these molecules using urea as the standard indicated second harmonic generation (SHG) efficiencies of approximately 50% that of urea for compounds containing a chiral substituent whereas the other derivatives were relatively inactive. Compounds 6a, b and 10 showed dual luminescence and the anomalous red-shifted fluorescence bands observed in polar solvents for these compounds were attributed to the formation of intramolecular charge transfer (ICT) excited states. The formation of ICT excited states in these classes of compounds and the thermodynamics of these processes were also studied in solvents of varying polarity.

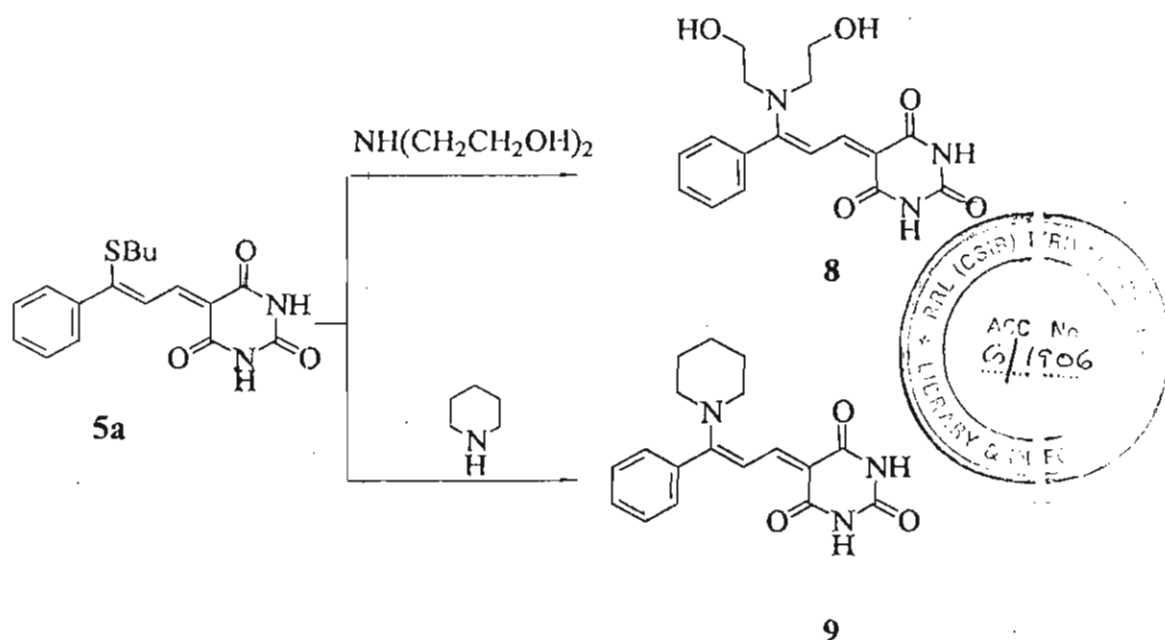
2.2. Introduction

The synthesis of new organic materials possessing nonlinear optical properties has been a subject of intense activity in recent years because of their potential applications in areas such as telecommunications, optical information processing and data storage.^{1,2} The interest in organic materials has been

primarily due to their ultrafast response times, the synthetic flexibility which permits the modification of molecular parameters required for optimizing the NLO properties as well as the ease with which these molecules can be incorporated into polymeric systems either by physical mixing or through covalent bonding.¹⁻⁴ Most studies so far have focused on donor-acceptor π -conjugated molecules which tend to possess large second-order molecular polarizability (β).⁵⁻¹¹ However, molecules possessing large β values tend to crystallize into centrosymmetric space groups, which nullify the contribution of the individual molecules. This problem can sometimes be overcome by introducing a chiral group in the molecule, which can ensure crystallization into noncentrosymmetric space-groups.^{1,12}

The second-order molecular polarizability, β is a function of the ground and excited state properties of the molecule. It is proportional to (i) the dipole moment changes between the ground and excited states and (ii) to the oscillator strength of the transition to the excited state. Molecules with large β values are therefore often characterized by strong intramolecular charge transfer (ICT) transitions, which are highly solvatochromic.^{5,6} This Chapter describes the synthesis and photophysical studies of some donor-acceptor linked butadiene derivatives, **6-10** and two bicyclic compounds, **14a, b**. The electron donor in some of these systems is L-(-)pyrrolidine-2-methanol (L-prolinol), which also ensures crystallization of the molecules into noncentrosymmetric space groups. Reaction of 4,4-bismethylthio-1,1-dicyano-2-aryl-1,3-butadienes (**13a-c**) with L-prolinol gives rearranged products, **15a-c**, in addition to the normal bicyclic products (**14a-c**) (Scheme 2.4).

butanethiol to the starting acetophenones **1a,b** and subsequent Vilsmeier formylation leads to the formation of **3a,b**.¹³ Aldol type condensation of **3a** and **3b** with indane-1,3-dione or barbituric acid gives the corresponding butylthio-substituted-dienones **4a,b** and **5a,b**. Substitution of the butylthio group of **4** and **5** by amines leads to compounds **6-9**. Compounds **4-9** were characterized on the basis of analytical results and spectral data.



Scheme 2. 2

The ^{13}C NMR spectra of compounds **6a, b** and **7a, b** show twin peaks for some of the carbon atoms (for example Figure 2.1a). This may be attributed to the presence of two isomeric forms due to restricted rotation around the N-C bond (involving prolinol), resulting from the delocalization of the nitrogen lone pair. The ^{13}C NMR spectrum of **6a** in CDCl_3 containing trifluoroacetic acid (TFA) indicated that only a single isomer was present (Figure 2.1b). Some of the twin

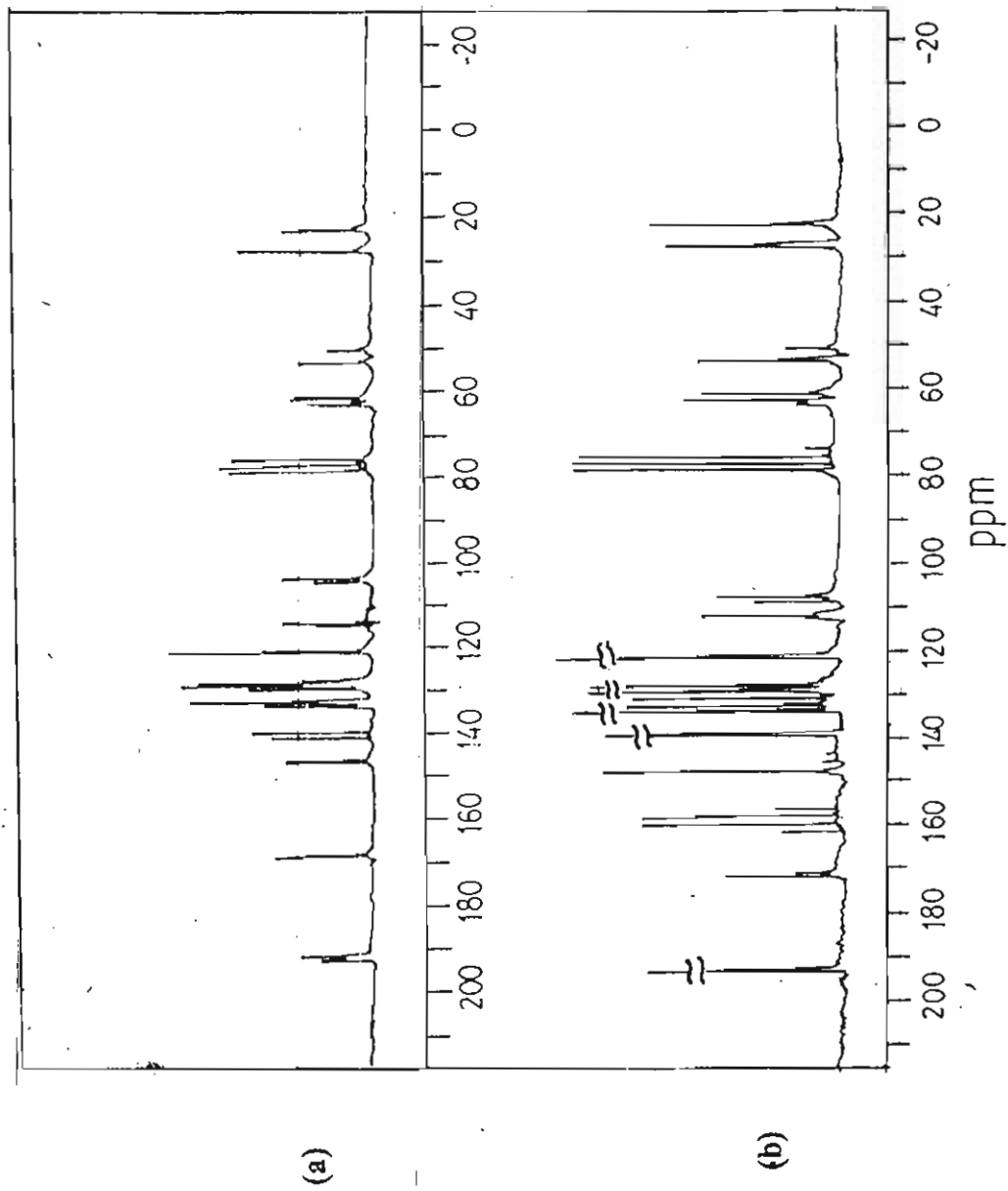
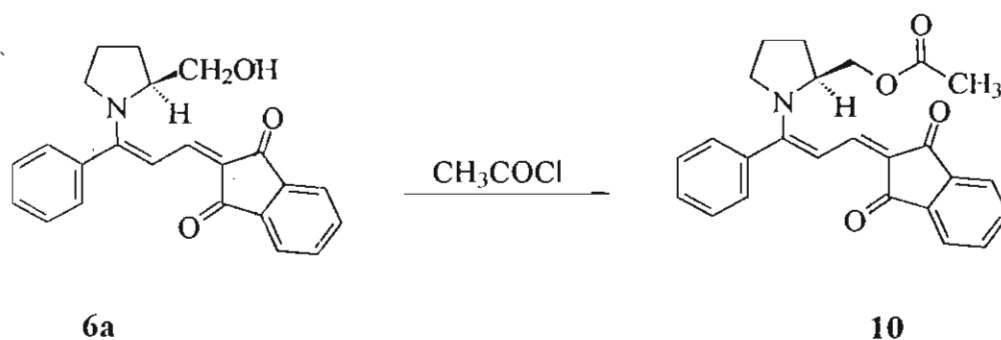


Figure 2.1. (a) ^{13}C NMR spectrum of 6a in CDCl_3 and (b) in CDCl_3 containing trifluoroacetic acid.



peaks appearing in the ^{13}C NMR of **6a** at δ 22.43, 22.97; 60.86, 61.61; 62.65, 63.04; 114.32, 114.80; 167.88, 168.36; 191.51, 191.72 and 191.89, 192.32 appear as single peaks in the ^{13}C NMR of **6a** on addition of trifluoro acetic acid (δ 22.61, 61.10, 62.29, 112.06, 171.64 and 193.09 respectively). Protonation of nitrogen would prevent delocalization of the nitrogen lone pair resulting in the formation of a single isomer, due to free rotation around the C-N bond. The ^{13}C NMR spectrum of the acylated form of **6a** (**10**, Scheme 2. 3) also showed twin peaks for some of the carbon atoms, thus ruling out the role of intramolecular hydrogen bonding in the formation of the isomers. It may be noted that these compounds can also exist in the E and Z isomeric forms.



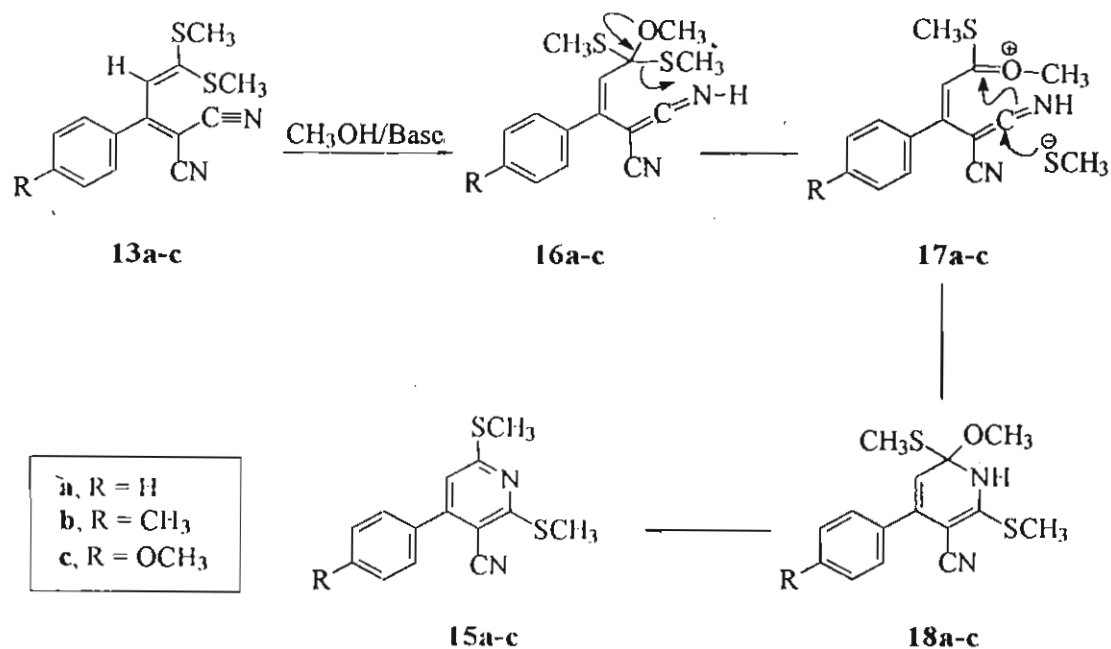
Scheme 2. 3

Two solid crystalline forms of the compound **6a** possessing different melting points could be separated by crystallizing them from different solvents. Crystallization from a mixture (1:1) of DMSO and water gave yellow needles (mp 219-220 $^{\circ}\text{C}$), while crystallization from benzene provided a red solid (mp 181-182 $^{\circ}\text{C}$). However, mixtures of both solids were obtained when other solvents such as ethanol and acetonitrile were used. In solutions, the two

isomeric forms exist in equilibrium and have identical IR, NMR, and UV spectra. Solid state reflectance spectra of the yellow and red isomers showed cut-off wavelengths at 550 nm and 590 nm respectively. It has been found that the red solid that was obtained from benzene could be converted to the yellow form by recrystallization from a mixture of DMSO-water. Similarly, the yellow form could be converted to the red form by recrystallizing it from benzene. However, the other compounds in the series **6b**, **7a** and **7b** were crystallized in a single form, in each case.

2.3.2. Synthesis of Bicyclic Compounds

Bicyclic compounds (**14a-c**) were synthesized as per Scheme 2.4. Knoevenagel condensation of substituted acetophenones with dicyanomethane leads to the formation of dicyano adducts, **12a-c**.¹⁴ Ketene dithioacetals **13a-c** were synthesized from **12a-c** by adopting a known procedure using potassium fluoride adsorbed on alumina as catalyst for the derivatization of compounds containing an active methylene group.¹⁵ Reaction of these 3-aryl-2-cyano-5,5-bis(methylthio)penta-2,4-dienedinitriles with (L)(-)-2-hydroxymethylpyrrolidine gave two types of products, the expected products **14a-c** and the pyridine derivative **15a-c**. It was observed that compounds **13a-c** undergo an intramolecular rearrangement (Scheme 2.5) to give the pyridine derivatives **15a-c**, respectively, when refluxed in dry methanol in presence of catalytic amounts of a base such as pyridine, secondary amines or potassium carbonate.¹⁶



Scheme 2.5

crystallized from a mixture (2:1) of chloroform and hexane. Molecular structure of **14a** incorporates a diene dinitrile skeleton attached to a pyrrolo-oxazolic unit at one end and a phenyl substituent at the C-2 carbon. The space group of the resulting tetragonal crystals was found to be $P4_32_12$, with unit cell dimensions $a = 9.877 \text{ \AA}$, $b = 9.877 \text{ \AA}$, $c = 35.36 \text{ \AA}$, and angle β was found to be 90° . The projection view of **14a** is shown in Figure 2.2.

Colourless rectangular crystals of **15c** obtained by slow crystallization from a mixture (1:4) of ethyl acetate and hexane was found to be monoclinic. The space group present in **15c** was $P2_1/c$ with unit cell dimensions $a = 10.598 \text{ \AA}$, $b = 7.575 \text{ \AA}$, $c = 19.053 \text{ \AA}$ and angle $\beta = 103.03^\circ$. The projection view of **15c** is shown in Figure 2.3.

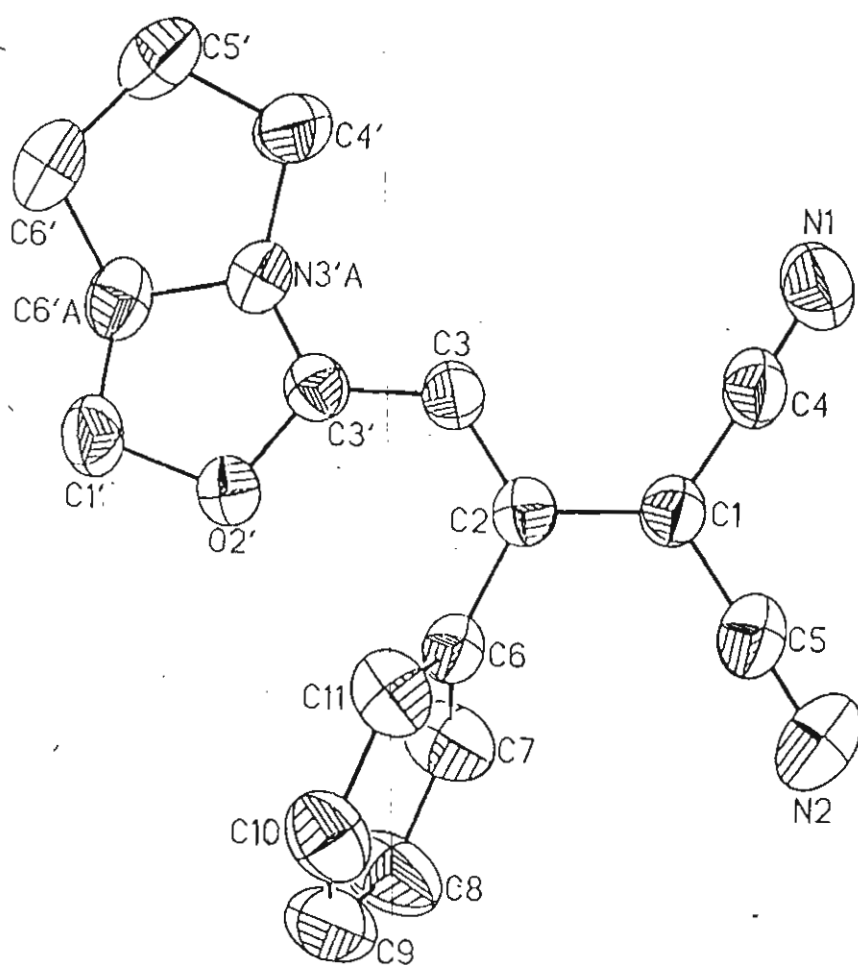


**Figure 2.2. Projection view drawing of the structure of 14a.
The thermal ellipsoids are drawn at 50 % probability**

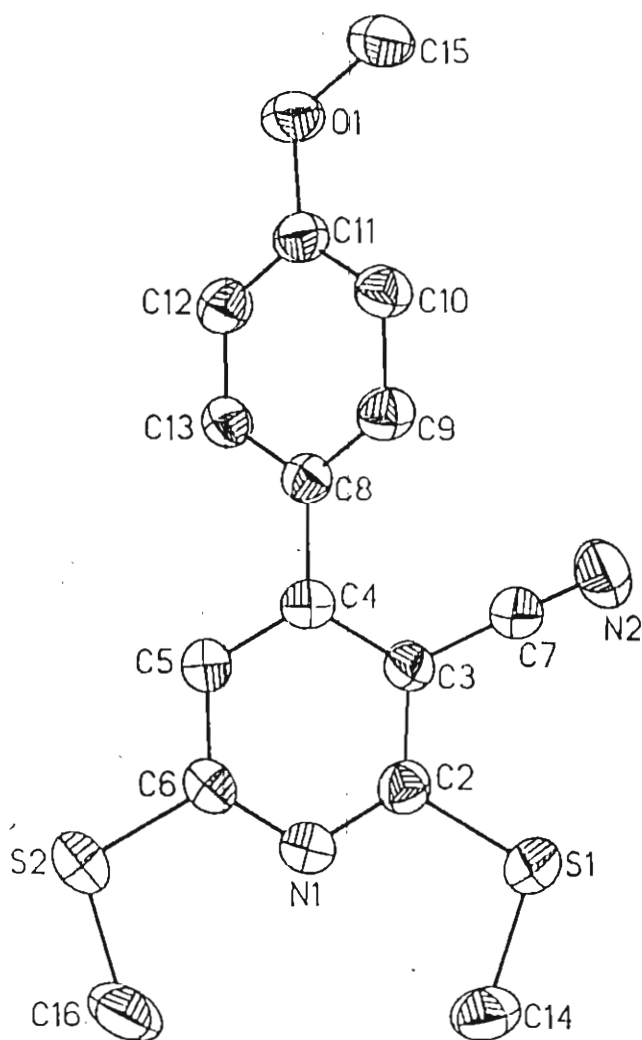


**Figure 2.3. Projection view drawing of the structure of 15c.
The thermal ellipsoids are drawn at 50 % probability**

3.3. Absorption and Emission Spectra

The absorption spectra of these compounds in acetonitrile are shown in figures 2.4-2.6. These spectra show fairly sharp absorption bands with maxima round 450 nm for 6a,b and 10 and around 420 nm for the other compounds. The bicyclic compounds 14a and 14c have absorption maxima around 385 nm. The absorption maxima of these compounds in a variety of solvents are shown in Table 2.1. It is evident from this Table that the absorption spectra of these compounds are not very sensitive to the polarity of the solvent.

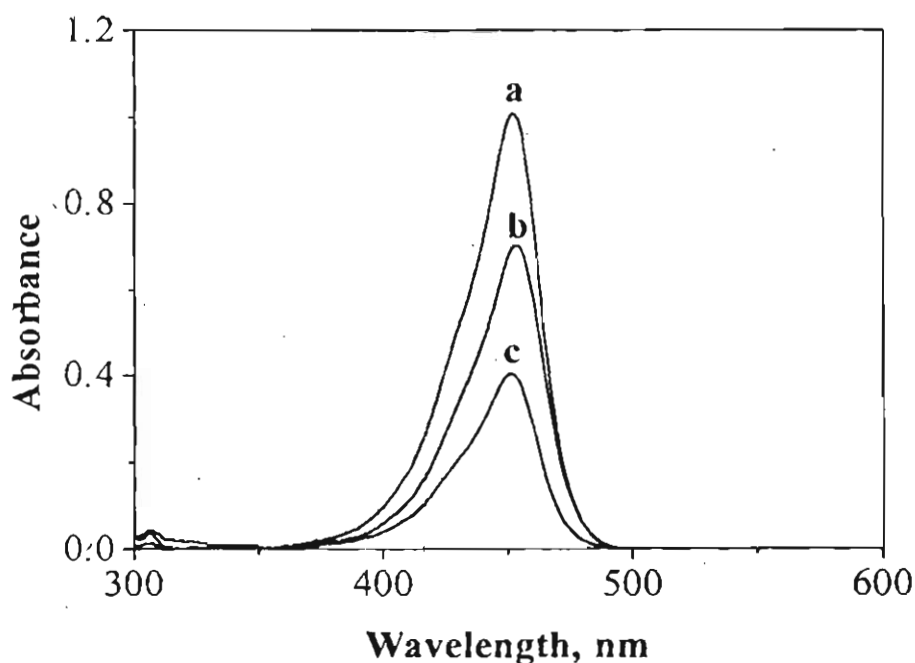


Figure 2.4. Absorption spectra of (a) 6a (6.8×10^{-5} M), (b) 6b (5.0×10^{-6} M), and (c) 10 (9.8×10^{-6} M) in acetonitrile.

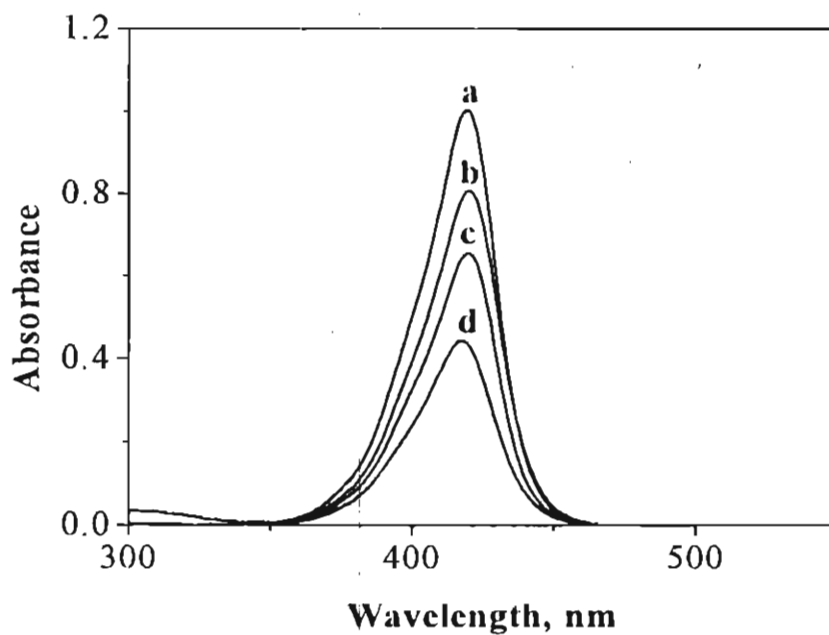


Figure 2.5. Absorption spectra of (a) 7a (1.7×10^{-5} M), (b) 7b (1.2×10^{-5} M), (c) 8 (8.0×10^{-6} M), and (d) 9 (9.0×10^{-6} M) in acetonitrile

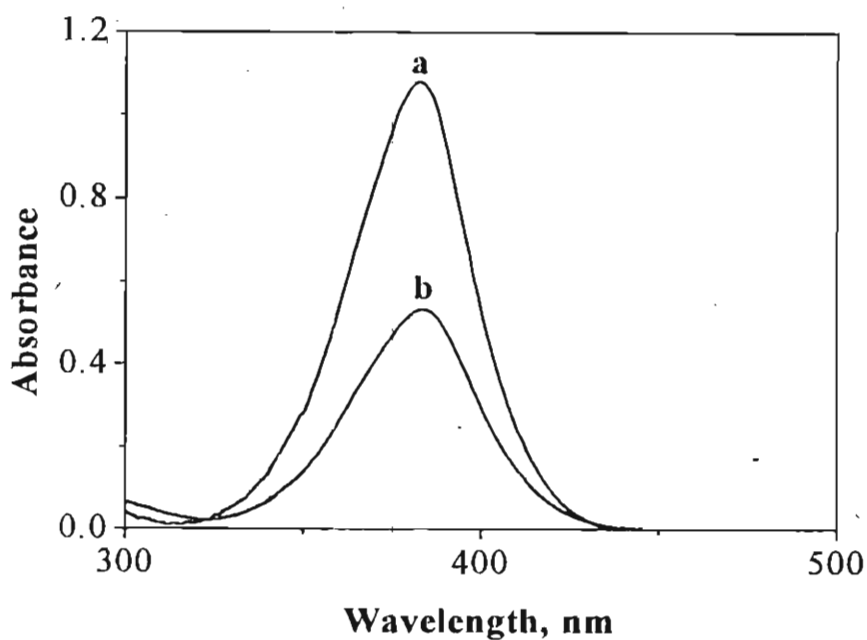


Figure 2.6. Absorption spectra of (a) 14a (1.8×10^{-5} M) and (b) 14b (1.1×10^{-5} M) in acetonitrile

Table 2.1. Absorption maxima (in nm) of 6-10 and 14a, b in different solvents

Solvent	6a	6b	7a	7b	8	9	10	14a	14b
Benzene	457	459	426	427	*	425	454	385	386
Dichloro- methane	456	458	424	425	*	422	455	386	386
Chloroform	458	460	425	425	*	423	457	386	386
Ethyl acetate	454	455	422	425	421	421	453	383	383
Acetone	454	455	422	422	421	420	453	383	384
Acetonitrile	452	453	419	419	420	417	452	383	384
DMF	456	457	424	423	424	423	456	386	387
DMSO	458	459	424	425	424	424	457	387	389
Methanol	452	452	419	420	420	417	453	382	383

* compound is insoluble in these solvents

2.3.3.1. Solvent Effects on Fluorescence Spectra

Although the effect of solvent polarity on the absorption spectra of 6a,b and 10 is small, its effect on the emission spectra is striking. Figures 2.7-2.9 show the emission spectra of 6a, 6b, and 10 in solvents of varying polarity. In less polar solvents such as benzene, the emission spectra show a maximum around 498 nm and a broad tail in the longer wavelength region (curve a, Figures 2.7-2.9), in each case. With increasing solvent polarity, there is a relative increase in the emission intensity at the longer wavelengths and in highly polar solvents such as acetonitrile, dimethyl sulfoxide and methanol, two distinct emission bands are clearly visible in each case. Whereas the positions of the shorter wavelength emission band remains fairly constant with increasing solvent polarity, the longer wavelength bands

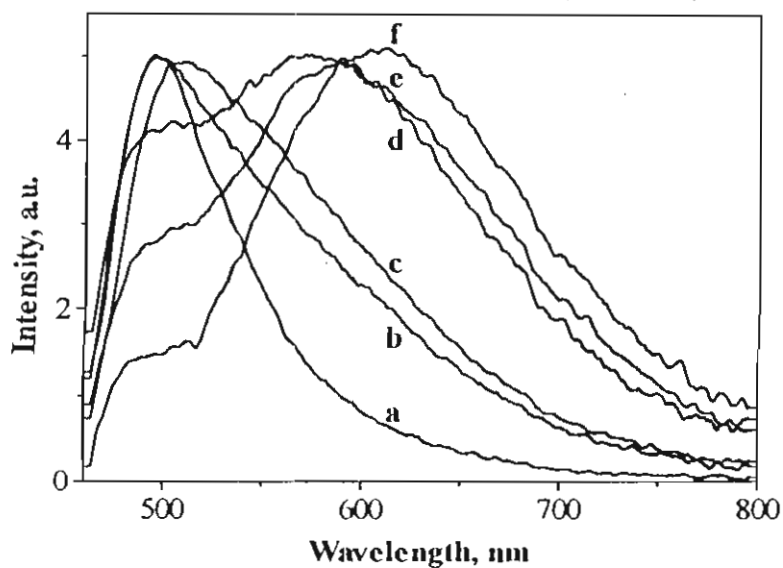


Figure 2.7. Emission spectra of 6a normalised at the λ_{max} in (a) benzene, (b) dichloromethane, (c) chloroform, (d) acetone, (e) dimethyl formamide, and (f) dimethyl sulfoxide

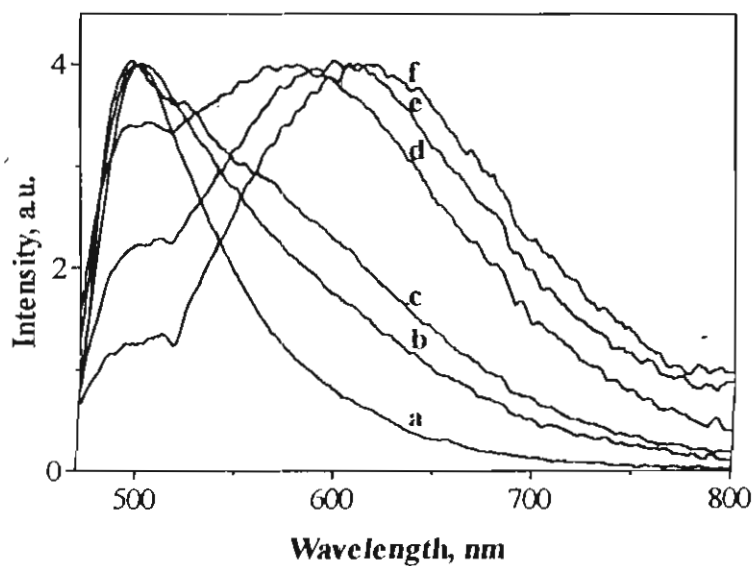


Figure 2.8. Emission spectra of 6b normalised at the λ_{max} in (a) benzene, (b) dichloromethane, (c) ethyl acetate, (d) acetone, (e) dimethyl formamide and (f) dimethyl sulfoxide

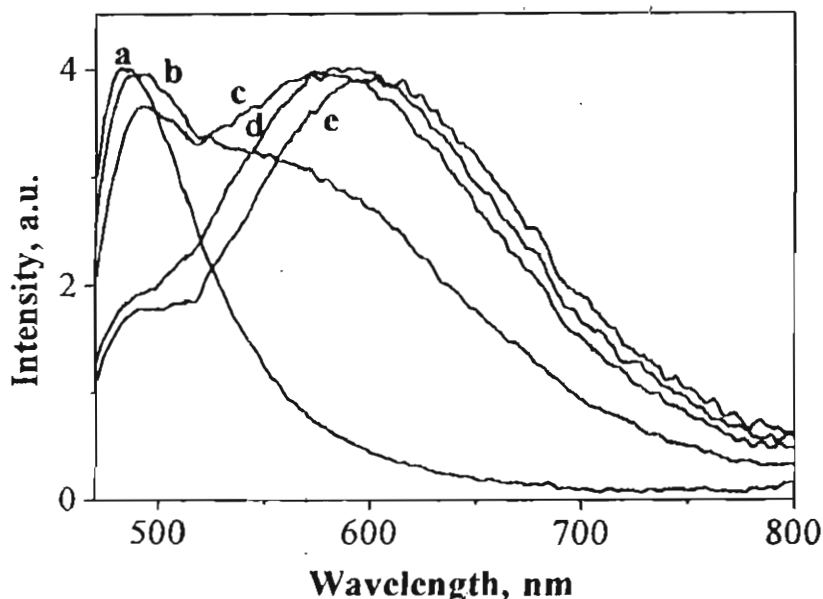


Figure 2.9. Emission spectra of 10 normalised at the λ_{\max} in (a) benzene, (b) acetone, c) acetonitrile, (d) dimethyl formamide and (f) dimethyl sulphoxide

shift to the red in each case, indicating their charge transfer character of the latter. These results are summarized in Table 2.2.

The increase in the Stokes shift with increasing solvent polarity reveals an increase in the dipole moment, on excitation. The difference of the dipole moment $\Delta\mu_{eg}$ between the excited and ground states can be calculated from the Lippert-Mataga equation,^{18,19}

$$\Delta\nu_{st} = \Delta\nu_{abs} - \Delta\nu_{em} = \frac{2\Delta\mu_{eg}^2}{hca^3} \Delta f + \text{constant} \quad 2.1$$

where, a is the radius in Å of the spherical cavity in Onsagers theory of reaction field and Δf is a solvent polarity parameter, dependent upon the solvent refractive index (n) and dielectric constant (ϵ) (equation. 2.2),

Table 2.2. Emission maxima of 6-10 (in nm) in different solvents

Solvent	6a	6b	7a	7b	8	9	10
Benzene	496	500	468	501	*	487	484
Dichloro- methane	496	500	461	460	*	460	488
Chloroform	508	511	456	466	*	471	490
Ethyl acetate	493	496	466	456	478	458	488
Acetone	495, [†] 570	501, [†] 575	451	458	448	460	490, 601 [†]
Acetonitrile	482, [†] 594	491, [†] 605	452	456	444	450	490, [†] 590
DMF	499, [†] 588	503, [†] 598	463	455	447	462	488, [†] 580
DMSO	489, [†] 610	489, [†] 615	452	455	454	460	491, [†] 603
Methanol	487, [†] 611	488, [†] 617	452	454	444	465	493, [†] 607

* compound is insoluble in these solvents

† shoulder peak

$$\Delta f = \frac{\epsilon - 1}{2\epsilon + 1} - \frac{n^2 - 1}{2n^2 + 1} \quad 2.2$$

Figure 2.10 shows the plots of Δv_{st} versus Δf for **6a** and **6b**. The observed scatter in the points may arise due to the difficulty in ascertaining the λ_{max} of the long wavelength bands in solvents where the two bands merge together.²⁰ $\Delta\mu_{cg}$ was estimated from the slope of these plots,²¹

$$\frac{\Delta v_{st}}{\Delta f} = \frac{2}{hc_0} \left(\frac{\Delta\mu_{cg}^2}{a^3} \right) \quad 2.3$$

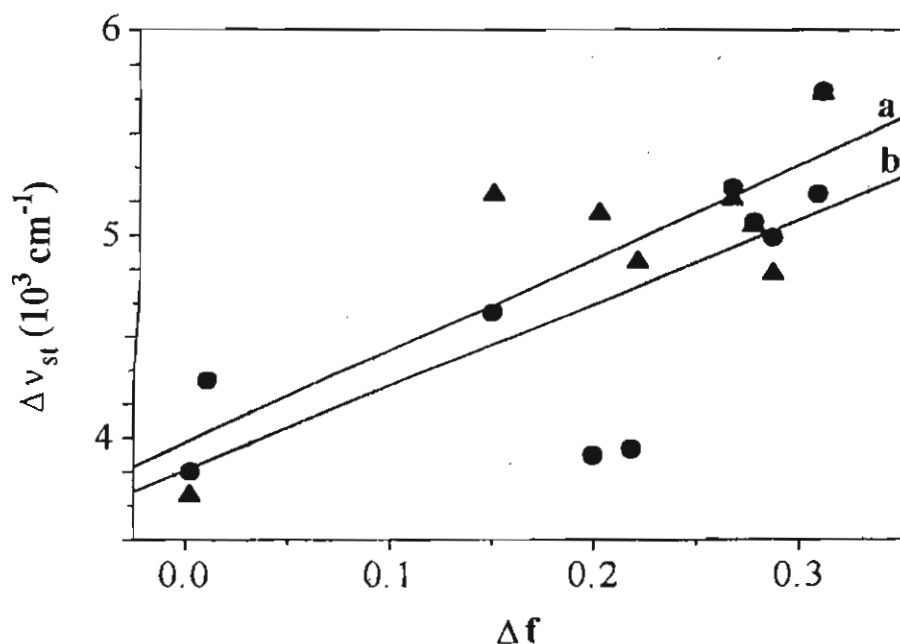


Figure 2.10. Solvatochromic plots of Stokes shift (Δv_{st}) for (a) 6a, and (b) 6b as a function of solvent polarity parameter (Δf)

$$\Delta\mu_{cg} = 0.01 \left(\frac{\Delta v_{st}}{\Delta f} \right) a^3 \quad 2.4$$

using $a = 4.8 \text{ \AA}$ and 4.9 \AA for 6a and 6b, respectively which were determined by the addition of atomic volumes.²² $\Delta\mu_{cg}$ was obtained as 7 and 6 for 6a and 6b, respectively. These values are relatively high indicating the CT nature of the long wavelength emission. In contrast to 6a,b and 10 the emission bands of 7-9 are relatively insensitive to solvent polarity (Table 2). The emission spectra of compounds 7a and 7b in different solvents are shown in Figures 2.11 and 2.12, respectively. Bicyclic compounds 14a,b did not show any fluorescence indicating efficient nonradiative decay to the ground state after excitation.

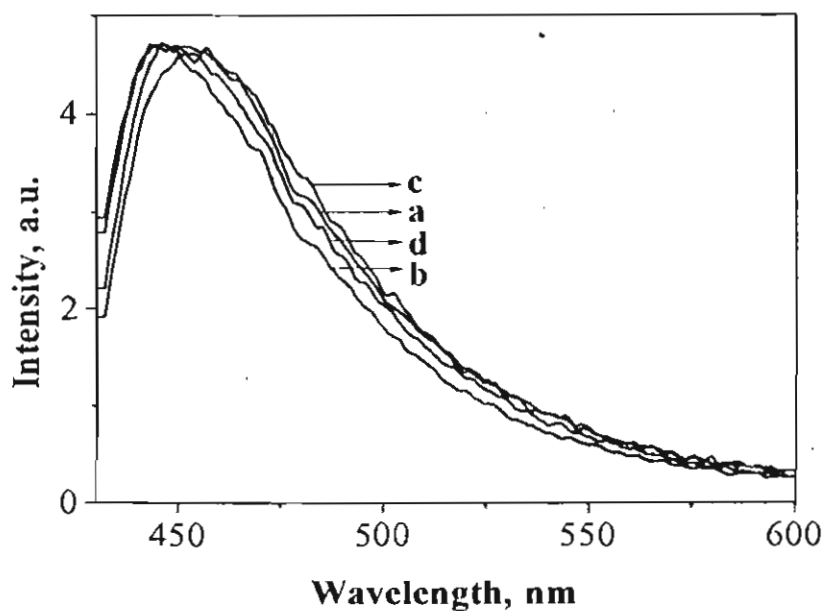


Figure 2.11. Emission spectra of 7a normalised at the λ_{\max} in (a) acetone, (b) acetonitrile, (c) dimethyl formamide, and (d) methanol

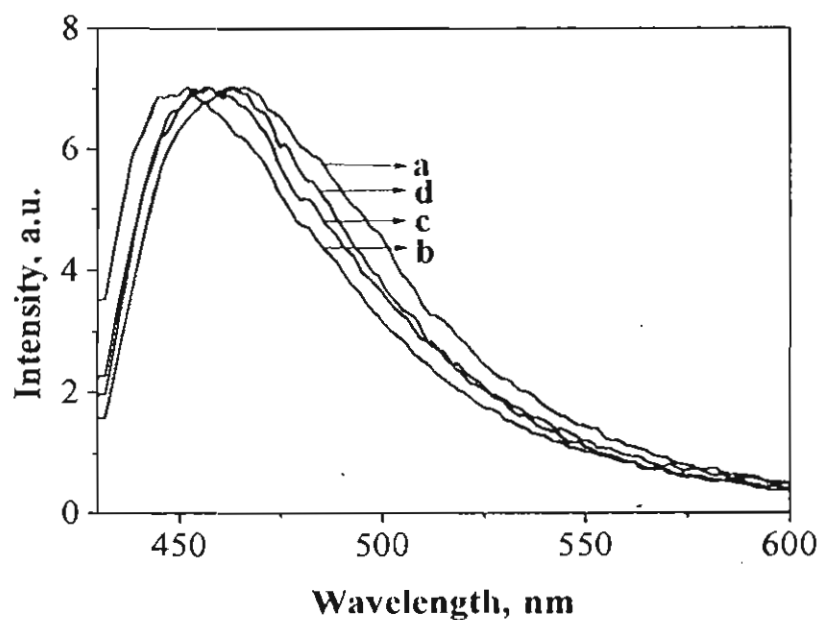
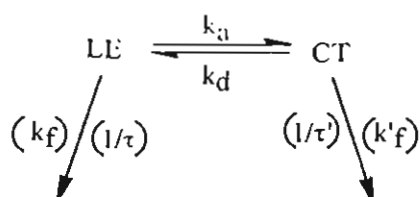


Figure 2.12. Emission spectra of 7b normalised at the λ_{\max} in (a) chloroform, (b) acetone, (c) acetonitrile, and (d) dimethyl sulphoxide

2.3.3.2. Effect of Temperature on Dual Fluorescence

The dual fluorescence of these compounds indicates the involvement of two excited states, which are close in energy. Since the short wavelength band is more pronounced in nonpolar solvents and the long wavelength band in polar solvents, these states can be attributed to the locally excited (LE) and charge transfer (CT) states as shown in Scheme 2.6.



Scheme 2.6

In this Scheme, k_a and k_d are the rate constants of the forward and backward reactions, respectively. τ (LE) and τ' (CT) are the fluorescence lifetimes. The radiative rate constants k_f (LE) and k'_f (CT) have also been indicated. The forward and backward reactions represented by Scheme 2.6 involve an orientational relaxation of the solvent molecules following the changes in the charge distribution as well as a concomitant structural relaxation by rotation of the nitrogen-containing ring.

The phenomenon of dual fluorescence was studied in detail for compound 6a. Figures 2.13-2.16 show the fluorescence spectra of 6a in DMSO, DMF, acetonitrile, acetone and toluene at different temperatures. Upon lowering the temperature, the intensity of the red-shifted CT band is strongly enhanced with respect to that of the LE band. The emission spectra can be resolved into LE and CT bands (Figure 2.17) using the emission spectrum of 6a in toluene at 40 °C as the model system, since under these conditions the CT

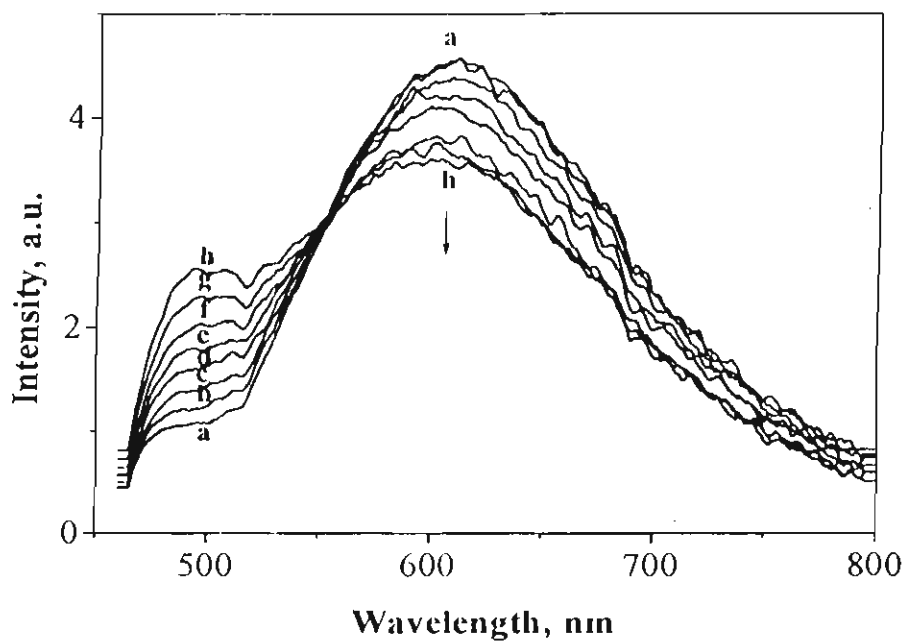


Figure 2.13. Temperature dependent emission spectra of 6a in DMSO. (a) 20 °C, (b) 25 °C, (c) 35 °C, (d) 47 °C, (e) 56 °C, (f) 67 °C, (g) 76 °C and (h) 87 °C.

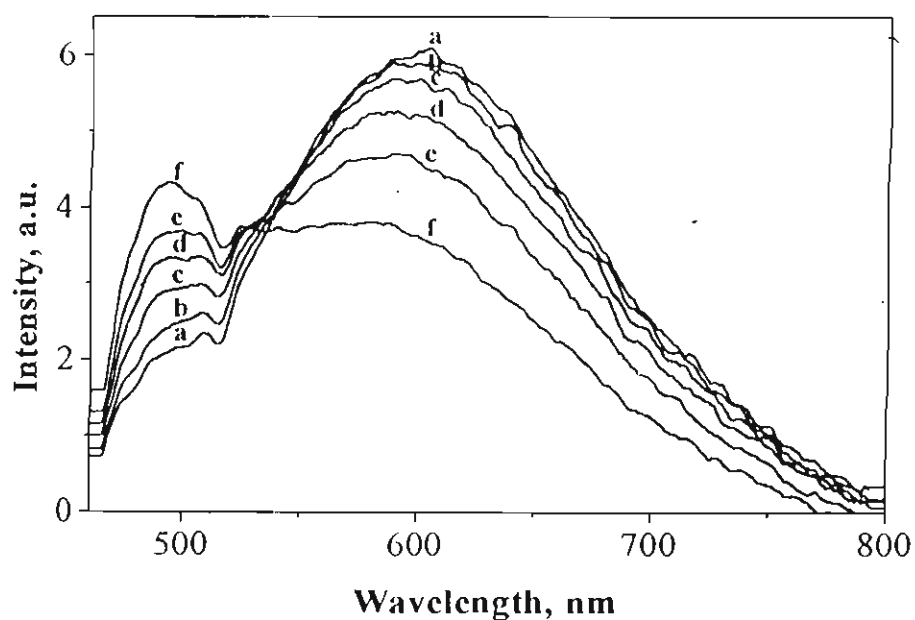


Figure 2.14. Temperature dependent emission spectra of 6a in DMF. (a) 11 °C, (b) 20 °C, (c) 30 °C, (d) 40 °C, (e) 50 °C and (f) 70 °C.

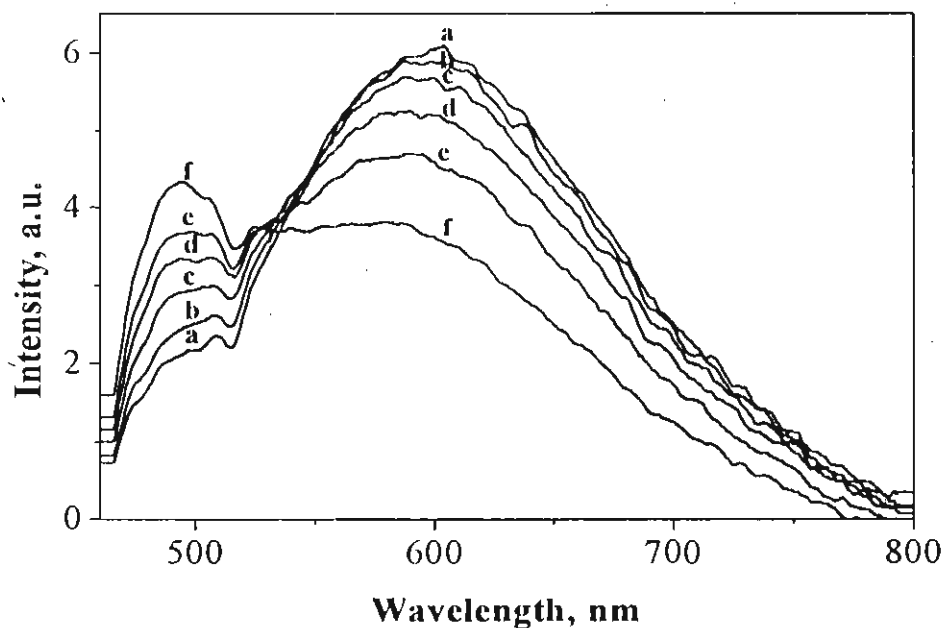


Figure 2.15. Temperature dependent emission spectra of 6a in acetonitrile. (a) 0 °C, (b) 10 °C, (c) 20 °C, (d) 30 °C and (e) 40 °C.

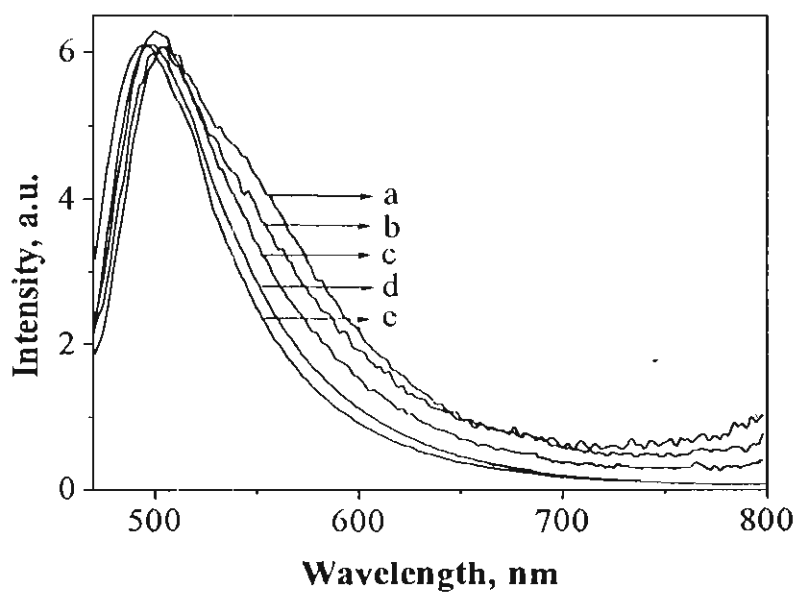


Figure 2.16. Temperature dependent emission spectra of 6a in toluene. (a) -49 °C, (b) -30 °C, (c) -10 °C, (d) 10 °C and (e) 40 °C.

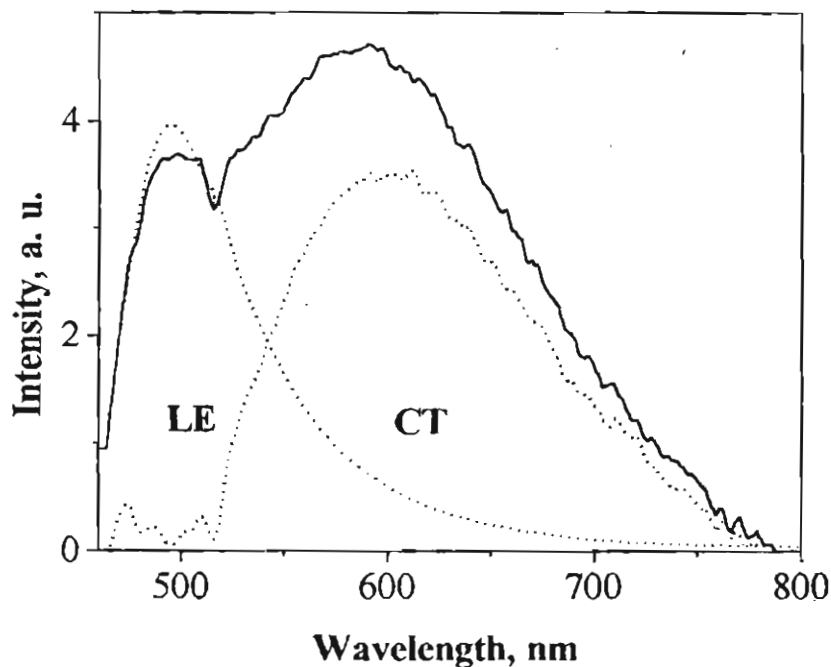


Figure 2.17. Fluorescence spectra of 6a in DMSO at 30 °C. The two emission bands, LE and CT were separated using the fluorescence spectrum of 6a in toluene at 40 °C.

band is not observed. The CT-to-LE fluorescence intensity ratio ($I(\text{CT})/I(\text{LE})$), is related to the quantum yields of fluorescence $\Phi(\text{LE})$ and $\Phi(\text{CT})$ as,²³

$$\frac{I(\text{CT})}{I(\text{LE})} = \frac{\Phi(\text{CT})}{\Phi(\text{LE})} = \frac{k'_f}{k_f} \frac{k_a}{k_d + 1/\tau'} \quad 2.5$$

The stabilization enthalpy of the CT state could be derived from the equation,

$$\ln K = -E/RT \quad 2.6$$

At higher temperatures, $k_d \gg 1/\tau'$ (Scheme 2.6). Since $k_u/k_d = K$, and k'_f/k_f and $1/\tau'$ are independent of temperature, equation 2.5 takes the form,

$$\ln \left[\frac{I(\text{CT})}{I(\text{LE})} \right] \propto \frac{-\Delta H}{RT} \quad 2.7$$

where, ΔH is the stabilization enthalpy of the CT state.

In a plot of $\ln(I(\text{CT})/I(\text{LE}))$ versus the absolute temperature (equation 2.7), a linear dependence is obtained at the high- and low-temperature limits, for which the conditions $k_d \gg 1/\tau'$ (HTL) and $k_d \ll 1/\tau'$ (LTE) hold. The slopes of these straight lines are $(E_d - E_a)/R = -\Delta H/R$ (for HTL) and $-E_a/R$ (for LTL), when k'/k_f and τ' are independent of temperature. Here E_a and E_d are the activation energies of k_a and k_d , respectively, whereas ΔH is the enthalpy change associated with the exciplex (CT) formation. Figure 2.18 represents the Arrhenius plot of $\ln(I(\text{CT})/I(\text{LE}))$ versus the reciprocal of absolute temperature for 6a in DMSO at different temperatures.

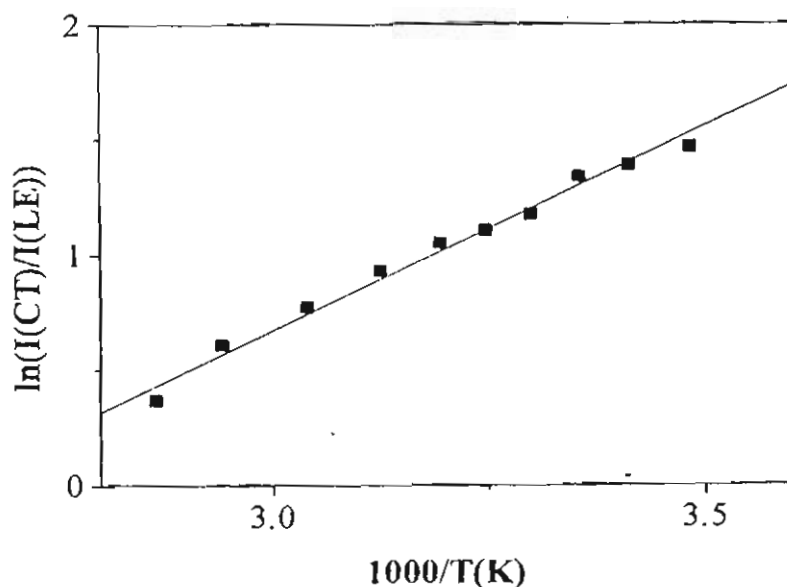


Figure 2.18. Arrhenius plot of LE-to-CT fluorescence intensity of 6a in DMSO at different temperatures.

From the pattern of this I(CT)/I(LE) plot, it would appear that compound **6a** in these solvents is in the higher temperature limit ($k_d \gg 1/\tau'$).²⁴⁻²⁶ From the slope of the Arrhenius plots ($= \Delta H/R$) the stabilization enthalpy, ΔH , the difference of the activation energies E_d and E_a could be obtained. The stabilization enthalpies of **6a** in different solvents are listed in Table 2.3.

Table 2.3. Stabilization enthalpy of 6a in different solvents

Solvent	$-\Delta H$ (kJmol ⁻¹)
Acetone	17.49
Acetonitrile	12.85
DMF	19.93
DMSO	14.68

2.3.3.3. Substitution Effects on Dual Fluorescence

In order to confirm that the dual fluorescence in **6a,b** and **10** was not due to the presence of a chiral group, achiral derivatives (**19-22**, Chart 2.1) were synthesized and the fluorescence properties were studied. Compounds **19-21** were synthesized using the procedure analogous to that outlined in Scheme 2.1. Compound **22** was synthesized by the condensation between cinnamaldehyde and indane-1,3-dione. The synthetic details are outlined in the experimental section (2.4). Among these nonchiral butadiene derivatives, compounds **19-21** exhibited dual fluorescence. Interestingly **22** was found to be nonfluorescent. Figure 2.19 shows the emission spectra of compound **19** in different solvents as a representative example. The absorption and emission maxima of these compounds in different solvents are summarized in Table 2.4. All the three

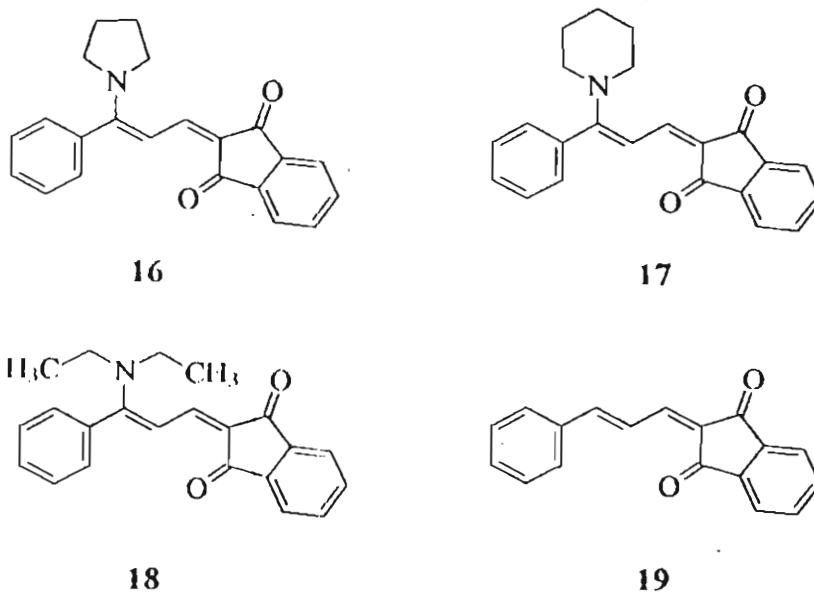


Chart 2.1

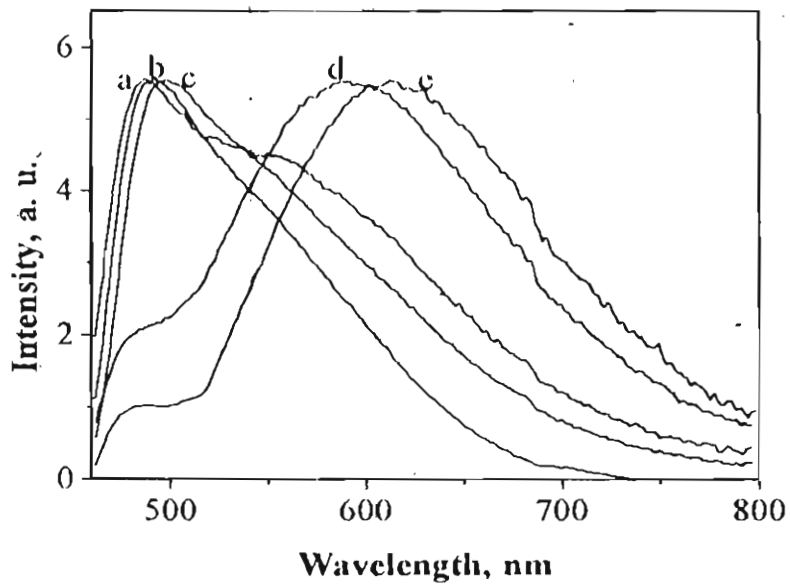


Figure 2.19. Emission spectra of 19 normalized at the maxima in (a) dichloromethane, (b) chloroform, (c) ethyl acetate, (d) acetone and (e) DMSO.

Table 2.4. Absorption and emission maxima (in nm) of 19-21 in different solvents

Solvent	19		20		21	
	Abs.	Em.	Abs.	Em.	Abs.	Em.
Benzene	455	486	456	491	454	487
Dichloro- methane	455	492	457	499	455	494
Chloroform	457	498	459	505	456	499
Ethyl acetate	453	487	453	490	451	485
Acetone	452	592	454	541	452	542
Acetonitrile	450	606	452	568	450	564
DMF	455	599	456	569	545	572
DMSO	455	613	458	581	456	582
Methanol	449	617	451	584	449	584

compounds are butadiene derivatives similar to the compounds previously discussed (6a,b), except that none of these compounds contain a chiral center or hydroxyl group capable of forming hydrogen bond with the acceptor moiety. The presence of dual fluorescence in all these compounds indicates that none of these factors are governing dual fluorescence.

The quantum yields of fluorescence of these molecules are very low. The overall quantum yield (Φ_f) decreases with increasing solvent polarity for 6a,b and 10. In non-polar solvents such as benzene, Φ_f values for 6a,b and 10 are 5.6×10^{-4} , 1.4×10^{-3} and 1.39×10^{-3} , respectively, whereas they are 1.5×10^{-4} , 2.0×10^{-4} and 1.96×10^{-4} respectively, in methanol. The quantum yields of fluorescence of 19-21 tend to increase slightly in polar solvents. For example, in benzene the quantum yields of fluorescence are 1.50×10^{-3} ,

1.15×10^{-3} , and 1.45×10^{-3} respectively, whereas in ethanol these values are 3.36×10^{-3} , 2.10×10^{-3} , and 1.52×10^{-3} respectively for compounds 19-21.

2.3.3.4. Discussion on the Mechanism of Dual Fluorescence

The discovery of the dual fluorescence of simple donor-acceptor substituted benzene derivatives such as 4-N,N-dimethylaminobenzonitrile (DMABN) by Lippert *et al.*²⁷ and the subsequent model compound studied by Grabowski *et al.*²⁸ including rigidized and pretwisted compounds gave birth to the idea of twisted intramolecular charge transfer (TICT) states (Fig. 2.20).

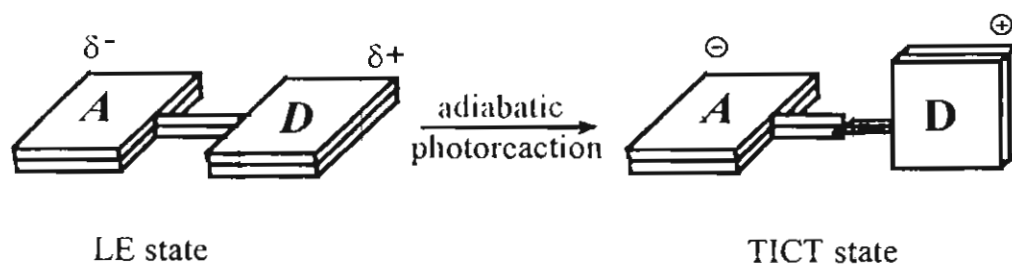


Figure 2.20. Grabowski's model of TICT formation in DMABN. LE state with near-planar conformation is the precursor for the TICT state with near-perpendicular geometry.

This model explains the dual fluorescence as occurring from two configurations of the excited state of the same molecule. The Franck-Condon excited state and a low lying TICT state with a perpendicularly twisted geometry in which the amine lone pair axis is twisted perpendicular to the phenyl group and involving charge transfer. The increasing dipole moment for increasingly twisted geometries provides the driving force for the twist towards the TICT conformation with maximum charge separation via the polar solvent induced energetic stabilization.^{27, 29-31}

Other models have also been proposed to explain the phenomenon of dual luminescence;³²⁻³⁴ however, TICT is currently the most favoured one. Since its discovery in DMABN, dual luminescence has been observed in numerous related singly bonded donor-acceptor molecules.²⁹ The results obtained for these donor-acceptor substituted butadienes can however be explained on the basis of the recently developed biradicaloid charge transfer model (BCT), in which the concept of TICT and biradicaloid states have been merged to understand the twisted single and double bonds within the same frame-work.²⁹⁻³³ This theory has been successfully applied to explain the photophysical properties of several stilbene dyes.³⁴ In such systems, the excited state can undergo a twist across one of the single bonds adjacent to the double bonds, leading to the TICT state. Alternatively, twisting of the double bond can occur. Upon introduction of substituents which produce large enough electronic asymmetry, TICT formation is favoured. In weaker donor-acceptor systems, intramolecular fluorescence quenching can occur due to twisting of the double bond, which will lead to ultrafast non-radiative deactivation.

Based on these mechanisms, for compounds **6a,b**, **10** and **19-21** in polar solvents, charge-transfer would be highly favoured which would lead to a large electronic asymmetry rendering the TICT pathway involving a twist of the N-C bond, much more competitive than the twisting of the double bonds, leading to relative enhancement of the long wavelength bands in polar solvents. The absence of dual emission in **7a,b**, **8** and **9** shows that the double bond twisting is much more efficient for these molecules. This may be attributed to the barbituric acid moiety in these compounds, being weaker acceptors relative to indane-1,3-dione moiety in **6a, b**, **10** and **19-21**.

Zachariasse *et al.* have extensively studied the phenomenon of dual fluorescence in aminobenzonitriles.^{23,35-37} According to their mechanism, dual fluorescence takes place from two different low lying singlet excited states and twisting of the amino moiety is not a prerequisite for dual fluorescence. The energy gap $\Delta E (S_1, S_2)$ between the two lowest singlet excited states determines the occurrence dual fluorescence. Another factor is the energetics of the change in configuration of the amino nitrogen from a (partly) pyramidal (sp^3) towards a planar (sp^2) hybridization. At present however, we are unable to distinguish between the two mechanisms for this class of butadiene derivatives.

2.3.4. Second Harmonic Generation Measurements

The second harmonic generation efficiency of these compounds were examined by the powder reflection technique using a Nd:YAG pulsed laser (1064 nm, 11 ns pulses). This technique is a convenient method for screening large numbers of powdered materials for second-order nonlinear optical activity without needing to grow large single crystals. The results are dependent on the particle size, and recrystallization from a range of solvents can lead to different SHG efficiencies. This method is reliable for phase matchable powders. For non-phase matchable powders, the intensity $I_{2\omega}$ decreases rapidly with increasing particle size, after reaching a maximum.³⁸ The reference compound used in these measurements was urea (particle size 100-150 μm). Powdered samples between 100 – 150 μm size were taken for the measurements. The results are shown in Table 2.6. The yellow crystals of **6a** showed an activity of 0.46 times that of urea, whereas the red solid did not show any activity. This may be due to reabsorption of the 532 nm by the red crystals. Compound **6b** recrystallized only in one form from all the solvents and these crystals were not found to be SHG active. Compound **7a** showed SHG activity of 0.45 x urea,

whereas **7b** showed an activity of 0.05 x urea. Substitution by the methoxy group as in **6b** and **7b** does not affect the solvatochromic properties. However, second harmonic generation is not observed with both **6b** and **7b**. This may be due to the possibility that the methoxy groups in **6b** and **7b** affect in some way the bulk properties. However, we could not get good quality crystals required for determining the X-ray structures of these compounds.

Table 2.6. Results of SHG measurements of 6-9, 14 and 15

Compound	SHG activity (x urea)
Urea	1.0
6a (red)	0.0
6a (yellow)	4.6×10^{-1}
6b	0.0
7a	4.5×10^{-1}
7b	4.0×10^{-2}
8	1.6×10^{-3}
9	6.4×10^{-3}
14a	6.0×10^{-2}
15a	6.9×10^{-3}

2.4. Experimental Section

Melting points are uncorrected and were recorded on a Mel-temp-II melting point apparatus. The IR spectra were determined on a Perkin-Elmer Model 882 infrared spectrophotometer. Absorption spectra were recorded on a GBC UV/Vis 918 spectrophotometer. Emission and excitation studies were

carried out on a SPEX-Fluorolog F-112X spectrofluorometer. Quantum yields were measured by the relative method using optically matched dilute solutions. Rhodamine 6G having a quantum yield of fluorescence of 0.90 in ethanol³⁹ was used as reference for **6a** and **6b**, whereas anthracene having a fluorescence quantum yield of 0.27 in ethanol⁴⁰ was used as the reference for **7a** and **7b**. Unless otherwise stated, NMR spectra were recorded on a JEOL 90 MHz NMR spectrometer with tetramethylsilane as internal standard. Optical rotations were measured using a Jasco DIP-370 Digital Polarimeter.

2.4.1. Measurement of Second Harmonic Generation Efficiency

The SHG activities of these compounds were compared with that of urea using the Kurtz and Perry method.⁴¹ The samples were ground and graded by use of standard sieves (100-150 μ) and loaded on a microscopic slide with a sample thickness of 1 mm.

Applied Photophysics Model LKS-50 laser kinetic spectrometer using a Spectra Physics GCR-12 series Nd: YAG laser (1064 nm, 11 ns, 400 mJ/pulse) was used for these studies. The laser beam was directed unfocussed on to the sample kept at 45° angle to the laser beam. The emission was collected from the front face of the sample at 90° angle to the laser beam. After removal of the fundamental beam using filters and a monochromator, the 532 nm signal was detected by a photomultiplier and stored on a Philips model PM 3323 digital oscilloscope. The signals were averaged over several shots.

2.4.2. Materials

Reagent grade reactants and solvents were used as received from chemical suppliers. Extremely dry solvents were prepared as per reported

procedures. Spectroscopic grade solvents were used for all measurements.

General Procedure for the Synthesis of 5-Butylthio-2,4-pentadienones (4a, b and 5a, b)

Equimolar amounts of the aldehydes **3a, b** and the corresponding active methylene compounds were dissolved in minimum amount of dry methanol. Few drops of 10% KOH solution was then added and the mixture was stirred at room temperature for 2 hours in each case. The products formed were filtered and purified by repeated recrystallization from suitable solvents.

1H-Indene-1,3(2H)-dione-2(3-butylthio-3-phenylpropenylidene) (4a)

Compound **4a** was prepared from 3-butylthio-3-phenylprop-2-enal (**3a**) (200 mg, 0.9 mmol) and indane-1,3-dione (132 mg, 0.9 mmol). The product was chromatographed using silica gel (230-400 mesh) in a flash column. Elution of the column with a mixture (1:9) of ethyl acetate and hexane yielded a pure sample of **4a** as an orange solid (250 mg, 80%), which melted at 116-117 °C. after recrystallization from a mixture (1:9) of ethyl acetate and hexane.

IR ν_{\max} (KBr): 3050, 2920 (CH), 1670 (C=O), 1570 (C=C) cm^{-1} ; UV λ_{\max} (CH_3OH): 248 (ϵ 25,600 $\text{M}^{-1} \text{cm}^{-1}$), 272sh (19,500), 391.3 (38,200), 438.0 nm (23,000); ^1H NMR (CDCl_3): δ 0.90-1.10 (3 H, t, CH_3), 1.25-1.91 (4 H, m, CH_2), 3.05-3.20 (2 H, t, SCH_2), 7.10-8.15 (11 H, m, aromatic and vinylic); ^{13}C NMR (CDCl_3): δ 13.42, 21.93, 29.59, 32.73, 117.07, 122.17, 122.37, 123.63, 128.44, 129.30, 130.02, 134.19, 134.34, 135.81, 140.01, 140.46, 141.65, 167.16, 190.31, 190.67. Exact mol wt calcd for $\text{C}_{22}\text{H}_{20}\text{O}_2\text{S}$ (M^+) 348.1184; found 348.1178 (EI, high resolution mass spectroscopy).

1H-Indene-1,3(2H)-dione-2(3-butylthio-3-anisylpropenylidene) (4b)

Treatment of 3b (2 g, 8 mmol) with indane-1,3-dione (1.17 g, 8 mmol) gave the crude product 4b, which was further purified by flash chromatography over silica gel using a mixture (1:1) of benzene and hexane. The orange solid of 4b (2.25 g, 74%) melted at 112-113 °C, after recrystallization from a mixture (1:1) of chloroform and hexane.

IR ν_{\max} (KBr): 2933, 2864 (CH), 1678 (C=O), 1599 (C=C) cm^{-1} ; UV λ_{\max} (CH₃OH): 267 (ϵ 11,500 $\text{M}^{-1}\text{cm}^{-1}$), 442 nm (71,900); ¹H NMR (CDCl₃): δ 0.90-1.10 (3 H, t, CH₃), 1.45-2.00 (4 H, m, CH₂), 3.00-3.20 (2 H, t, SCH₂), 3.9 (3 H, s, OCH₃) 6.95-7.35 (2 H, dd, vinylic), 7.45-8.10 (10 H, m, aromatic); ¹³C NMR (CDCl₃): δ 13.42, 21.93, 29.68, 32.87, 55.16, 113.97, 116.86, 122.11, 122.32, 123.21, 128.20, 130.94, 134.10, 134.25, 140.49, 140.58, 141.65, 161.31, 167.61, 190.55, 190.79. Exact mol wt calcd for C₂₃H₂₃O₃S (MH⁺) 379.1368; found 379.1642 (FAB, high resolution mass spectroscopy).

2,4,6(1H,3H,5H)-Pyrimidinetrione-5-(3-butylthio-3-phenylpropenylidene) (5a)

Treatment of 3a (200 mg, 0.09 mol) with barbituric acid (116 mg, 0.09 mol) and work-up in the usual manner gave 221 mg (74%) of 5a, mp 227-228 °C, after recrystallization from a mixture (1:1) of ethyl acetate and methanol.

IR ν_{\max} (KBr): 3200 (NH), 3000, 2920, 2860 (CH), 1670 (C=O), 1560 (C=C) cm^{-1} ; UV λ_{\max} (CH₃OH): 248 (ϵ 8,700 $\text{M}^{-1}\text{cm}^{-1}$), 372 nm (25,900); ¹H NMR (DMSO-d₆): δ 0.70-1.00 (3 H, t, CH₃), 1.15-1.85 (4 H, m, CH₂), 2.95-3.05 (2 H, t, SCH₂), 7.30-8.20 (7 H, m, aromatic and vinylic), 11.10 (2 H, s, NH); ¹³C NMR (DMSO-d₆): δ 16.84, 25.01, 32.98, 35.69, 114.57, 121.38, 132.23,

132.74, 133.97, 139.13, 151.84, 153.78, 166.70, 167.05, 171.47. Exact mol wt calcd for $C_{17}H_{19}N_2O_3S$ (MH^+) 331.1116; found 331.1166 (FAB, high resolution mass spectroscopy).

2,4,6(1*H*,3*H*,5*H*)-Pyrimidinetrione-5-(3-butylthio-3-anisylpropenylidene) (5b)

Compound **5b** was prepared from **3b** (2 g, 8 mmol) and barbituric acid (1.02 g, 8 mmol). The reddish brown product obtained was purified by flash chromatography over silica gel using a mixture (1:4) of ethyl acetate and chloroform to give 1.9 g (65%) of a pure sample of **5b** which melted at 191-192 °C, after recrystallization from acetone.

IR ν_{max} (KBr): 3745 (NH), 3048, 2842 (CH), 1653 (C=O), 1604, 1575 (C=C) cm^{-1} ; UV λ_{max} (CH₃OH): 229 (ϵ 20,000 $M^{-1}cm^{-1}$), 262sh (9,700), 418 nm (37,000); ¹H NMR (DMSO-*d*₆): δ 0.75-1.10 (3 H, t, CH₃), 1.25-1.85 (4 H, m, CH₂), 2.90-3.15 (2 H, t, SCH₂), 3.85 (3 H, s, OCH₃), 7.00-8.15 (6 H, m, aromatic and vinylic), 11.05 (2 H, s, NH); ¹³C NMR (DMSO-*d*₆): δ 13.39, 21.57, 29.60, 32.37, 55.43, 110.48, 114.30, 114.59, 117.61, 127.84, 130.23, 131.06, 149.02, 150.37, 161.29, 163.29, 163.73, 168.60. Exact mol wt calcd for $C_{18}H_{21}N_2O_4S$ (MH^+) 361.1215; found 361.1222 (FAB, high resolution mass spectroscopy).

General Procedure for the Synthesis of 5-Pyrollidino(2-methanol)-2,4-pentadienones (6a, b and 7a, b)

Equimolar amounts of butylthio-substituted-pentadienone (4a, b and 5a, b) and L-prolinol were dissolved in dry methanol and refluxed for 2 h. The product formed was purified in each case by column chromatography.

1H-Indene-1,3(2H)-dione-2-[3-pyrrolidino(2-methanol)-3-phenylpropylidene] (6a)

Treatment of 1H-indene-1,3(2H)-dione-2(3-butylthio-3-phenylpropenylidene) **4a** (152 mg, 0.47 mmol) with L-prolinol (47 mg, 0.47 mmol) gave reddish brown solid, which was chromatographed over silica gel (230-400 mesh) using a flash column. Elution with a mixture (3:17) of ethyl acetate and chloroform gave reddish brown crystals of **6a** (95 mg, 60%), mp 181-182 °C, after recrystallization from benzene.

IR ν_{\max} (KBr): 3300 (OH), 3060, 2950, 2880 (CH), 1630 (C=O), 1590 (C=C) cm^{-1} ; UV λ_{\max} (CH₃OH): 239 (ϵ 4,250 $\text{M}^{-1}\text{cm}^{-1}$), 452 nm (14,800); ¹H NMR (CDCl₃): δ 1.60-2.40 (5 H, m, CH₂ and OH), 3.10-3.40 (2 H, m, NCH₂), 3.45-4.05 (2 H, m, OCH₂), 4.20-4.60 (1 H, m, NCH), 7.10-7.90 (11 H, m, aromatic and vinylic); ¹³C NMR (CDCl₃):⁴² δ 22.44, 22.97, 27.59, 50.24, 52.95, 60.86, 61.61, 62.65, 63.04, 103.58, 104.27, 114.32, 114.80, 120.62, 120.80, 120.98, 127.51, 128.08, 128.64, 129.78, 132.58, 132.76, 133.42, 139.59, 141.00, 146.52, 167.88, 168.36, 191.51, 191.72, 191.89, 192.31. Exact mol wt calcd for C₂₃H₂₁NO₃ (M⁺) 359.15214; found 359.1504 (FAB, high resolution mass spectroscopy). $[\alpha]_{\text{D}}^{25}$ -328.82 ($c = 0.01$ in methanol).

1H-Indene-1,3(2H)-dione-2-[3-pyrrolidino(2-methanol)-3-anisylpropylidene] (6b)

Treatment of **4b** (2 g, 5.65 mmol) with L-prolinol (570 mg, 5.65 mmol) gave a crude product, which was further purified by flash chromatography over silica gel using a mixture (1:1) of ethyl acetate and chloroform. Recrystallization from benzene gave 1.90 g (87%) of **6b** as reddish brown crystals, mp. 198-199 °C.

IR ν_{\max} (KBr): 3444 (OH), 2915, 2875 (CH), 1643 (C=O), 1615, 1569 (C=C) cm^{-1} ; UV λ_{\max} (CH_3OH): 240sh (ϵ 75,750 $\text{M}^{-1}\text{cm}^{-1}$), 268 (111,100), 452 nm (132,500); ^1H NMR (CDCl_3): δ 1.80-2.40 (5 H, m, CH_2 and OH), 3.10-3.40 (2 H, m, NCH_2), 3.45-4.05 (2 H, m, OCH_2), 3.90 (3 H, s, OCH_3), 4.25-4.55 (1 H, m, NCH), 6.9-7.85 (10 H, m, aromatic and vinylic); ^{13}C NMR (CDCl_3):⁴² δ 22.37, 22.94, 27.44, 50.21, 53.04, 55.04, 60.68, 61.49, 62.62, 103.94, 104.66, 113.76, 114.29, 120.77, 124.41, 125.27, 128.73, 129.66, 131.15, 132.34, 132.64, 139.45, 140.85, 146.52, 160.30, 160.51, 168.15, 168.62, 191.48, 191.78, 192.16. Exact mol wt calcd for $\text{C}_{24}\text{H}_{24}\text{NO}_4$ (MH^+) 390.1705; found 390.1740 (FAB, high resolution mass spectroscopy). $[\alpha]_{\text{D}}^{26}$ 353.91 ($c = 0.0112$ in methanol).

2,4,6(1*H*,3*H*,5*H*)-Pyrimidinetrione-5-[3-pyrrolidino(2-methanol)-3-phenylpropylidene] (7a)

Treatment of 2,4,6(1*H*,3*H*,5*H*)-pyrimidinetrione-5-(3-butylthio-3-phenylpropylidene) **5a** (100 mg, 0.303 mmol) with L-prolinol (30 mg, 0.303 mmol) gave an yellow product, which was purified by flash chromatography over silica gel (230-400 mesh). Elution of the column with a mixture (1:4) of methanol and ethyl acetate gave **7a** (53.9 mg, 52%), mp 270-271 $^{\circ}\text{C}$ after recrystallization from methanol.

IR ν_{\max} (KBr): 3480 (NH), 3120 (OH), 3000, 2920, 2840 (CH), 1660 (C=O) and 1600 (C=C) cm^{-1} ; UV λ_{\max} (CH_3OH): 237 (ϵ 11,300 $\text{M}^{-1}\text{cm}^{-1}$), 419 nm (60,600); ^1H NMR (500 MHz) (DMSO-d_6):⁴³ δ 1.85-2.02 (2 H, m, CH_2), 2.03-2.20 (2 H, m, CH_2), 3.00-3.15 (2 H, m, NCH_2), 3.30-3.48 (2 H, m, OCH_2), 4.25-4.30 (1 H, m, NCH), 4.85 and 5.15 (1 H, t, OH), 7.10-7.64 (7 H, m, aromatic and vinylic), 10.22-10.25 (1 H, d, NH), 10.25-10.30 (1 H, s, NH);

^{13}C NMR (DMSO- d_6):⁴² δ 25.40, 26.11, 30.11; 30.74, 56.83, 62.90, 62.63, 65.44, 66.75, 101.42, 101.95, 108.28, 108.79, 131.40, 131.73, 132.33, 133.25, 133.43, 136.32, 137.34, 154.40, 156.61, 167.65, 167.92, 172.57, 172.90. Exact mol wt calcd for $\text{C}_{18}\text{H}_{20}\text{N}_3\text{O}_4$ (MH^+) 342.1454; found 342.1464 (FAB, high resolution mass spectroscopy). $[\alpha]_D^{25}$ -152.13 ($c = 0.095$ in methanol).

2,4,6(1*H*,3*H*,5*H*)-Pyrimidinetrione-5-[3-pyrrolidino(2-methanol)-3-anisyl-propylidene] (7b)

Compound **7b** was prepared from **5b** (1.5 g, 4.16 mmol) and L-prolinol (420 mg, 4.16 mmol). Purification by flash chromatography over silica gel using a mixture (1:19) of methanol and ethyl acetate gave 1.18 g (76%) of **7b**, which melted at 280-281 °C after recrystallization from methanol.

IR ν_{max} (KBr): 3434 (NH), 3109 (OH), 2999, 2824 (CH), 1664 (C=O), 1615(C=C) cm^{-1} ; UV λ_{max} (CH_3OH): 232sh (ϵ 24,350 $\text{M}^{-1}\text{cm}^{-1}$), 267 (41,500), 420 nm (67,900); ^1H NMR (DMSO- d_6):⁴³ δ 1.75-2.40 (4 H, m, CH_2), 3.05-3.25 (2 H, m, NCH_2), 3.65-3.80 (2 H, m, OCH_2), 3.85 (3 H, s, OCH_3), 4.20-4.55 (1 H, m, NCH), 7.05-7.75 (6 H, m, aromatic and vinylic), 10.25 (2 H, s, NH); ^{13}C NMR (DMSO- d_6):⁴² δ 25.61, 26.32, 31.23, 30.86, 58.99, 63.14, 66.93, 101.00, 101.57, 109.03, 109.53, 117.92, 128.42, 129.40, 133.73, 154.61, 156.79, 163.89, 164.01, 167.83, 168.19, 173.20, 173.53. Exact mol wt calcd for $\text{C}_{19}\text{H}_{22}\text{N}_3\text{O}_5$ (MH^+) 372.1556; found 372.1559 (FAB, high resolution mass spectroscopy). $[\alpha]_D^{25}$ 213.94 ($c = 0.012$ in methanol).

5-(3-Diethanolamine-3-phenylprop-2-enylidene)pyrimidine-2,4,6(1*H*,3*H*,5*H*)-trione (8)

Treatment of pyrimidinetrione **5a** (2.0 g, 6.06 mmol) with diethanolamine (636

mg, 6.06 mmol) gave a yellow product, which was purified by flash chromatography over silica gel (230-400 mesh). Elution of the column with a mixture (1:9) of methanol and chloroform gave the title compound **8** (1.35 g, 65%), mp 245-346 °C, after recrystallization from methanol.

IR ν_{\max} (KBr): 3673 (NH), 3175, 3129 (OH), 3032, 2930, 2823 (CH), 1723, 1674 (C=O), 1639, 1578 (C=C) cm^{-1} ; UV λ_{\max} (CH₃OH): 237 (ϵ 15,517 $\text{M}^{-1}\text{cm}^{-1}$), 419 nm (82,715); ¹H NMR (DMSO-*d*₆): δ 3.10-3.55 (8 H, m, N(CH₂CH₃)), 4.90 (1 H, br s, OH), 5.25 (1 H, br s, OH), 7.0-7.85 (7 H, m, aromatic and vinylic), 10.25 (2 H, s, NH); ¹³C NMR (DMSO-*d*₆): δ 56.69, 59.56, 60.93, 62.15, 102.01, 107.89, 132.12, 132.54, 133.10, 133.37, 136.41, 154.49, 156.84, 167.71, 167.92, 175.98. Exact mol wt calcd for C₁₇H₂₀N₃O₅ (MH⁺) 346.1403; found 346.1410 (FAB, high resolution mass spectroscopy).

5-(3-piperidinyl-3-phenylprop-2-enylidene)pyrimidine-2,4,6(1*H*,3*H*,5*H*)-trione (9)

Compound **9** was prepared from pyrimidenetrione **5a** (1 g, 3.04 mmol) and piperidine (256 mg, 3.04 mmol). Purification by flash chromatography on silica gel using a mixture (1:9) of methanol and chloroform gave the title compound **9** (520 mg, 56%), mp 321-322 °C, after recrystallization from methanol.

IR ν_{\max} (KBr): 3620 (NH), 3093, 3004, 2954 (CH), 1716, 1670 (C=O), 1610, 1559 (C=C) cm^{-1} ; UV λ_{\max} (CH₃OH): 237 (ϵ 10,000 $\text{M}^{-1}\text{cm}^{-1}$) 417 nm (50,000); ¹H NMR (DMSO-*d*₆): δ 1.50-1.85 (6 H, m, CH₂), 3.70-3.95 (4 H, m, NCH₂), 7.05-7.90 (7 H, m, aromatic and vinylic), 10.30 (2 H, s, NH); Exact mol wt calcd for C₁₈H₂₀N₃O₃ (MH⁺) 326.1505; found 326.1515 (FAB, high resolution mass spectroscopy).

1H-Indene-1,3(2H)-dione-2-[3-pyrrolidino(2-methylacetate)-3-phenylpropylidene] (10)

Treatment of 1H-Indene-1,3(2H)-dione-2-[3-pyrrolidino(2-methanol)-3-phenylpropylidene], **6a** (100 mg, 0.28 mmol) with acetyl chloride (22 mg, 0.28 mmol) in refluxing benzene (dry, 20 mL) for 2 h gave **8**, which was further purified by flash chromatography over silica gel using a mixture (1:1) of ethyl acetate and chloroform. The brown solid obtained (109 mg, 95%) melted at 113-114 °C after recrystallization from a mixture (1:1) of chloroform and hexane).

IR ν_{\max} (KBr): 2984, 2372 (CH), 1650 (C=O) and 1563 (C=C) cm^{-1} ; UV λ_{\max} (CH₃OH): 240sh (ϵ 27,000 $\text{M}^{-1}\text{cm}^{-1}$), 268 (43,300), 452 nm (40,850); ¹H NMR (CDCl₃): δ 1.60-2.4 (7 H, m, CH₂ and COCH₃), 3.60-3.90 (2 H, m, NCH₂), 4.20-4.50 (2 H, m, OCH₂), 4.60-4.80 (1 H, m, NCH), 6.90-8.00 (11 H, m, aromatic and vinylic); ¹³C NMR (CDCl₃):⁴² δ 20.52, 22.22, 22.82, 27.62, 49.52, 52.03, 53.28, 58.00, 59.01, 62.74, 63.84, 102.96, 103.46, 115.58, 116.14, 120.80, 121.19, 127.60, 127.90, 128.26, 128.56, 128.82, 129.75, 132.43, 132.64, 132.82, 133.54, 139.83, 141.18, 146.37, 166.98, 167.58, 169.94, 170.59, 191.18, 191.98. Exact mol wt calcd for C₂₅H₂₄NO₄ (MH⁺) 402.1705; found 402.1707 (FAB, high resolution mass spectroscopy). $[\alpha]_{\text{D}}^{26}$ -71.84 ($c = 0.01$ in methanol).

General Procedure for the Synthesis of Bicyclic Compounds (14a-c)

Condensation of carbon disulfide and active methylene compounds **12a-c** with subsequent alkylation in the presence of potassium fluoride afforded the corresponding ketene dithioacetals **13a-c**. Refluxing **13a-c** with equimolar amount of pyrrolidine-2-methanol for 16 h yielded the condensation products **14a-c** or the rearranged products **15a-c**, depending on the reaction conditions.

4,4-Bismethylthio-1,1-dicyano-2-phenyl-1,3-butadiene (13a)

Treatment of 1,1-dicyano-2-phenyl propene, **12a** (8.4 g, 50 mmol) with carbon disulphide (4.56 g, 60 mmol) followed by alkylation using methyl iodide (14.5 g, 102 mmol) in the presence of potassium fluoride gave the crude product. Purification by column chromatography using a mixture (1:4) of ethyl acetate and hexane gave the title compound as orange crystals (8 g, 60%), which melted at 117-118 °C after recrystallization from chloroform.

IR ν_{\max} (KBr): 3066, 2992 (CH), 2208 (CN) cm^{-1} ; UV λ_{\max} (acetone): 410 nm (ϵ 24200 $\text{M}^{-1}\text{cm}^{-1}$); ^1H NMR (CDCl_3): δ 2.2 (3 H, s, SCH_3), 2.7 (3 H, s, SCH_3), 6.5 (1 H, s, vinylic), 7.30-7.90 (5 H, m, aromatic); ^{13}C NMR (CDCl_3): δ 16.23, 17.27, 113.52, 113.64, 113.97, 128.10, 128.32, 128.56, 130.67, 134.07, 165.19, 167.31.

4,4-Bismethylthio-1,1-dicyano-2-(4-tolyl)-1,3-butadiene (13b)

Compound **13b** was synthesized from 1,1-dicyano-2-(4-tolyl)propene, **12b** (5.47 g, 30 mmol), carbon disulphide (3.34 g, 36 mmol) and methyl iodide (9.0 g, 61 mmol). The crude product was purified by column chromatography using a mixture (1:5) of ethyl acetate and hexane to give 6 g (70%) of the title compound, mp 126-127 °C, after recrystallization from benzene.

IR ν_{\max} (KBr): 2999 (CH), 2213 (CN), 1607 (C=C) cm^{-1} ; UV λ_{\max} (acetone): 410 nm (ϵ 34500 $\text{M}^{-1}\text{cm}^{-1}$); ^1H NMR (CDCl_3): δ 2.30 (3 H, s, CH_3), 2.45 (3 H, s, SCH_3), 2.60 (3 H, s, SCH_3), 6.50 (1 H, s, vinylic), 7.10-7.45 (4 H, m, aromatic); ^{13}C NMR (CDCl_3): δ 16.32, 17.39, 21.27, 113.94, 114.32, 128.38, 129.48, 131.27, 141.62, 161.64, 163.34, 164.48, 167.85.

4,4-Bismethylthio-1,1-dicyano-2-anisyl-1,3-butadiene (13c)

This compound was synthesized from 1,1-dicyano-2-anisylpropene, **12c** (9.9 g, 50 mmol) and carbon disulfide (4.6 g, 60 mmol), followed by alkylation using methyl iodide (15 g, 105 mmol). The crude product was purified by column chromatography using a mixture (1:5) of ethyl acetate and hexane to give 10 g (61%) of a pure sample of **13c**, which melted at 150-151 °C, after recrystallization from chloroform.

IR ν_{max} (KBr): 2939, 2838 (CH), 2205 (CN), 1605, 1588 (C=C) cm^{-1} ; UV λ_{max} (acetone): 406 nm (ϵ 26900 $\text{M}^{-1}\text{cm}^{-1}$); ^1H NMR (CDCl_3): δ 2.2 (3 H, s, SCH_3), 2.75 (3 H, s, SCH_3), 3.8 (3 H, s, OCH_3), 6.5 (1 H, s, vinylic), 6.90-7.40 (4 H, m, aromatic); ^{13}C NMR (CDCl_3): δ 17.20, 18.16, 55.94, 79.36, 115.01, 115.19, 115.40, 126.94, 131.33, 162.95, 164.57, 168.26.

1-Propene-1,1-dinitrile-3-phenyl-3-(1*H*,3*H*)-pyrrolo[1,2-*c*]oxazole-3-ylidene (14a)

Compound **14a** was synthesized by refluxing 4,4-bismethylthio-2-phenyl-1,3-butadiene, **13a** (200 mg, 0.734 mmol) and prolinol (74 mg, 0.734 mmol) using dry methanol (50 mL) as the solvent for 16 h. The product mixture was purified by column chromatography over silica gel (100-200 mesh). Elution with a mixture (2:1) of chloroform and hexane gave **14a**, 150 mg (73%), which melted at 132-133 °C along with the rearranged product, **15a**, (40 mg, 20%), which melted at 125-126 °C.

Compound 14a

IR ν_{max} (KBr): 3053, 2960, 2887 (CH), 2203 (CN), 1598, 1565 (C=C) cm^{-1} ; UV λ_{max} (acetone): 385 nm (ϵ 61500 $\text{M}^{-1}\text{cm}^{-1}$); ^1H NMR (CDCl_3): δ 1.2-2.5 (4

H, m, CH₂), 3.35 (2 H, m, NCH₂), 3.85-4.40 (3 H, m, OCH₂ and CH), 5.25 (1 H, s, vinylic), 7.00-7.80 (5 H, m, aromatic); ¹³C NMR (CDCl₃): δ 27.36, 30.01, 46.96, 61.73, 61.96, 73.42, 79.75, 117.01, 117.34, 127.78, 129.27, 136.46, 166.74, 170.38. Exact mol wt calcd for C₁₇H₁₆N₃O (MH⁺) 278.1293; found 278.1311 (FAB, high resolution mass spectroscopy).

2,6-Bismethylthio-3-cyano-4-phenyl pyridine (15a)

IR ν_{\max} (KBr): 3064, 2936 (CH), 2213 (CN), 1563 (C=C) cm⁻¹; UV λ_{\max} (acetone): 336 nm (ϵ 12900 M⁻¹cm⁻¹); ¹H NMR (CDCl₃): δ 2.65 (3 H, s, SCH₃), 2.70 (3 H, s, SCH₃), 6.95 (1 H, s, vinylic), 7.45-7.70 (5 H, m, aromatic); ¹³C NMR (CDCl₃): δ 12.97, 13.27, 99.85, 115.64, 115.94, 127.93, 128.53, 129.60, 135.30, 151.68, 163.82, 164.15; Analysis calcd for C₁₄H₁₂N₂S₂: C, 61.73, H, 4.44, N, 10.29; found C, 61.96, H, 4.41, N, 10.37.

1-Propene-1,1-dinitrile-3-(4-tolyl)-1,3-(1*H*,3*H*)-pyrrolo[1,2-*c*]oxazole-3-ylidine (14b)

Compound 14b was synthesized from 4,4-bismethylthio-2-(4-tolyl)-1,3-butadiene, 13b (500 mg, 1.75 mmol) and prolinol (176 mg, 1.75 mmol). The crude product was chromatographed over silica gel (100-200 mesh). Elution with a mixture (1:1) of ethyl acetate and hexane gave the bicyclic compound 14b, 150 mg (29%), which melted at 147-148 °C, after recrystallization from chloroform, and the rearranged product 15b (270 mg, 54%), mp 144-145 °C, after recrystallization from a mixture (1:9) of ethyl acetate and hexane.

Compound 14b

IR ν_{\max} (KBr): 2995, 2972 (CH), 2202 (CN), 1600, 1552 (C=C) cm⁻¹; UV λ_{\max} (acetone): 386 nm (ϵ 48000); ¹H NMR (CDCl₃): δ 1.20-1.75 (2 H, m, CH₂),

1.85-2.20 (2 H, m, CH₂), 2.3 (3 H, s, CH₃), 3.10-3.60 (2 H, m, NCH₂), 3.95-4.40 (3 H, m, OCH₂ and NCH) 5.15 (1 H, s, vinylic), 6.95-7.45 (4 H, m, aromatic); ¹³C NMR (CDCl₃): δ 21.03, 27.15, 29.80, 46.90, 60.95, 61.84, 73.24, 79.51, 117.07, 117.49, 127.69, 128.35, 133.18, 139.30, 166.74, 170.35. Exact mol wt calcd for C₁₈H₁₈N₃O (MH⁺) 292.1450; found 292.1443 (FAB, high resolution mass spectroscopy).

Compound 15b

IR ν_{\max} (KBr): 2930, 2859 (CH), 2219 (CN), 1614, 1573 (C=C) cm⁻¹; UV λ_{\max} (acetone): 337 nm (ϵ 11900 M⁻¹cm⁻¹); ¹H NMR CDCl₃: δ 2.35 (3 H, s, CH₃), 2.65 (3 H, s, SCH₃), 2.75 (3 H, s, SCH₃), 6.85 (1 H, s, vinylic), 7.10-7.55 (4 H, m, aromatic); ¹³C NMR (CDCl₃): δ 13.03, 13.33, 21.06, 54.33, 99.91, 113.64, 115.88, 127.93, 129.33, 132.49, 139.92, 151.80, 163.73, 164.18. Exact mass calcd for C₁₅H₁₅N₂S₂ (MH⁺) 287.0677; found 287.0648 (FAB, high resolution mass spectroscopy).

2,6-Bismethylthio-3-cyano-4-anisyl pyridine 15c

Treatment of 4,4-bismethylthio-2-anisyl-1,3-butadiene, **13c** (500 mg, 1.7 mmol) and prolinol (172 mg, 1.7 mmol) in dry methanol (50 mL) gave the crude product. This was purified by column chromatography using a mixture (1:9) of ethyl acetate and hexane to give 340 mg (68%) of a pure sample of **15c** which melted at 157-158 °C, after recrystallization from a mixture (1:4) of ethyl acetate and hexane.

IR ν_{\max} (KBr): 3205, 2936 (CH), 2216 (CN), 1614, 1579 (C=C) cm⁻¹; UV λ_{\max} (acetone): 335 nm (ϵ 11600 M⁻¹cm⁻¹); ¹H NMR (CDCl₃): δ 2.65 (3 H, s, SCH₃), 2.70 (3 H, s, SCH₃), 3.90 (3 H, s, OCH₃), 6.90 (1 H, s, vinylic), 7.00-7.75 (4 H,

m, aromatic); ^{13}C NMR (CDCl_3): δ 13.09, 13.42, 55.25, 113.58, 114.20, 115.85, 116.17, 127.66, 129.60, 151.56, 160.93, 163.70, 164.33; Analysis calcd for $\text{C}_{15}\text{H}_{14}\text{N}_2\text{OS}_2$: C, 59.57, H, 4.67, N, 9.27; found C, 59.74, H, 4.68, N, 9.33.

General Procedure for the Synthesis of 3-amino-substituted propenylidene indanediones (19-21)

Equimolar amounts of sulfanyl-substituted indane-1,3-dione derivative 4a and the corresponding secondary amine were dissolved in methanol and refluxed for 10 h. The product formed was purified in each case by column chromatography over silica gel (100-200 mesh).

2-(3-Pyrrolidine-3-phenylprop-2-enylidene)indane-1,3-dione (19)

Treatment of 1H-indane-1,3(2H)-dione-2-(3-butylthio-3-phenylpropenylidene) (4a, 500 mg, 1.5 mmol) with pyrrolidine (102 mg, 1.5 mmol) gave a reddish brown solid which was further purified by column chromatography using chloroform as eluent. Recrystallization from a mixture (1:9) of methanol and chloroform afforded 530 mg (88%) of a pure sample of 19 as reddish brown crystals, which melted at 274-275 °C.

IR ν_{max} (KBr): 2983, 2875 (CH), 1648 (C=O), 1587 (C=C) cm^{-1} ; UV λ_{max} (CHCl_3): 242 (ϵ 20900 $\text{M}^{-1}\text{cm}^{-1}$), 456 nm (88900), ^1H NMR (CDCl_3): δ 1.65-2.25 (4 H, m, CH_2), 3.05-3.35 (2 H, t, NCH_2), 3.60-3.85 (2 H, t, NCH_2), 7.00-7.90 (11 H, m, aromatic and vinylic); ^{13}C NMR (CDCl_3): δ 24.73, 25.06, 49.49, 51.88, 102.81, 114.95, 120.65, 121.07, 128.17, 128.82, 129.84, 132.46, 132.70, 133.39, 139.92, 141.29, 146.31, 167.61, 191.45, 192.16. Exact mass calcd for $\text{C}_{22}\text{H}_{20}\text{NO}_2$ (MH^+) 330.1512; found 330.1494 (FAB, high resolution mass spectroscopy).

2-(3-Piperidine-3-phenylprop-2-enylidene)indane-1,3-dione (20)

Treatment of **4a** (200 mg, 0.6 mmol) with piperidine (51 mg, 0.6 mmol) gave a crude product, which was further purified by column chromatography. Elution with a mixture (3:7) of ethyl acetate and petroleum ether gave a pure sample of **20**, (225 mg 90%), which melted at 243-244 °C, after recrystallization from benzene.

IR ν_{\max} (KBr): 2939, 2861 (CH), 1703, 1659 (C=C), 1563 (C=C) cm^{-1} ; UV λ_{\max} (CHCl_3): 458 nm (ϵ 70200 $\text{M}^{-1}\text{cm}^{-1}$); ^1H NMR (CDCl_3): δ 1.4-2.0 (6 H, m, $(\text{CH}_2)_3$), 3.1-3.4 (2 H, m, NCH_2), 3.7-4.0 (2 H, m, NCH_2), 6.9-7.9 (11 H, m, aromatic and vinylic); ^{13}C NMR (CDCl_3): δ 23.72, 25.48, 101.88, 114.95, 120.47, 120.89, 128.61, 129.90, 132.37, 132.58, 132.79, 139.74, 141.09, 147.44, 169.40, 191.00, 191.92. Exact mass calcd for $\text{C}_{23}\text{H}_{22}\text{NO}_2$ (MH^+) 344.1662; found 344.1651 (FAB, high resolution mass spectroscopy).

2-(3-Diethylamino-3-phenylprop-2-enylidene)indane-1,3-dione (21)

Treatment of **4a** (200 mg, 0.6 mmol) with diethylamine (42 mg, 0.6 mmol) gave an orange solid, which was further purified by column chromatography using a mixture (3:7) of ethyl acetate and petroleum ether as eluent. The pure sample (175 mg, 85%) melted at 172-173 °C, after recrystallization from benzene.

IR ν_{\max} (KBr): 3060, 2990 (CH); 1698, 1651 (C=O), 1566 (C=C) cm^{-1} ; UV λ_{\max} (CHCl_3): 455 nm (ϵ 86500 $\text{M}^{-1}\text{cm}^{-1}$); ^1H NMR (CDCl_3): δ 0.80-1.30 (3 H, t, CH_3), 1.35-1.70 (3 H, t, CH_3), 3.00-3.30 (2 H, q, NCH_2), 3.50-3.90 (2 H, q, NCH_2), 6.80-7.90 (11 H, m, aromatic and vinylic); ^{13}C NMR (CDCl_3): δ 11.96, 14.14, 44.75, 47.26, 102.24, 115.16, 120.71, 121.19, 128.53, 128.76, 129.84,

132.58, 132.79, 139.98, 141.29, 147.41, 169.43, 191.42, 192.37. Exact mass calcd for $C_{22}H_{22}NO_2$ (MH^+) 332.1655; found 332.1651 (FAB, high resolution mass spectroscopy).

2.5. References

1. *Nonlinear Optical Properties of Organic Molecules and Crystals*, Chemla, D. S.; Zyss, J. Eds., Vols. 1 and 2, Academic Press, London, 1987.
2. *Organic Materials for Nonlinear Optics*, Hann, R. A; Bloor, D. Eds., Special Publication No. 69, Royal Society of Chemistry, Oxford, 1989.
3. Burland, D. M.; Miller, R. D.; Walsh, C. A. *Chem. Rev.*, 1994, 94, 31.
4. Groh, W.; Lupo, D.; Sixl, H. *Adv. Mater.* 1989, 1, 1548.
5. Paley, M. S.; Harris, M. J. *J. Org. Chem.* 1991, 56, 568.
6. Stiegman, A. E.; Graham, E.; Perry, K. J.; Khundkar, L. R.; Cheng, L.-T.; Perry, J. W. *J. Am. Chem. Soc.* 1991, 113, 7658.
7. Jen, A. K. -Y.; Rao, V. P.; Wang, K. Y.; Drost, K. J. *J. Chem. Soc. Chem. Commun.* 1993, 90.
8. Ching, K. C.; Lequan, M.; Lequan, R. M. *J. Chem. Soc. Faraday Trans.* 1991, 87, 2225.
9. Pucetti, G.; Blanchard-Desce, M.; Ledoux, I.; Lehn, J.-M.; Zyss, J. *J. Phys. Chem.* 1993, 97, 9385.
10. Slama-Schwok, A.; Blanchard-Desce, Lehn, J.-M. *J. Phys. Chem.* 1990, 94, 3894.
11. Marder, S. R.; Gorman, C. B.; Tiemann, B. G.; Cheng, L.-T. *J. Am. Chem. Soc.* 1993, 115, 3006.
12. *International Tables for X-ray Crystallography*, Henry, N. F. M.; Lonsdale, K. Eds. Vol 1, Kynoch Press, Brimingham, 1969.

13. Asokan, C. V.; Mathews, A. *Tetrahedron Lett.* **1994**, *35*, 2585.
14. Mowry, D. T. *J. Am. Chem. Soc.* **1943**, *65*, 991.
15. Villemin, D.; Alloum, A. B. *Synthesis* **1991**, 301.
16. Peseke, K.; Zahn, K.; Michalik, M. *J. Prakt. Chem.* **1994**, *336*, 357 and references cited therein.
17. X-ray structure determinations were carried out by Dr. Rath, N. P. at the Department of Chemistry, University of Missouri St. Louis, St. Louis, MO 63121, USA.
18. Lippert, E.; *Z. Naturforsch.* **1955**, *10a*, 541.
19. Mataga, N.; Kaifu, Y.; Koizumi, M. *Bull. Chem. Soc. Jpn.* **1956**, *29*, 465.
20. The λ_{max} of the CT bands were estimated by subtracting the LE band from the observed emission spectrum assuming a symmetric shape of the LE bands.
21. Méyer, M.; Mialocq, J. C. *Opt. Commun.* **1987**, *64*, 264.
22. Edward, J. T. *Chem. Ind.* **1956**, 774.
23. Leinhos, U.; Kuhnle, W.; Zachariasse, K. A. *J. Phys. Chem.* **1991**, *95*, 2013.
24. *Photophysics of aromatic Molecules* Birks, J. B. Ed., Wiley-Interscience, New York, **1970**.
25. Zachariasse, K. A.; Kuhnle, W.; Weller, A. *Chem. Phys. Lett.* **1978**, *59*, 375.
26. Zachariasse, K. A.; Duveneck, G.; Kuhnle, W. *Chem. Phys. Lett.* **1985**, *113*, 337.
27. Lippert, E.; Luder, W.; Boos, H. in *Advances in Molecular Spectroscopy*, Mangini, A. Ed. Pergamon Press, Oxford, **1962**, pp. 443-457.

28. Grabowski, Z. R.; Rotkiewicz, K.; Siemiarczuk, A.; Cowley, D. J.; Baumann, W. *New J. Chem.* **1979**, *3*, 443.
29. Rettig, W. *Angew. Chem. Int. Ed. Engl.* **1986**, *25*, 971.
30. Nag, A.; Kundu, T.; Bhattacharyya, K. *Chem. Phys. Lett.* **1989**, *160*, 257.
31. Chandross, E. A.; Thomas, H. T. *Chem. Phys. Lett.* **1971**, *9*, 397.
32. Weisenborn, P. C. M.; Huizer, A. H.; Varma, C. A. G. O. *J. Chem. Phys.* **1989**, *133*, 437.
33. Rettig, W. *Proc. Indian Acad. Sci. (Chem. Sci.)*, **1992**, *104*, 89.
34. Rettig, W.; Majenz, J. *Chem. Phys. Lett.* **1989**, *154*, 335.
35. Zachariasse, K. A.; von der Haar, Th.; Hebecker, A.; Leinhos, U.; Kuhnle, E. *Pure and Appl. Chem.* **1993**, *65*, 1745.
36. Schuddeboom, W.; Jonker, S. A.; Warman, J. M.; Leinhos, U.; Kuhnle, W.; Zachariasse, K. A. *J. Phys. Chem.* **1992**, *96*, 10809.
37. Zachariasse, K. A.; Grobys, M.; von der Haar, Th.; Hebecker, H. A.; Il'chev, Yu. V.; Jiang, Y.-B.; Morawski, O.; Kuhnle, W. *J. Photochem. Photobiol. A: Chem.* **1996**, *102*, 59.
38. Williams, D. J. *Angew. Chem. Int. Ed. Engl.* **1984**, *23*, 690.
39. *Kodak Laser Dyes*, Kodak Publication JJ-169, **1987**.
40. *CRC Handbook of Organic Photochemistry*, Scaiano, J. C. Ed.; CRC Press Inc., New York, **1989**, Vol. 1, 235.
41. Kurtz, S. K.; Perry, T. T. *J. Appl. Phys.* **1968**, *39*, 3798.
42. ¹³C NMR showed peaks more than the number of carbon atoms present in the molecule due to the existence of two different conformers in equilibrium in solution.
43. The -OH proton shows two signals due to restricted rotation of C-N bond.

CHAPTER 3

STUDIES OF SUBSTITUENT EFFECTS ON THE NLO PROPERTIES OF SOME DONOR-ACCEPTOR SYSTEMS

3.1. Abstract

The effect of varying the substitution on the donor side of some butadiene derivatives on their NLO properties was studied. The acceptor moiety in all these cases was derived from Meldrum's acid. Two classes of compounds were examined, containing either butylthio- or prolinol as the donor moiety attached to butadiene. The NLO coefficient (d_{33}) of these butadiene derivatives was obtained by aligning these molecules in a polymer matrix using the electric field poling method. Most of the derivatives studied showed large d_{33} coefficients. The alkylthio derivatives possessed slightly higher d_{33} values compared to the corresponding prolinol derivatives, which could be attributed to better alignment of the alkylthio derivatives. Absorption studies of alkylthio derivatives in poled films showed marginally higher order parameter compared to those of prolinol derivatives. The β values of these molecules were measured using the hyper-Rayleigh scattering technique. In this case the prolinol derivatives had marginally higher β values, which can be attributed to the better electron donating ability of the prolinol compared to the butylthio- group. The β values of these compounds

were also calculated theoretically using MOPAC (version 6.12) package, and good trend was obtained with the experimentally determined values. The Kurtz and Perry powder measurements method showed that 5a had an SHG efficiency same as that of urea whereas all the others showed negligible efficiencies, indicating that compounds 5b-e crystallizes in a centrosymmetric fashion. It is noteworthy that substituting both electron donating as well as electron accepting groups on the donor side predisposes these molecules to crystallize in a centrosymmetric fashion in spite of the presence of a chiral group.

3.2. Introduction

The optimization of materials for nonlinear optical (NLO) devices requires an in-depth understanding of the NLO properties on the microscopic or molecular level. Reliable structure-property relationships are required for rational design of optimized materials for photonic devices such as electrooptic modulators and optical switches. The development of organic NLO materials for device applications is a multidisciplinary effort involving both theoretical and experimental studies. Quantum chemical calculations have made an important contribution to the understanding of the electronic polarization at the molecular level underlying the NLO processes and the establishment of structure-property relationships.^{1,2}

The molecular origin of β in organic molecules has been studied by many methods. One of the first structure-function relationships developed showed that donor/acceptor organic molecules consisting of a donor (D) and an acceptor (A) pair linked by a π -electron conjugated hydrocarbon bridge have a large β value that is proportional to the difference in dipole moment between the first molecular excited state compared to the ground state ($\Delta\mu$).³ Research into increasing β has

often concentrated on the development of stronger donors and acceptors, with less attention paid to the structure of the molecular bridge connecting the two. Theoretical studies have also predicted that as donor and acceptor strengths are increased, β is expected to reach a maximum and then decrease.⁴⁻⁶

The macroscopic nonlinear response of second-order materials depends both on the magnitude of the molecular nonlinearities and the ordering of the chromophores in the medium. The overall nonlinear response of a material can therefore be improved using techniques that can bring about optimal alignment of the chromophores in the bulk material.

One of the most promising approaches to development of materials with optimal orientation for second order NLO application is that of electric field poling, where an active nonlinear molecule is dissolved in a polymer and the matrix is heated and poled above the glass transition temperature of the polymer (T_g) to orient it in the direction of the applied field. Cooling the polymer matrix in the presence of the electric field helps to lock in its activity.⁷ This procedure has also been used to determine the NLO coefficient (d_{33}) of several newly synthesized molecules.

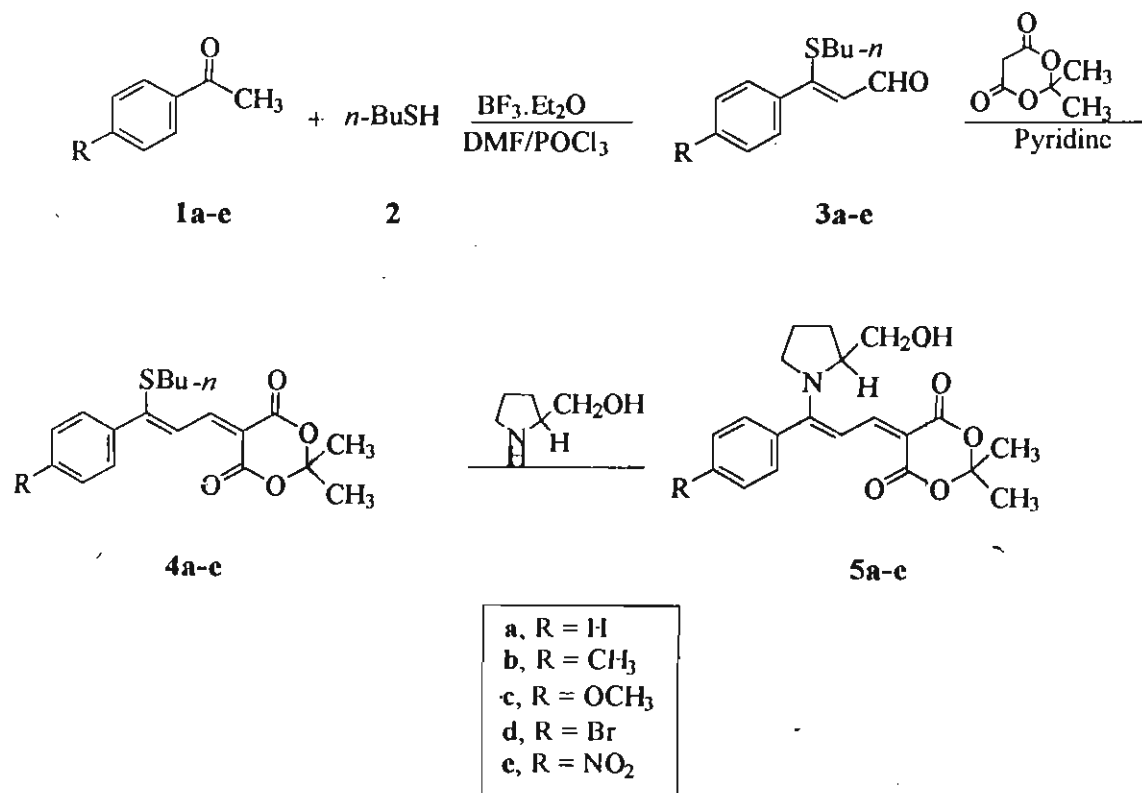
Another method that can be used to determine the β values of NLO chromophores is the hyper-Rayleigh (light) scattering technique.^{8,9} This method is intrinsically a very powerful technique for the measurement of β . Hyper-Rayleigh scattering has been used to determine the first- and second-order hyperpolarizabilities of a variety of intramolecular charge transfer NLO chromophores¹⁰ as well as those of proteins in solution.¹¹ Since an external electric field is not required for such studies, the hyperpolarizability of ionic and mixed-valence metal complexes can also be determined by the hyper-Rayleigh scattering technique.¹²

Important insights into the structure-property relationship on β can be gained through the study of simple models. In this work, the effect of changing the substituent at the donor side of some butadiene derivatives, keeping the acceptor moiety the same on their SHG properties has been examined.

3.3. Results and Discussion

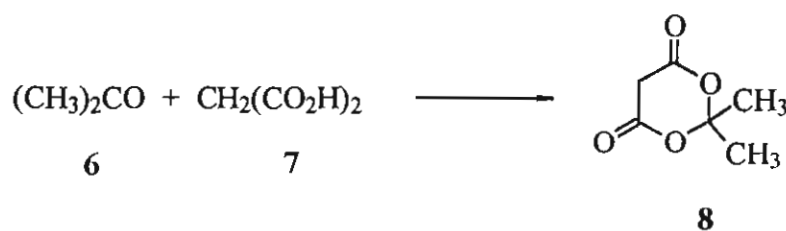
3.3.1. Synthesis

The procedure for the synthesis of butadiene derivatives **4a-e** and **5a-e** is outlined in Scheme 3.1. The strategy involves three types of reactions, namely,



Scheme 3.1

Vilsmeier formylation of 4-substituted acetophenone, Knoevenagel condensation of the resulting aldehyde with Meldrum's acid and finally substitution of the butylthio group of **4a-e** with prolinol. Meldrum's acid was prepared from acetone and malonic acid as per Scheme 3.2.



Scheme 3.2

3.3.2. Absorption Properties

The absorption properties of these compounds were examined in a variety of solvents of varying polarity. The absorption maxima of these compounds in different solvents are summarized in Table 3.1. There is a small but definite hypsochromic shift in the absorption maxima of these compounds with increasing solvent polarity. This 'negative solvatochromism'¹³ is indicative of the ground state being more polar than the excited state. The absorption band maxima of compounds **5a-e** are in the region of 410 nm which is substantially blue shifted compared to the compounds derived from indane-1,3-dione and barbituric acid (compounds **6a,b** and **7a,b** described in Chapter 2). This is indicative of the weak electron accepting nature of the Meldrum's acid moiety. Thus the weak charge transfer between donor and acceptor in the excited state will lead to enhanced

nonradiative decay via twisting of the double bond. Emission studies revealed that these compounds are not fluorescent ($\Phi < 10^{-4}$).

Table 3.1. Absorption maxima (in nm) of compounds 5a-e in different solvents

Solvent	5a	5b	5c	5d	5e
Benzene	412	410	412	413	409
Dichloromethane	410	410	411	410	412
Chloroform	411	411	412	412	413
Ethyl acetate	408	408	408	408	400
Acetone	407	406	407	407	402
Acetonitrile	404	405	405	406	404
DMF	408	407	407	409	405
DMSO	407	407	409	410	410
Methanol	404	403	404	404	404

3.3.3. Nonlinear Optical Studies

3.3.3.1. Determination of d_{33} Values by the Electric Field Poling Method

The effects of substitution on the NLO properties of these donor-acceptor substituted butadiene derivatives were studied by electric field poling as well as hyper-Rayleigh scattering methods. Electric field poling of chromophores embedded in polymer matrix at a temperature above the glass transition temperature (T_g) of the polymer causes the dipole of the chromophores to align parallel to the direction of the applied electric field. SHG measurements were

carried out in films of uniform thickness immediately after poling. The highest order nonlinear coefficient (d_{33}) of these aligned chromophores was estimated using equation 3.1.¹⁴⁻¹⁷

$$\frac{d_{33}^S}{d_{33}^Q} = \left(\frac{n_s}{n_q} \right)^{3/2} \frac{I_s^{2\omega}}{I_q^{2\omega}} \frac{l_c}{lF} \quad 3.1$$

where, d_{33}^S and d_{33}^Q are the SH coefficients of the substrate and quartz, respectively. n_s and n_q are the refractive indices of the sample and quartz, respectively. $I_s^{2\omega}$ and $I_q^{2\omega}$ are the SH intensities corresponding to the polymer film and quartz, respectively. l_c and l are the coherence lengths of quartz and polymer film, respectively, and F is a factor defined as per equation 3.2, where, ϵ is the

$$F^2 = \left(\frac{l_c}{2l} \right)^2 \exp - \left(\frac{1}{2} \epsilon l \right) \left[\cosh \left(\frac{1}{2} \epsilon l \right) - \cos(\pi l / l_c) \right] \quad 3.2$$

absorption coefficient and l_c is the coherence length of fundamental and harmonic waves in the film. Since the compound has no absorption near the fundamental wavelength, substituting for $\epsilon = 0$, in equation 3.2 we get $F^2 = (l_c^2/2l^2)[1 - \cos(\pi l/l_c)]$. Under our experimental conditions $l < l_c$ and $F = 1.2$. The d_{33} values of all the compounds estimated disregarding the difference in the refractive indices of the polymer film and quartz (i.e., $n_s = n_q$), are listed in Table 3.2.

The d_{33} values of the butylthio derivatives (**4a-c**) are marginally higher than those of the corresponding prolinol derivatives (**5a-e**). The difference could be

attributed to a better alignment of the butanethiol derivatives in the electric field poled films. The order parameter S is defined as¹⁸

$$S = 1 - A_{\perp}/A_{\parallel} \quad 3.3$$

where, A_{\parallel} is the optical density of the film before poling and A_{\perp} , the optical density of the film after poling. For example, the order parameter S was marginally higher for the butanethiol derivative **4e** (0.52) than for the corresponding prolinol derivative **5e** (0.50).

Table 3.2. First hyperpolarizability of 4a-e and 5a-e measured by electric field poling and hyper-Rayleigh scattering techniques

Compound	d_{33} (pm/V)		β ($\times 10^{-30}$ esu)	
	4	5	4	5
a	0.35	0.13	10	17
b	1.52	1.35	23	28
c	1.93	1.55	33	42
d	3.48	1.93	18	24
e	5.80	2.30	19	24

From Table 3.2 it is clear that all the compounds except **4a** and **5a** have larger d_{33} coefficients compared to some known materials such as potassium dihydrogen phosphate (KDP) ($d_{33}=1.0$ pm/V) or 4-dimethylamino-4'-nitrostilbene (DANS) ($d_{33}=0.55$ pm/V).¹⁹

3.3.3.2. Determination of β by Hyper-Rayleigh Scattering Method

SHG efficiencies of these compounds were also measured using the hyper-Rayleigh scattering (HRS) technique. HRS measurements were carried out by measuring the intensity of the frequency-doubled light that is generated by focusing an intense laser beam on to an isotropic solution. The fact that second-order optical processes can occur in an isotropic solution is due to the fluctuations in molecular orientations that instantaneously break the centrosymmetry of the solution. The term *hyper-Rayleigh* scattering is used because the intensity of scattered light varies as the square of the incident laser intensity and the scattered photons appear at frequency 2ω . In ordinary Rayleigh scattering, the scattered intensity varies linearly with the incident laser intensity and the scattered photons have the same frequency as that of the incident light.

Since the average second order optical susceptibility in the electric dipole approximation vanishes in an isotropic system, the contribution to the nonlinear polarization $P(2\omega)$ associated with second order nonlinear scattering is proportional to the fluctuation in the second order susceptibility $\chi(-2\omega, \omega, \omega)$. Two different mechanisms may contribute to $\chi(-2\omega, \omega, \omega)$, namely the fluctuations in the number density of the NLO chromophores and the fluctuation in the orientation of the chromophores. The fluctuation in NLO number density results in a spatial inhomogeneity and hence removes local centrosymmetry. The fluctuation in the chromophore orientation results in a depolarized light scattering intensity, which is found to be small, compared to the polarized component. Therefore we may consider the hyper-Rayleigh scattered light intensity to arise mainly from the concentration fluctuation of the NLO chromophores.

Assuming that the values of β_{ijk} at two different points are correlated only over small distances compared to a wavelength, the intensity of the HRS signal is given by the equation 3.4,

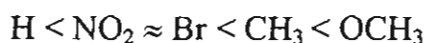
$$I_{2\omega} = G \sum N_k \beta_k^2 I_\omega^2 \quad 3.4$$

where, G is an instrument factor and depends on the scattering geometry, N is the molecular number density, β is the first order hyperpolarizability of individual molecules, and I_ω and $I_{2\omega}$ are the incident and scattered intensities, respectively. For a two-component mixture of solvent and solute the scattering signal $I_{2\omega}$ is given by the equation 3.5.

$$I_{2\omega} = G \{ N_{\text{solvent}} \beta_{\text{solvent}}^2 + N_{\text{solute}} \beta_{\text{solute}}^2 \} I_\omega^2 \quad 3.5$$

The quadratic coefficient $I_{2\omega}/I_\omega^2$ is a linear function of the number density of the solute, N_{solute} if β and N for the solvent are fixed. The intercept can be used to calculate the proportionality factor G , provided β_{solvent} is known. The factor G depends on the wavelength, the distance between the cell and detector, the solid angle of photon collection, and the PMT gain. This approach effectively eliminates the need for the knowledge of local field factors, since these factors are divided by measuring in nearly the same local field. The number densities of the solvent, N_{solvent} , and solute, N_{solute} are calculated from the molecular weight and density. From the intercept and slope of the plot of $I_{2\omega}/I_\omega^2$ vs. number density, β_{solute} can be calculated provided β_{solvent} is known. The β values of several solvents are known in the literature and that of chloroform is 0.48×10^{-30} esu.²⁰

The β values of compounds 4a-c and 5a-c measured by using this technique are summarized in Table 3.2. The values show that prolinol derivatives have marginally higher coefficients compared to the corresponding butylthio derivatives indicating that prolinol is a slightly better donor moiety than butylthio group. Among the various substituents, β increases in the order:



The general trend is in agreement with expectations, since the NO_2 group is electron attracting and the methoxy group is the most electron donating among these compounds.

3.3.3.3. Theoretical Calculations

The structures of all the molecules were fully optimized by the Austin Modell (AM1) method²¹ of the MOPAC package.²² The ground state dipole moment, μ_g , and the first hyperpolarizabilities were computed using the same program. All 27 components of the SHG tensor are calculated in the Cartesian frame, but the most appropriate quantity is the vector component, β_x , theoretically defined as²³

$$\beta_x = \beta_{\mu\mu\mu} + 1/3 \sum (\beta_{\mu ii} + \beta_{ii\mu}) \quad 3.6$$

where, β_x is aligned along the direction of the molecular dipole moment and is therefore directly related to the nonlinear coefficients derived from the electric field poling method where molecules are oriented along the direction of their

dipole moments by a strong dc field. The intrinsic hyperpolarizability also is calculated for all these compounds, using equation 3.7.²³

$$\beta = (\beta_x^2 + \beta_y^2 + \beta_z^2)^{1/2} \quad 3.7$$

The results of computational calculations are summarized in Table 3.2. All the prolinol derivatives except 5a have higher dipole moments than the corresponding butylthio derivative. Electron delocalization is more in 4-substituted compounds, which is true even in the case of electron withdrawing substituents, though the values are smaller than that of electron releasing substituents. Because the dipole moment lies on an axis running from a point somewhere between the two donors to the acceptor, there are two major components

Table 3.2. Results of theoretical calculations. The β values reported are in 10^{-30} esu

Compound	μ (Debye)	β_x	β_y	β_z	β_o
4a	6.22	9.05	-1.31	0.94	7.63
4b	3.88	-13.34	0.55	-0.51	11.19
4c	6.51	10.98	1.96	0.27	8.66
4d	4.87	8.86	-3.80	0.012	8.36
4e	4.84	-8.45	-4.80	-0.44	1.70
5a	5.33	5.92	0.87	-0.39	4.51
5b	6.79	6.08	-0.07	-0.79	5.87
5c	7.14	7.24	0.39	0.90	6.46
5d	6.00	6.42	-2.39	-0.98	5.91
5e	6.53	5.83	-2.57	-0.94	2.80

to the hyperpolarizability. The positive value of β is obtained along the dipole axis and for other axes, its value is negative.

The calculated β values for the lowest energy conformations are plotted against the experimentally determined β values in Figure 3.1. Except for the nitro group a good correlation between the theoretical and experimental β values is observed for different substituents.

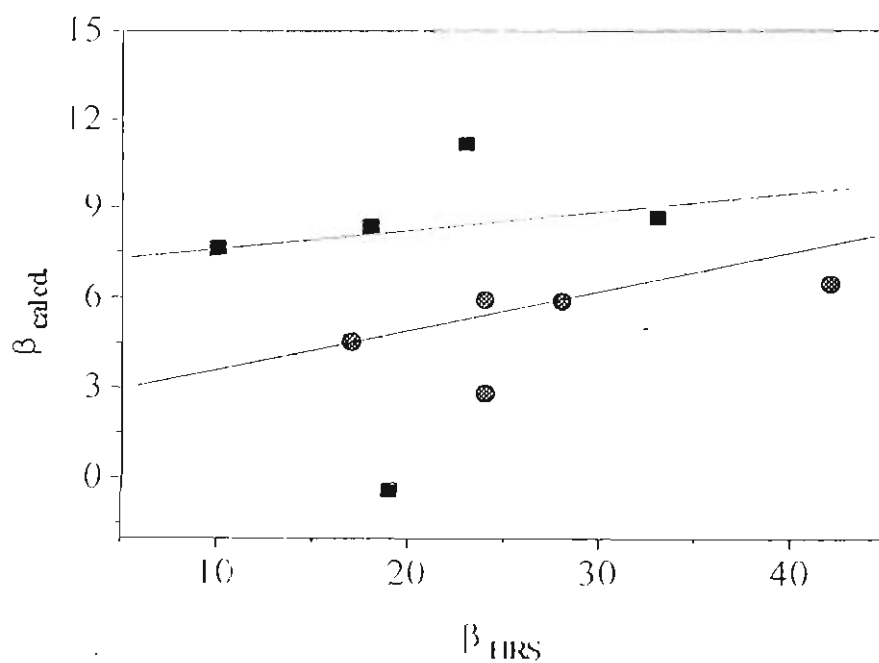


Figure 3.1. Correlation between the experimental and theoretical molecular values of β for (a) butylthio- (■) and (b) prolinol (●) substituted butadiene derivatives.

3.3.3.4. Determination of SHG Efficiency by Kurtz and Perry Powder Method

Powder NLO efficiencies of compounds **5a-e** were measured by Kurtz and Perry powder technique.²⁴ The results are summarized in Table 3.3. Compound **5a** has efficiency same as that of urea whereas all other compounds in this series are only slightly active. The low activity of other derivatives may be due to the centrosymmetric packing of the molecules in the bulk. Even though the molecules are chiral, dipole-dipole and other kinds of interactions may prevent the crystals from packing in a noncentrosymmetric arrangement.

Table 3.3. NLO efficiencies of compounds 5a-e measured by Kurtz and Perry powder method

Compound	$\lambda_{\text{cut off}}$	SHG intensity
Urea		1
5a	450	1
5b	450	1.53×10^{-3}
5c	450	1.09×10^{-2}
5d	455	6.43×10^{-3}
5e	460	3.72×10^{-3}

3.4. Experimental Section

Melting points are uncorrected and were recorded on a Mel-temp-II melting point apparatus. The IR spectra were determined on a Perkin Elmer Model 882 infrared spectrophotometer. Absorption studies were carried in a Shimadzu 2100 UV-vis spectrophotometer. Emission studies were carried out using a SPEX-

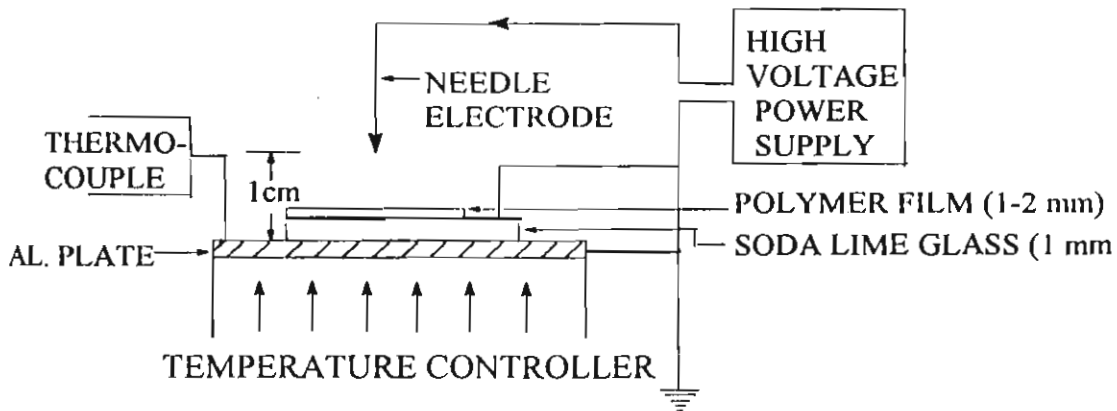
Fluorolog F-112 X spectrofluorimeter. NMR spectra were recorded on JEOL 90 MHz NMR spectrometer with tetramethylsilane as internal standard.

3.4.1. Second Harmonic Generation Measurements

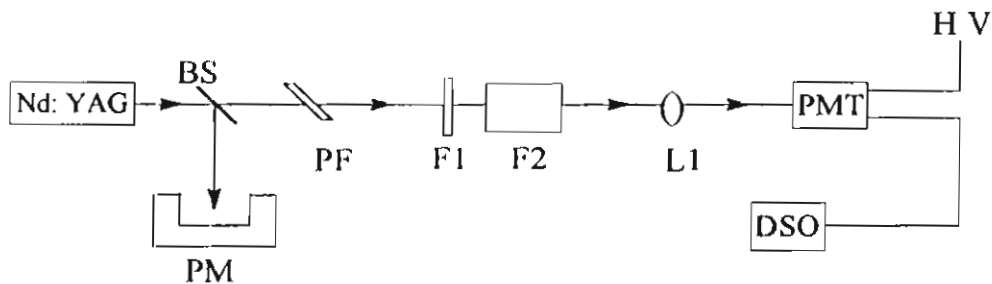
3.4.1.1. Electric Field Poling Method

The experimental setup for measurement of nonlinear coefficient is shown in Figure 3.2. Poly(methyl methacrylate) (PMMA) ($n^{20} = 1.4900$, $d = 1.188$, $mw = 120000$) used in this study was purchased from Aldrich Chemical Co. (USA) and used without further purification. A small quantity of the polymer along with 5 wt % of the chromophore (4a-c and 5a-c) was dissolved in spectroscopic grade chloroform and filtered. The resulting solution was spin coated on soda-lime glass slides. The films were dried at 60 °C for 6 h followed by heating at an elevated temperature above the glass transition temperature (T_g) for several hours in order to remove as much solvents as possible since the residual solvent acts as a plasticizer. The film uniformity was checked by measuring the absorbance (at λ_{max}) at various points in the film. Poling was performed using a corona discharge nearer the T_g of the polymer. The soda lime glass plate holding the film was heated to 100 °C on a hot plate. The dc field was applied through a stainless-steel needle electrode placed 1 cm above the grounded planar aluminium electrode, which was positioned on the hot plate. The applied voltage was 6 kV. SH intensities were measured using a Nd:YAG laser (spectra-physics, 10 Hz, 8 ns). The incident vertically polarized beam at 1064 nm was filtered (Schott BG 38 filter as well as copper sulfate solution) and the signal at 532 nm was collected using a UV-Vis PMT (Hamamatsu R 2059) the output of which was fed into a

digital oscilloscope. The SH intensities (in the doped polymer films) were obtained relative to a quartz plate (0.5 mm thickness, $l_c = 20.6$ mm, $d_{33} = 0.5$ pm/V).



(a)



(b)

Figure 3.2. (a) Schematic experimental setup for electric field poling and (b) for d_{33} measurement. BS – beam splitter, PM - power meter, PF - polymer film, F1 -filter (BG38), F2-filter (copper sulphate solution), L1-lens, PMT-photomultiplier tube, HV-high dc voltage, DSO- digital oscilloscope.

3.4.1.2. Hyper-Rayleigh Scattering (HRS) Measurements

The β values of compounds 4a-e and 5a-e were measured in chloroform by HRS technique. The experimental set up is schematically shown in Figure 3.3.

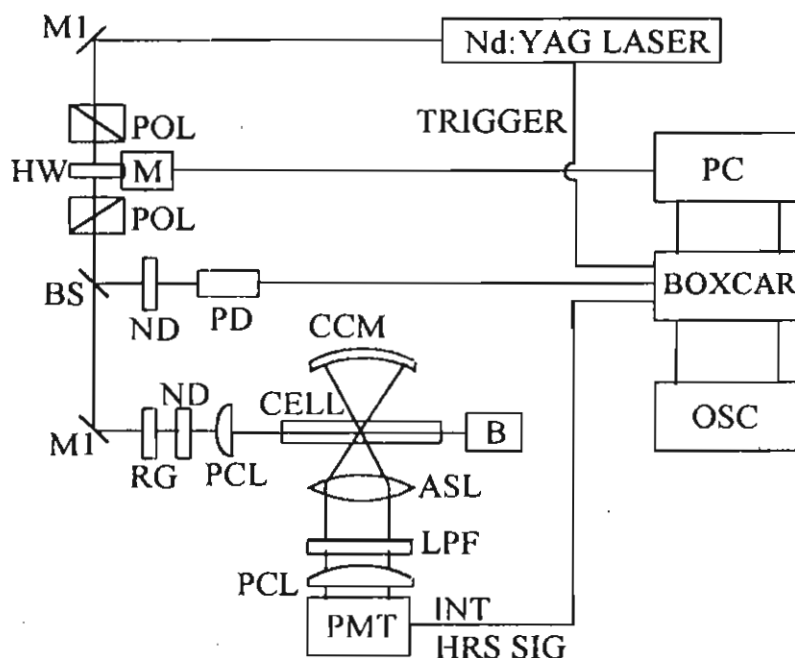


Figure 3.3. Experimental HRS setup: ASL - aspheric lens condenser, B - beam splitter, CCM - concave mirror, HW - half-wave plate, INT - 532 nm interference filter, LPF - low-pass filter, M - stepping mirror, M1 - mirror, ND - neutral density filter, OSC - oscilloscope, PC - personal computer, PCL - plano convex lens, PD - photodiode, PMT - photomultiplier tube, POL - polarizer, RG - high-pass filter, SIG - signal.

The fundamental of a Q-switched Nd:YAG laser (Spectra Physics, 8 ns) is focused on to a glass cell containing the solution. The second harmonic scattered light is collected into a sensitive UV-Visible photomultiplier tube. Other harmonics are

eliminated by a set of filters. A small fraction of the 1064 nm fundamental is directed toward an IR sensitive photomultiplier tube (PMT) for monitoring the incident light intensity. Signals from both PMTs are fed into a gated boxcar averager (SRS 250) to record the intensities of the incident and second order scattered light pulses after averaging over 1000 shots. All data were collected at laser powers (6.12 mJ/pulse) well below the threshold for stimulated Raman and Brillouin scattering, self-focusing or self-defocusing and dielectric breakdown.

3.4.1.3. Kurtz and Perry Powder Method

Nonlinear optical property of bulk materials was determined by this technique. The experimental details are described in Chapter 2.

3.4.2. Materials

Reagent grade reactants and solvents were used as received from chemical suppliers. Extremely dry solvents were prepared as per reported procedures. Spectroscopic grade solvents were used for all measurements.

Synthesis of 5-butylthio-2,4-pentadienones (4a-e)

Equimolar amounts of the aldehydes **3a-e** and Meldrum's acid were dissolved in the minimum amount of dry methanol. Few drops of 10% KOH solution were then added and the mixture was stirred at room temperature for 5 h, in each case. The products formed were purified by column chromatography.

2,2-Dimethyl-1,3-dioxane-4,6-dione-5(3-butylthio-3-phenylpropenylidene) (4a)

This compound was synthesized from 3-butylthio-3-phenylprop-2-enal (**3a**, 1 g, 4.55 mmol) and Meldrum's acid (655 mg, 4.55 mmol). The product formed was

purified by column chromatography using a mixture (1:9) of ethyl acetate and petroleum ether as eluent to give 1.2 g (76%) of a pure sample of **4a**, which melted at 79-80 °C, after recrystallization from benzene.

IR ν_{\max} (KBr): 2950, 2875 (CH), 1720 (C=O), 1575 (C=C) cm^{-1} ; UV λ_{\max} (CHCl_3): 314 (ϵ 5000 $\text{M}^{-1}\text{cm}^{-1}$), 411 nm (23700); ^1H NMR (CDCl_3): δ 0.85-1.10 (3 H, t, CH_3), 1.25-2.05 (4 H, m, CH_2), 1.75 (6 H, s, CH_3), 3.0-3.20 (2 H, t, SCH_2), 7.25-7.95 (7 H, m, aromatic and vinylic); ^{13}C NMR (CDCl_3): δ 13.39, 21.93, 27.36, 29.53, 33.02, 104.00, 105.79, 118.26, 128.64, 129.27, 130.61, 135.63, 152.60, 161.40, 163.37, 172.32. Exact mol wt calcd for $\text{C}_{19}\text{H}_{23}\text{O}_4\text{S}$ (MH^+) 347.1317; found 347.1310 (FAB, high resolution mass spectroscopy).

2,2-Dimethyl-1,3-dioxane-4,6-dione-5(3-butylthio-3-tolylpropenylidene) (4b)

Treatment of 3-butylthio-3-tolylprop-2-enal (**3b**, 2.5 g, 10.7 mmol) with Meldrum's acid (1.54 g, 10.7 mmol) gave **4b** as a red oily liquid. This was further purified by column chromatography using a mixture (1:4) of ethyl acetate and hexane as eluent to afford 3.6 g (93%) of a pure sample of **4b**, mp 89-90 °C, after recrystallization from benzene.

IR ν_{\max} (KBr): 2975, 2960, (CH), 1722, 1651 (C=O), 1556, 1530 (C=C) cm^{-1} ; UV λ_{\max} (CHCl_3): 413 nm (ϵ 24300 $\text{M}^{-1}\text{cm}^{-1}$); ^1H NMR (CDCl_3): δ 0.70-1.05 (3 H, t, CH_3), 1.20-1.60 (4 H, m, CH_2), 1.65 (6 H, s, CH_3), 2.35 (3 H, s, CH_3), 2.85-3.15 (2 H, t, SCH_2), 7.15-8.0 (6 H, m, aromatic and vinylic); ^{13}C NMR (CDCl_3): δ 13.24, 13.87, 21.06, 21.78, 27.15, 29.41, 31.65, 32.84, 103.73, 105.22, 117.90, 126.32, 128.61, 129.12, 129.18, 132.64, 141.00, 152.62, 163.28, 172.65. Exact

mol wt calcd for $C_{20}H_{25}O_4S$ (MH^+) 361.1474; found 361.1483 (FAB, high resolution mass spectroscopy).

2,2-Dimethyl-1,3-dioxane-4,6-dione-5-(3-butylthio-3-anisylpropenylidene) (4c)

Compound **4c** was prepared from 3-butylthio-3-anisyloropenal (**3c**, 1 g, 4 mmol) and Meldrum's acid (864 mg, 6 mmol). The product formed was purified by column chromatography over silica gel. Elution with a mixture (2:3) of hexane and chloroform gave 1.14 g (76%) of a pure sample of **4c** as a reddish brown solid, which melted at 61-62 °C, after recrystallization from benzene.

IR ν_{max} (neat): 2976, 2935, 2881 (CH), 1728, 1707 (C=O), 1575 (C=C) cm^{-1} ; UV λ_{max} ($CHCl_3$): 421 (ϵ 287050 $M^{-1}cm^{-1}$), 347 nm (7900); 1H NMR ($CDCl_3$): δ 0.85-1.10 (3 H, t, CH_3), 1.28-1.60 (4 H, m, CH_2), 1.75 (6 H, s, CH_3), 2.9-3.15 (2 H, t, SCH_2), 3.85 (3 H, s, OCH_3), 6.8-8.0 (6 H, m, aromatic and vinylic); ^{13}C NMR ($CDCl_3$): δ 12.97, 20.91, 21.45, 26.85, 29.18, 32.64, 54.80, 103.40, 104.60, 113.67, 113.79, 117.43, 127.54, 130.14, 130.61, 152.48, 161.40, 166.86, 172.20. Exact mol wt calcd for $C_{20}H_{24}O_5S$ (M^+) 376.1344; found 376.1329 (FAB, high resolution mass spectroscopy).

2,2-Dimethyl-1,3-dioxane-4,6-dione-5[3-butylthio-3-(4-bromophenyl)propenylidene] (4d)

Compound **4d** was synthesized from 3-butylthio-3-(4-bromophenyl) prop-2-enal (**3d**, 5 g, 16 mmol) and Meldrum's acid (2.4 g, 16 mmol). Purification by column chromatography using a mixture (1:9) of ethyl acetate and hexane gave 2.34 g (34%) of a pure sample of **4d**, as a yellowish brown liquid.

IR ν_{\max} (KBr): 3080, 2975, 2884 (CH), 1722 (C=O), 1579, 1560 (C=C) cm^{-1} ; UV λ_{\max} (CHCl_3): 252 (ϵ 12800 $\text{M}^{-1}\text{cm}^{-1}$), 407 nm (42500); ^1H NMR (CDCl_3): δ 0.80-1.10 (3 H, t, CH_3), 1.40-1.70 (4 H, m, CH_2), 1.75 (6 H, s, CH_3), 2.95-3.20 (2 H, t, SCH_2), 7.2-7.9 (6 H, m, aromatic and vinylic); ^{13}C NMR (CDCl_3): δ 13.33, 21.84, 27.29, 29.38, 32.99, 104.03, 106.27, 118.32, 125.12, 130.70, 131.87, 134.43, 151.74, 170.12.

2,2-Dimethyl-1,3-dioxane-4,6-dione-5[3-butylthio-3-(4-nitrophenyl)propenyli-dene] (4e)

Treatment of 3-butylthio-3-(4-nitrophenyl)prop-2-enal (**3e**, 2.5 g, 9.4 mmol) with Meldrum's acid (1.36 g, 9.4 mmol) gave **4e** as brown viscous liquid. This was further purified by column chromatography using a mixture (3:7) of ethyl acetate and hexane as eluent to afford 2.78 g (75%) of a pure sample of **4e**, which melted at 72-73 $^{\circ}\text{C}$, after recrystallization from benzene.

IR ν_{\max} (KBr): 3125, 3095, 2975, 2944 (CH), 1722 (C=O), 1579, 1560 (C=C) cm^{-1} ; UV λ_{\max} (CHCl_3): 295 (ϵ 17100 $\text{M}^{-1}\text{cm}^{-1}$), 408 nm (31800); ^1H NMR (CDCl_3): δ 0.75-1.10 (3 H, t, CH_3), 1.15-1.65 (4 H, m, CH_2), 1.75 (6 H, s, CH_3), 3.00-3.25 (2 H, t, SCH_2), 7.55-8.55 (6 H, m, aromatic and vinylic); ^{13}C NMR (CDCl_3): δ 13.18, 21.12, 27.18, 29.18, 31.56, 32.96, 104.15, 107.28, 118.80, 123.60, 129.42, 130.17, 141.68, 148.48, 150.42, 162.75, 167.22. Exact mol wt calcd for $\text{C}_{19}\text{H}_{21}\text{NO}_6\text{S}$ (M^+) 391.1076; found 391.4441 (FAB, high resolution mass spectroscopy).

Synthesis of 5-pyrrolidino (2-methanol)-2,4-pentadienones (5a-e)

Equimolar amounts of butylthio-substituted-pentadienones (4a-e) and L-prolinol were dissolved in dry methanol and refluxed for 10 h. The products formed were purified in each case by column chromatography.

2,2-Dimethyl-1,3-dioxane-4,6-dione-5[3-pyrrolidino(2-methanol)-3-phenyl propylidene] (5a)

Treatment of 2,2-dimethyl-1,3-dioxane-4,6-dione-5(3-butylthio-3-phenylpropenylidene) (4a, 2 g, 5.8 mmol) with pyrrolidine-2-methanol (0.39 g, 5.8 mmol) gave the crude product which was further purified by column chromatography using ethyl acetate as eluent to give 1.34 g (65%) of a pure sample of 5a, which melted at 88-89 °C, after recrystallization from ethyl acetate.

IR ν_{\max} (KBr): 3406 (CH), 1658 (C=O), 1573, 1551 (C=C) cm^{-1} ; UV λ_{\max} (CHCl_3): 246 (ϵ 10100 $\text{M}^{-1}\text{cm}^{-1}$), 410 nm (58400 $\text{M}^{-1}\text{cm}^{-1}$); ^1H NMR (CDCl_3): δ 1.65 (6 H, s, CH_3), 1.8-2.4 (5 H, m, CH_2 and OH), 3.2-3.5 (2 H, m, NCH_2), 3.7-4.1 (2 H, m, OCH_2), 4.2-4.4 (1 H, m, NCH), 7.1-7.8 (7 H, m, aromatic and vinylic); ^{13}C NMR (CDCl_3):²⁵ δ 22.22, 22.91, 26.58, 27.15, 27.36, 50.33, 53.31, 60.59, 61.67, 62.50, 62.89, 92.28, 93.05, 102.60, 105.34, 105.88, 127.24, 129.84, 128.32, 128.64, 129.39, 129.93, 132.31, 133.21, 155.76, 162.36, 162.78, 163.40, 163.76, 165.13, 169.43, 169.76. Exact mol wt calcd for $\text{C}_{20}\text{H}_{24}\text{NO}_5$ (MH^+) 358.1654; found 358.1630 (FAB, high resolution mass spectroscopy).

2,2-Dimethyl-1,3-dioxane-4,6-dioxane-5[3-pyrrolidino(2-methanol)-3-tolyl-propylidene] (5b)

Compound **5b** was synthesized from **4b** (2.5 g, 7.2 mmol) and prolinol (0.73 g, 7.2 mmol). Purification of the crude product by column chromatography using ethyl acetate as eluent gave **5b** as a reddish brown solid 2.02 g (72%), which melted at 123-124 °C, after recrystallization from benzene.

IR ν_{\max} (KBr): 3427 (OH), 3012, 2960, 2892 (CH), 1722, 1677 (C=O), 1534 (C=C) cm^{-1} ; UV λ_{\max} (CHCl_3): 410 nm (ϵ 57600 $\text{M}^{-1}\text{cm}^{-1}$); ^1H NMR (CDCl_3): δ 1.60 (6 H, s, CH_3), 1.75-2.30 (5 H, m, CH_2 and OH), 2.40 (3 H, s, CH_3), 3.10-3.35 (2 H, m, NCH_2), 3.65-3.95 (2 H, m, OCH_2), 4.25-4.55 (1 H, m, NCH), 7.0-7.65 (6 H, m, aromatic and vinylic); ^{13}C NMR (CDCl_3):²⁵ δ 13.42, 20.55, 21.78, 22.28, 25.95, 26.61, 49.91, 52.92, 59.70, 61.25, 61.73, 62.62, 91.11, 91.83, 101.97, 105.05, 105.70, 126.74, 127.39, 128.79, 129.75, 139.50, 155.02, 163.01, 163.31, 164.75, 169.91. Exact mol wt calcd for $\text{C}_{21}\text{H}_{25}\text{NO}_5$ (M^+) 371.1733; found 371.1742 (FAB, high resolution mass spectroscopy).

2,2-Dimethyl-1,3-dioxane-4,6-dione-5[3-pyrrolidino(2-methanol)-3-anisylpropylidene] (5c)

Treatment of **4c** (750 mg, 2 mmol) with prolinol (202 mg, 2 mmol) gave a crude product which was further purified by column chromatography using ethyl acetate as eluent to give a pure sample of **5c**, 500 mg (65%), mp 129-130 °C, after recrystallization from benzene.

IR ν_{\max} (KBr): 3430, 2249 (CH), 1715, 1658 (C=O), 1551 (C=C) cm^{-1} ; UV λ_{\max} (CHCl_3): 412 nm (ϵ , 41000 $\text{M}^{-1}\text{cm}^{-1}$); ^1H NMR (CDCl_3): δ 1.65 (6 H, s, CH_3),

1.75-2.30 (5 H m, CH₂ and OH), 3.15-3.45 (2 H, m, NCH₂), 3.55-3.75 (2 H, m, OCH₂), 3.85 (3 H, s, OCH₃), 4.25-4.50 (1 H, m, NCH), 6.85-7.70 (6 H, m, aromatic and vinylic); ¹³C NMR (CDCl₃):²⁵ δ 13.60, 17.45, 20.28, 22.04, 22.64, 26.22, 27.00, 40.60, 51.91, 53.34, 54.86, 59.96, 61.43, 90.99, 91.77, 102.39, 102.48, 105.94, 106.51, 113.40, 121.93, 123.93, 124.86, 129.51, 145.86, 155.41, 160.33, 160.54, 163.49, 163.97, 165.31, 166.98, 168.41, 169.13, 169.85, 170.26, 174.23. Exact mol wt calcd for C₂₁H₂₅NO₆ (M⁺) 387.1682; found 387.1655 (FAB, high resolution mass spectroscopy).

2,2-Dimethyl-1,3-dioxane-4,6-dione-5[3-pyrrolidino(2-methanol)-3-(4-bromophenyl)propylidene] (5d)

Compound **5d** was synthesized from 2,2-dimethyl-1,3-dioxane-4,6-dione-5[3-butylthio-3-(4-bromophenyl)propenylidene] (**4d**, 2.43 g, 5.5 mmol) and prolinol (0.55 g, 5.5 mmol). The product formed was purified by column chromatography using ethyl acetate as eluent to give 2.0 g (83%) of the pure sample of **5d** as a waxy solid.

IR ν_{\max} (KBr): 3373 (OH), 2987, 2952, 2884 (CH), 1718, 1673 (C=O), 1538, 1530 (C=C) cm⁻¹; UV λ_{\max} (CHCl₃): 413 nm (ϵ 46000 M⁻¹cm⁻¹); ¹H NMR (CDCl₃): δ 1.65 (6 H, s, CH₃), 1.80-2.45 (5 H, m, CH₂ and OH), 3.10-3.35 (2 H, m, NCH₂), 3.70-3.95 (2 H, m, OCH₂), 4.25-4.50 (1 H, m, NCH), 7.0-7.85 (6 H, m, aromatic and vinylic); ¹³C NMR (CDCl₃): δ 22.64, 26.37, 27.06, 53.25, 60.11, 61.73, 92.25, 92.87, 102.51, 105.11, 124.14, 129.51, 131.06, 131.87, 155.14, 163.07, 163.46, 165.01, 168.00, 168.33.

2,2-Dimethyl-1,3-dioxane-4,6-dione-5[3-pyrrolidino(2-methanol)-3-(4-nitrophenyl)propylidene] (5e)

Treatment of **4e** (1 g, 2.55 mmol) and prolinol (0.26 g, 2.55 mmol) gave a crude product which was further purified by column chromatography using ethyl acetate as eluent to give a pure sample of **5e**, 800 mg (78%), which melted at 138-139 °C, after recrystallization from chloroform.

IR ν_{\max} (KBr): 3383 (OH), 2979, 2960, 2899 (CH), 1727, 1667 (C=O), 1569, 1537 (C=C) cm^{-1} ; UV λ_{\max} (CHCl_3): 415 nm (ϵ 32800 $\text{M}^{-1}\text{cm}^{-1}$); ^1H NMR (CDCl_3): δ 1.35-1.75 (6 H, s, CH_3), 1.80-2.35 (5 H, m, CH_2 and OH), 3.15-3.60 (2 H, m, NCH_2), 3.80-4.00 (2 H, m, OCH_2), 4.15-4.50 (1 H, m, NCH), 7.15-7.85 (6 H, m, aromatic and vinylic); ^{13}C NMR (CDCl_3):²⁵ δ 22.82, 26.55, 26.70, 27.36, 53.28, 60.35, 62.11, 62.59, 63.16, 93.68, 94.30, 103.02, 104.87, 105.31, 124.05, 129.27, 138.91, 139.47, 148.31, 148.46, 155.05, 163.13, 163.52, 164.95, 166.51, 166.77. Exact mol wt calcd for $\text{C}_{20}\text{H}_{22}\text{N}_2\text{O}_7$ (M^+) 402.1404; found 402.4048 (FAB, high resolution mass spectroscopy).

3.5. References

1. Bredas, J. L. in *Organic Materials for Photonics: Science and Technology*; Zerbi, G. Ed. Elsevier Science, Amsterdam, 1993, p 127.
2. Prasad, P. N.; Williams, D. J. *Introduction to Nonlinear Optical Effects in Molecules and Polymers*; Wiley-Interscience, New York, 1991, p. 42 and references cited therein.
3. Lalama, S. J.; Garito, A. F. *Phys. Rev. A*. 1979, 20, 1179.
4. Marder, S. R.; Beratan, D. N.; Cheng, L. -T. *Science* 1991, 252, 103.

5. Stahelin, M.; Burland, D. M.; Rice, J. E. *Chem. Phys. Lett.* **1992**, *191*, 245.
6. Ramesha, S.; Das, P. K. *Chem. Phys.* **1990**, *145*, 343.
7. Willand, C. S.; Feth, S. E.; Scozzafava, M.; Williams, D. J.; Green, G. D.; Weinschenk, J. I.; in *Nonlinear Optical and Electroactive Polymers*; Prasad, P. N.; Ulrich, D. R. Eds.; Plenum, New York, 1998.
8. Clays, K.; Persoons, A.; De Mayer, L. *Adv. Chem. Phys.* **1994**, *85*, 455.
9. Zyss, J.; Van, T. C.; Dhenaut, C.; Ledoux, T. I. *Chem. Phys.* **1993**, *177*, 281.
10. Clays, K.; Persoons, A. *Phys. Rev. Lett.* **1991**, *66*, 2980.
11. Clays, K.; Hendrickx, E.; Triest, M.; Verbiest, T.; Persoons, A.; Dehu, C.; Bredas, J.-L. *Science*, **1993**, *262*, 1419.
12. Laidlaw, M.; Denning, R. G.; Verbiest, T.; Chauchard, E.; Persoons, A. *Nature* **1993**, *363*, 58.
13. Reichardt, C. *Chem. Rev.* **1994**, *94*, 2319.
14. Hojo, M.; Masuda, R.; Okada, E. *Synthesis* **1990**, 425.
15. Mortazavi, M. A.; Knoesen, A.; Kowel, S. T.; Higgins, B. G.; Dienes, A. J. *Opt. Soc. Am. B.* **1989**, *6*, 733.
16. Erich, M.; Sen, A.; Looser, H.; Bjorklund, G. C.; Swalen, J. D.; Tweig, R.; Yoon, D. Y. *J. Appl. Phys.* **1989**, *66*, 2559.
17. Hampsch, H. L.; Yang, Y.; Wong, G. K.; Torkelson, J. M. *Macromolecules* **1988**, *21*, 526.
18. Hayashi, A.; Goto, Y.; Nakayama, M.; Kaluzynski, K.; Sato, H.; Kato, K.; Kondo, K.; Watanabe, T.; Miyata, S. *Chem. Mater.* **1992**, *4*, 555.
19. Meredith, G. R.; van Dusen, J. G.; Williams, D. J. *Macromolecules* **1982**, *15*, 1385.
20. Ray, P. C.; Das, P. K. *J. Phys. Chem.* **1995**, *99*, 14414.

21. Dewar, M. S. J.; Zoebisch, E. G.; Healy, E. F.; Stewart, J. *J. Am. Chem. Soc.* **1985**, *107*, 3902.
22. QCOMP program 137 Version 6.12, Department of Chemistry, Indiana University, Bloomington, IN 47405.
23. Docherty, V. J.; Pugh, D.; Morley, J. O. *J. Chem. Soc. Faraday Trans.* **1985**, *81*, 1179.
24. Kurtz, S. K.; Perry, T. T. *J. Appl. Phys.* **1968**, *39*, 3798.
25. ^{13}C NMR spectrum shows peaks more than the number of carbon atoms due to the restricted rotation of the C-N bond leading to the existence of two different conformers.

CHAPTER 4

SYNTHESIS AND STUDIES OF NONLINEAR OPTICAL AND PHOTOSWITCHING PROPERTIES OF SOME CHOLESTEROL-LINKED AZOBENZENE DERIVATIVES

4.1. Abstract

The synthesis and photophysical characterization of some azobenzene linked cholesterol derivatives has been described. The liquid crystalline properties of these compounds were studied by differential scanning calorimetry (DSC) and polarizing optical microscopy (POM) techniques. It has been observed that these compounds exhibit liquid crystalline phase over a wide range of temperature, which depends on the nature of the substituents linked to the azobenzene chromophore. All these compounds exhibited a cholesteric mesophase on heating, whereas smectic mesophase appeared on cooling. The presence of donor and acceptor substituted azobenzene imparts electrooptical and nonlinear optical (NLO) properties to these molecules. Their NLO properties have been studied by electric field poling as well as hyper-Rayleigh scattering techniques. The highest nonlinear coefficient was obtained for compound 5a. This can be attributed to the greater dipole moment of this molecule, brought about by the proper donor (OC_2H_4) and acceptor (NO_2) combination. The presence of azobenzene moiety also imparts photochromic properties to these compounds. *Trans-cis* photoisomerization of these compounds in eutectic mixtures consisting of cholesteryl oleyl

carbonate, cholesteryl chloride and cholesteryl nonanoate was studied by irradiating at 355 nm. Thin films of cholesteric liquid crystals made from eutectic mixtures of cholesterol derivatives containing the azobenzene-linked cholesterols, which show a reflectance band in the visible region were prepared. Photoinduced *trans-cis* isomerization of the azobenzene chromophore in these films leads to a large shift in the reflectance band resulting in visual change in the colour of the films. These processes have been examined in detail.

4.2. Introduction

Certain molecules do not show a single phase transition from the crystalline to the liquid state on heating, but rather a series of transformations involving new phases possessing a state of aggregation intermediate between those of highly ordered crystals and of isotropic liquids. For this reason they are termed as liquid crystals (LC) or mesogens. Liquid crystals can be roughly categorized as lyotropic or thermotropic liquid crystals. Lyotropic liquid crystals are formed from compounds with amphiphilic properties dissolved in a solvent, which is most commonly water. At intermediate concentrations of the compound in solution, anisotropic properties characteristic of liquid crystal phases can be obtained. Common examples of such lyotropic liquid crystals are those produced from soaps and other detergent systems in water. Thermotropic liquid crystals are formed from predominantly organic compounds, which are mainly either rod- or disc-shaped. Heating such crystalline solids or cooling them from their isotropic liquid phase can give rise to liquid crystalline phases. Several materials exist in the LC phase at room temperature, and many other room temperature LC materials can be produced by using mixtures of compounds. All components of the mixture need not necessarily be individually capable of forming LC phases in the latter case. An

essential requirement for liquid crystalline or mesomorphic behaviour is that the molecules must be geometrically anisotropic in shape.

The vast majority of thermotropic liquid crystals are composed of rod-like molecules and can be classified into three types, namely smectic, nematic and cholesteric mesophases.¹ The smectic mesophase is a turbid, viscous state with certain properties reminiscent of those found for soaps. The term 'smectic' is derived from the Greek, 'smectos' (soap like). They have stratified structures and a variety of molecular arrangements are possible within each stratification.^{2,3} Smectic mesophases adopt three different textures depending on: (i) the nature of the compound under consideration, (ii) the way in which the mesophase is produced, e.g., by heating the crystals, by cooling the isotropic liquid, or by cooling the nematic mesophase, and (iii) the nature and the cleanliness of the supporting surface employed to mount the specimen.

Nematic liquid crystals have a high degree of long range orientational order of molecules, but no long-range translational order. On surfaces such as glass, the mesophase frequently adopts a characteristic 'threaded' texture, clearly visible between crossed polaroids, and the word 'nematic' again stems from the Greek, 'nematos', meaning thread-like. The point group symmetry of the nematic phase is $D_{\infty h}$. A notable difference between the smectic and nematic mesophases lies in the way in which the two mesophase types separate from the isotropic liquid. Whilst the smectic mesophase appears as batonnets, the nematic mesophase separates as tiny, spherical droplets, which coalesce to form a nematic texture.

The third class of thermotropic liquid crystals is very similar to nematics except that the molecules contain chiral groups. This type of LC phase is known as chiral nematic or cholesteric mesophase since this type of texture was first

observed in derivatives of cholesterol or other sterols such as cholesteryl esters derived from open chain aliphatic acids.⁴ However, compounds derived from other systems also exhibit cholesteric mesophase as in the case of optically active amyl *p*-(4-cyanobenzylideneamino)cinnamate. It may also be noted that not all cholesteric compounds exhibit cholesteric LC phase. Many of the open-chain aliphatic esters of cholesterol exhibit smectic mesophase in addition to cholesteric mesophase. However there is no known case of a compound which gives both a cholesteric and a nematic mesophase.¹

The difference between cholesteric and nematic mesophases is that in cholesterics the director (the unit vector describing the average direction of the molecular long axis) is not constant in space, but undergoes a helical distortion.⁵ The structure may be envisaged as composed of layers or sheets of nematic liquid crystal, as shown in Figure 4.1. The director of an individual layer is rotated through a small angle with respect to the director in adjacent layers. As a succession of layers is passed through, the director turns through 360° and this thickness represents the pitch length (p) for the helix. The twist may be right handed or left handed depending on the molecular conformation. The energy of twist forms only a minute part (10^{-5}) of the total energy associated with the parallel alignment of the molecules.⁶ The spiral arrangement of the molecules in the cholesteric phase is responsible for its optical properties, namely selective reflection of circularly polarized light and a rotatory power about a thousand times greater than that of an ordinary optically active substance.

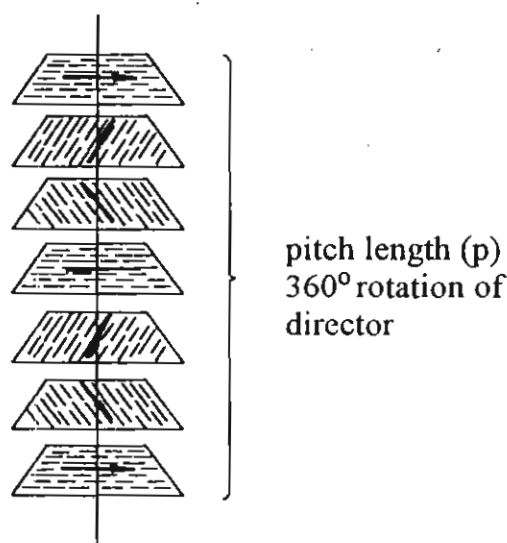


Figure 4.1. The cholesteric liquid crystal: schematic representation of the helical structure

The unique optical properties of cholesteric phase are due to the presence of helical structure. Classically, isotropic liquids containing chiral molecules, e.g., sugar solutions, are described as optically active, since the right- and left-handed components of plane polarized light propagates at different velocities, causing the plane of propagation of the emerging beam to be rotated. This property is often referred to as circular birefringence and gives rise to rotations of about $10^\circ/\text{mm}$. In the case of cholesteric liquid crystals, there is therefore a twofold optical activity: (i) molecular and (ii) macromolecular, associated with the helical structure. When plane polarized light propagates through this structure its right handed and left handed components see different refractive indices, resulting in phase retardation between them. Therefore the resultant plane of polarized light is rotated. The

important difference in this case is that the rotation is much greater, of the order of $1000^\circ/\text{mm}$.

A unique feature of the helical structure is the selective light reflection, which is the origin of brilliant colours that are displayed under certain conditions. The reflected wavelength is related to the pitch length (p) and refractive index (n) of the film as,

$$\lambda = np \quad 4.1$$

The selective reflection is analogous to Bragg X-ray diffraction.^{7,8} This can be explained by considering Fig. 4.1. Each layer represents the director orientation in that direction. Therefore for each layer or sheet, two refractive indices may be defined: n_c parallel to the director and n_o at right angles to it in the same plane. If a plane polarized beam with the same wavelength as the helix enters the structure with its plane of polarization parallel to the director, and if the helix is right handed, then one circularly polarized component will propagate seeing some average refractive index and be transmitted. However the other component will see a sinusoidal variation in refractive index along the helix axis with n_c repeat at every 180° rotation or $p/2$ spacing and be scattered. The scattered light from each $p/2$ plane constructively interferes and is reflected as right handed circularly polarized light, whose wavelength is given by,

$$\lambda = n_c p \quad 4.2$$

By the same process, incident plane polarized light with its plane orthogonal to the director will have 50% of its intensity reflected and its wavelength is given by,

$$\lambda' = n_o p \quad 4.3$$

When ordinary white light is incident on the helix, all wavelengths between λ and λ' are reflected so that the band width is given by,

$$\Delta\lambda = p(n_c - n_o) \quad 4.4$$

where,

$$n = n_c - n_o \quad 4.5$$

As a consequence of this circular dichroism, cholesteric LCs show an anomalous dispersion in their rotatory power at the selective reflection wavelength. This is analogous to the Cotton effect given by optically active isotropic liquids containing a chromophore.⁹

Although in the above description of selective reflection, an analogy was drawn to Bragg reflection, there are two important features which are different and are not adequately or easily explained by this simple model: (i) only first-order reflections occur at normal incidence, and (ii) the reflected wavelength dependence on the angle of incidence does not obey Bragg's law ($\lambda = n_2 d \sin\theta$). To explain these points accurately, more detailed theoretical arguments based on Maxwell's equation have been proposed by several authors.¹⁰⁻¹²

The optical properties of cholesterics were recognized by both Reinitzer and Lehmann at the time of their early investigations which culminated in the discovery of the liquid crystalline state.^{13,14} White light is incident on a 'planar' sample whose optic axis is perpendicular to the glass surface, selective reflection

takes place, the wavelengths of the reflected maxima varying with the angle of incidence in accordance with Bragg's law.

The pitch of cholesteric liquid crystals may be changed by weak external physical perturbations such as temperature, pressure, electrical and magnetic fields¹⁵⁻¹⁷ as well as by dissolved molecules. Ferguson reported the colour change of cholesteric phases by traces of dissolved gases.^{18,19} In the late 1960s, Haas *et al.* reported a change in the selective reflectivity of the cholesteric LC mixture composed of cholesteryl bromide and other cholesteryl derivatives on photoirradiation.²⁰ This change in the reflectivity arose from a change in the helical pitch of the cholesteric LC resulting from the photochemical reaction of cholesteryl bromide in the LC mixture. They also found that irradiation with UV light of LC cells containing mesogens with stilbene units in the molecules brought about *trans-cis* isomerization of the stilbene units, causing simultaneously nematic (N) to isotropic (I) phase transition of the host LC. The irreversible change in the selective reflectivity of cholesteric pitch was also reported by Haas *et al.* in 1974.²¹

In most pure cholesteric materials, the pitch is a decreasing function of the temperature. An elementary picture of the temperature dependence of the pitch can be given in analogy with the theory of thermal expansion in crystals.²² The strong temperature dependence of the pitch has practical applications in thermography, as was first demonstrated by Ferguson.^{23, 24} The material has to be so chosen that the pitch is of the order of the wavelength of visible light in the temperature range of interest. This is achieved by preparing suitable mixtures. Small variations of temperature are shown up as changes in the colour of the scattered light and can be used for visual display of surface temperatures,^{25,26} imaging of infrared²⁷⁻²⁹ and microwave³⁰ patterns, etc.

Pollmann and Stegemeyer investigated the effect of pressure on the pitch of cholesteryl oleyl carbonate (COC) mixed with cholesteryl chloride and found that the pitch increases very rapidly with pressure,¹⁶ the effect being more pronounced the greater the concentration of COC. This is attributed to the increase in the transition temperature with increasing pressure,³²⁻³⁴ so that the pitch at room temperature may be expected to rise accordingly.

The dependence of pitch on composition was first described by Friedel.¹ For a given composition there is an inversion of the rotatory power as the temperature is varied, indicating a change in the handedness of the helix. The inverse pitch exhibits a linear dependence on temperature, passing through zero at the nematic point where there is an exact compensation of the right- and left-handed forms. A similar reversal of handedness takes place as the composition is varied.³⁵ The inverse pitch shows a linear relationship with composition around the nematic point, but there are significant departures when one of the components has a smectic phase at a lower temperature.³⁶ It is well known that a nematic liquid crystal readily adopts a helical configuration if a small amount of a cholesteric is added to it. For low concentrations of the cholesteric, the inverse pitch is a linear function of the concentration, but at higher concentrations, the linear law is not obeyed.³⁷ A small quantity of a non-mesomorphic optically active compound may also transform a nematic into a cholesteric.³⁸ However, the handedness of the helix does not seem to be directly related to the absolute configuration of the solute as has been shown by Saeva.³⁹

Liquid crystals can be switched by relatively modest electric and magnetic fields and hence they are particularly suited for applications in nonlinear optics⁴⁰⁻⁴² and optical switching⁴³ devices. Liquid crystals usually consist of organic molecules with aromatic cores and there is considerable experimental⁴⁴ and

theoretical^{45,46} evidence to indicate that the dominant contribution to the polarizabilities in the molecular level originate from the delocalized π -electrons in conjugated portions of these molecules. The bulk susceptibilities of liquid crystals are related to the orientational order of the non-spherical molecules in the material, which results in anisotropic susceptibilities. For uniaxial phases, different linear susceptibilities are found for fields parallel and perpendicular to the local symmetry axis or director. The director tends to reorient in the presence of an external field and results in a large change in dielectric tensor of the material. Therefore director reorientation is mainly responsible for large nonlinear susceptibilities in liquid crystals. Optical nonlinearity in liquid crystals can also originate from changes in the degree of orientational order, and from changes in density due to the action of the optical field,⁴⁷⁻⁴⁹ and may involve laser heating^{50,51} or other mediating mechanisms.^{52,53}

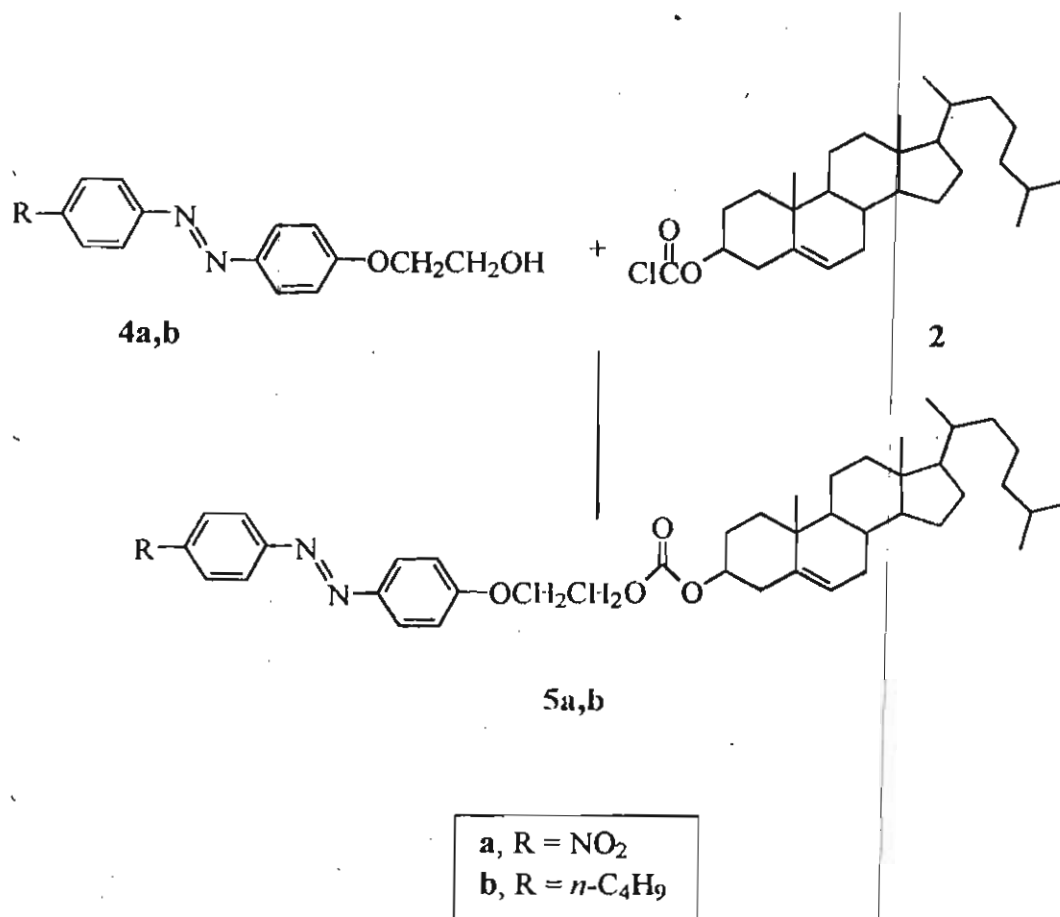
SHG was one of the first areas of investigation in the field of nonlinear optics of liquid crystals. SHG coefficient is nonzero only if the molecule is noncentrosymmetric. Nematic liquid crystals possess $D_{\infty h}$ symmetry and therefore they would not be expected to give rise to SHG. However SHG was observed in aligned samples of MBBA,^{54,55} with the suggestion that the nematic phase may not be centrosymmetric. Detailed theoretical studies of SHG in nematics however, indicated that the electric quadrupole effects and not the lack of centrosymmetry is responsible for the experimentally observed SHG in nematics.⁵⁶⁻⁵⁸

Ferroelectric chiral smectic C phases are distinguished by spontaneous polarization and hence lack centrosymmetry. The first experiment to measure SHG from ferroelectric liquid crystals was carried out by Vtyurin *et al.* using unaligned samples under a dc electric field.⁵⁹ When the fundamental and the SH waves propagate with the same phase velocity, phase matching SHG occurs. Phase

matched SHG from ferroelectric liquid crystals was first observed by Barnik et al. who used an electric field to unwind the helix and obtained the phase matching by adjusting the temperature and thus the tilt angle.⁶⁰ In recent reports also electric fields were applied to induce uniform director alignment, but the cell was rotated to achieve phase matching.^{61,62}

Cholesteric liquid crystals are noncentrosymmetric and as such they might be expected to give rise to SHG. However studies showed that the SH signals originate from crystalline particles present in the sample, and the melting of these leads to disappearance of the SH signal.⁶³ SHG in cholesteric liquid crystals were first observed in cholesteryl carbonate.⁶⁴ Electric field induced SHG in cholesterics was reported recently by Ozaki *et al.*⁶⁵ The electric field dependence of SHG was interpreted in terms of the increase in polarization density due to flexoelectric deformation.⁶⁶ SH intensity in this case was found to vary with the square of the applied electric field.

Several reports are there in the literature on the study of NLO properties of azobenzene derivatives⁶⁷⁻⁷¹ and on their optical switching applications.^{43,72,73} Azobenzene derivatives have been investigated for their nonlinear optical behaviour, because of their large dipole moments and the stability of the azo linkage. Additionally, the bathochromic shift induced by substitution with donor and acceptor groups in these systems facilitates resonance enhancement effects, and can be easily functionalized chemically. Some cholesterol linked azobenzene derivatives have been synthesized and their photoinduced ionic conductivity and gelation properties have been investigated.⁷³⁻⁷⁵ The nonlinear optical properties of these compounds were studied by electric field poling⁷⁶ as well as hyper-Rayleigh scattering techniques.⁷⁷



Scheme 4.2

4.3.1. Liquid Crystalline Properties

Phase transition characteristics of these compounds were studied by differential scanning calorimetry (DSC) and hot stage polarized optical microscopy (POM). POM of **3a** showed oily streak mesophase characteristics of a cholesteric phase⁷⁸ on first heating in the temperature range 170–221 °C (Figure 4.2, A, 50 times magnified). This phase remained as such till isotropization was

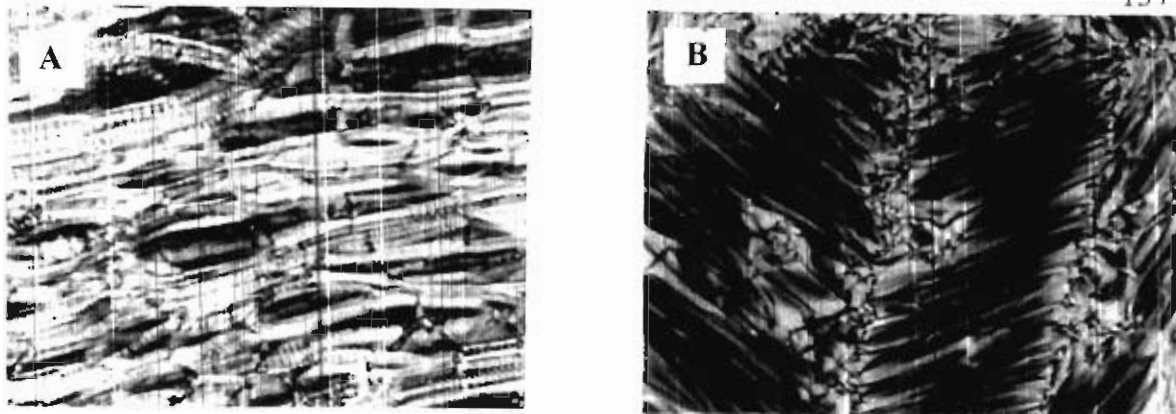


Figure 4.2. Optical micrographs of 3a: (A) oily streak of cholesteric phase and (B) focal conic texture of smectic phase.

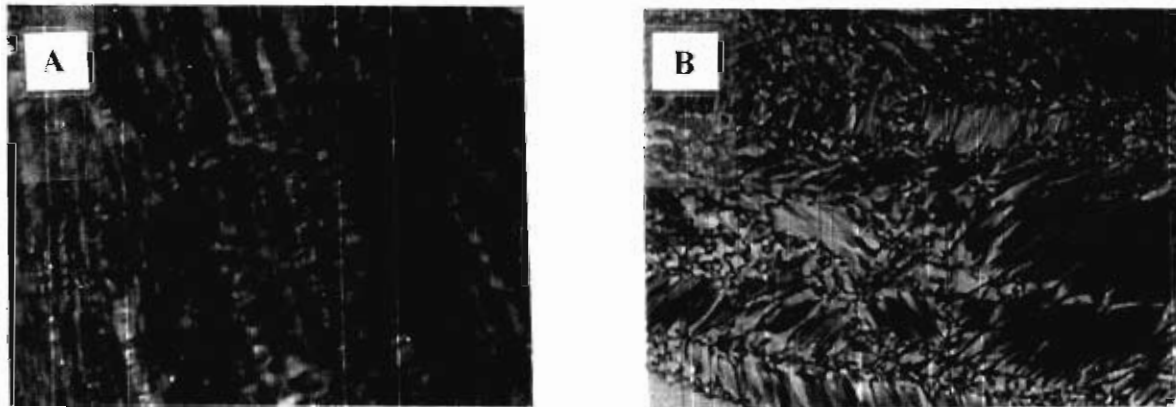


Figure 4.3. Optical micrographs of 3b: (A) cholesteric phase and (B) focal conic texture of smectic phase.



Figure 4.4. Optical micrographs of 3c: cholesteric phase.

observed at 221 °C. On cooling, however, focal conic texture of the smectic phase⁷⁸ appeared between 220-120 °C (Figure 4.2, B, 50 times magnified) and the compound crystallized at 110 °C. Focal conic texture of smectic mesophase and cholesteric texture with oily streaks are common for conventional low molecular liquid crystals.⁷⁸ The phase transition temperatures are highly reproducible over several heating and cooling cycles. The reproducibility was confirmed by DSC measurements, shown in Figure 4.5. However, DSC measurements showed only the transition from crystal to cholesteric phase on heating and crystallization exotherm on cooling. No isotropization endotherm or smectic transition was observed under DSC. It is not very clear as to why the phase

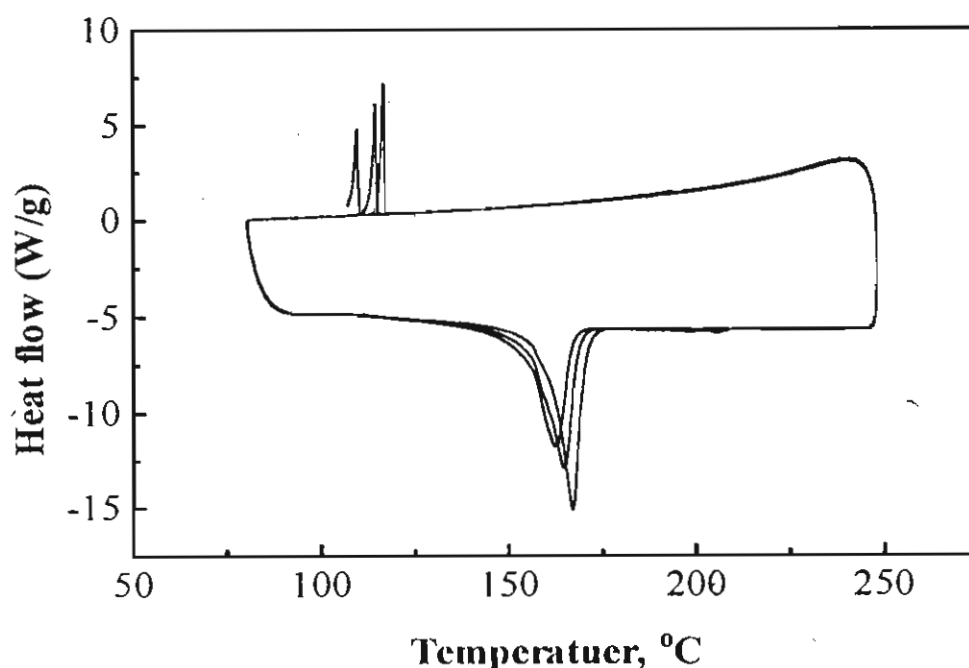


Figure 4.5. DSC trace of 3a showing several heating and cooling cycles

transitions observed under POM were not fully reflected in the DSC measurements. The thermal stability of 3a was studied by TGA and the decomposition curve is shown in Figure 4.6. From Figure 4.6 it is clear that the compound is stable up to 275 °C, under air and inert atmosphere. All the other

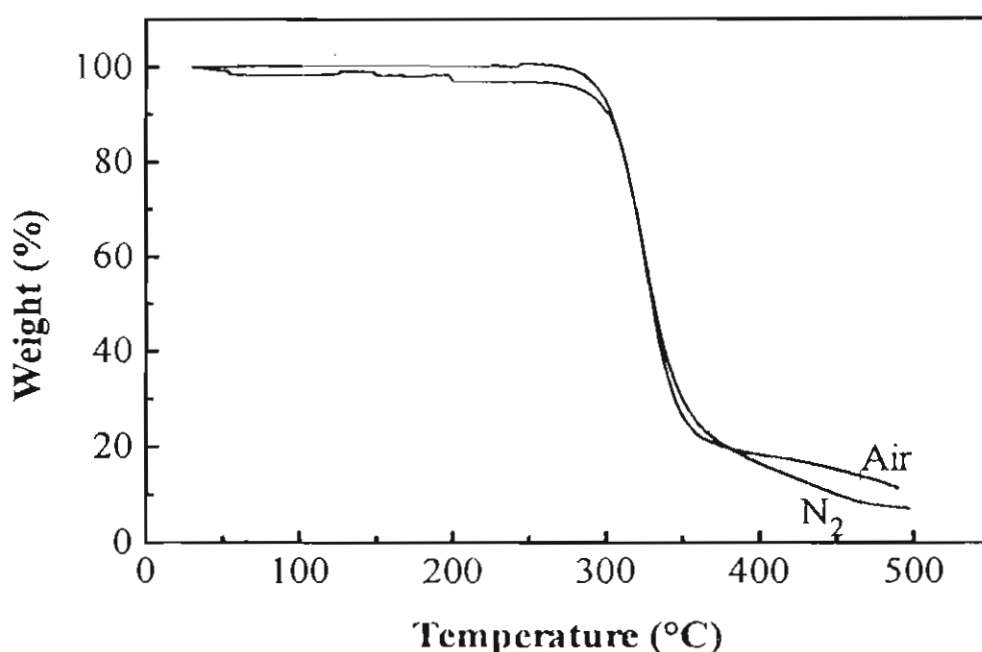


Figure 4.6. TGA curve of compound 3a under air and nitrogen atmosphere.

compounds in the series except 3c and 5a also showed characteristic oily streak textures of cholesteric phase on heating and smectic A (S_A) phase, on cooling. Compound 3c decomposed on heating just at its isotropization point whereas 5a showed cholesteric mesophase on cooling with the finger print texture (Figure 4.8, B). Figures 4.3, 4.4 and 4.7- 4.9 show the optical micrographs of cholesteric and smectic mesophases of compounds 3b-d and 5a, b. The phase transition temperatures of 3b-d and 5a,b were however, not reproducible on repeated heating

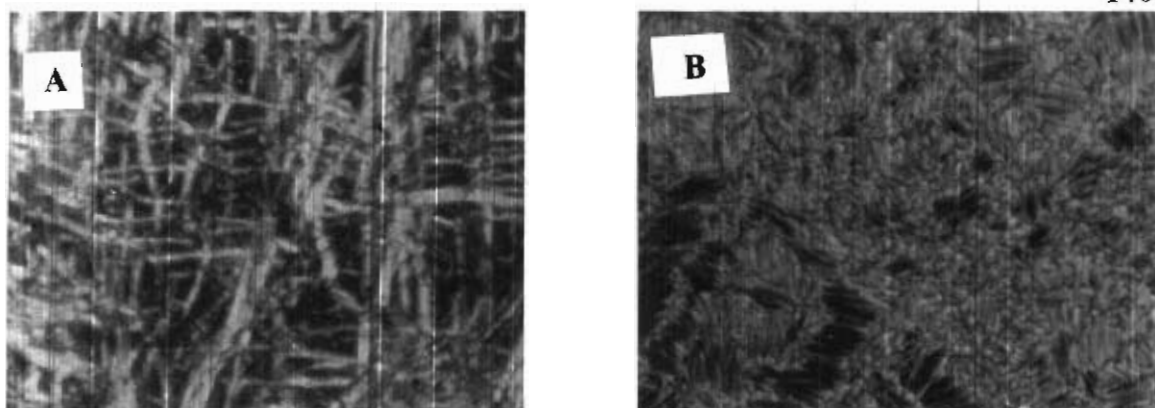


Figure 4.7. Optical micrographs of 3d: (A) oily streak of cholesteric phase and (B) focal conic texture of smectic phase.

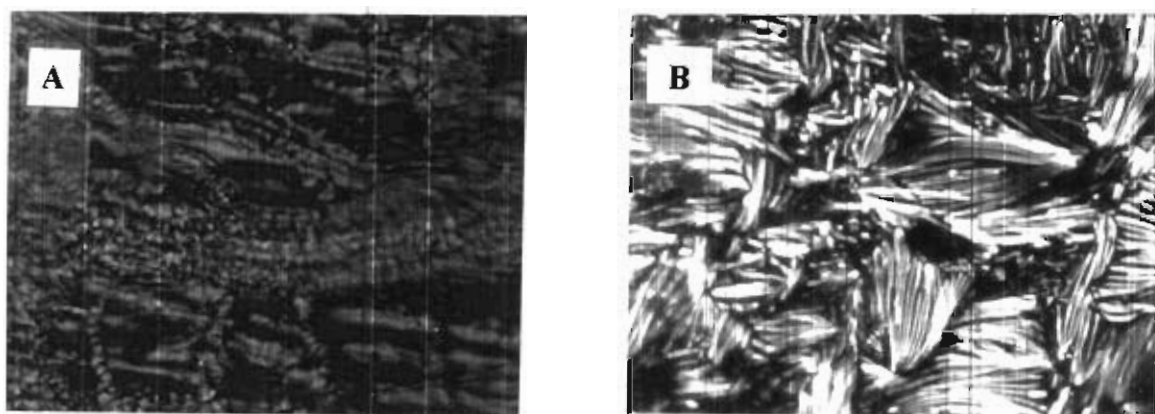


Figure 4.8. Optical micrographs of 5a: (A) oily streak of cholesteric phase on heating and (B) finger print texture of cholesteric phase on cooling.

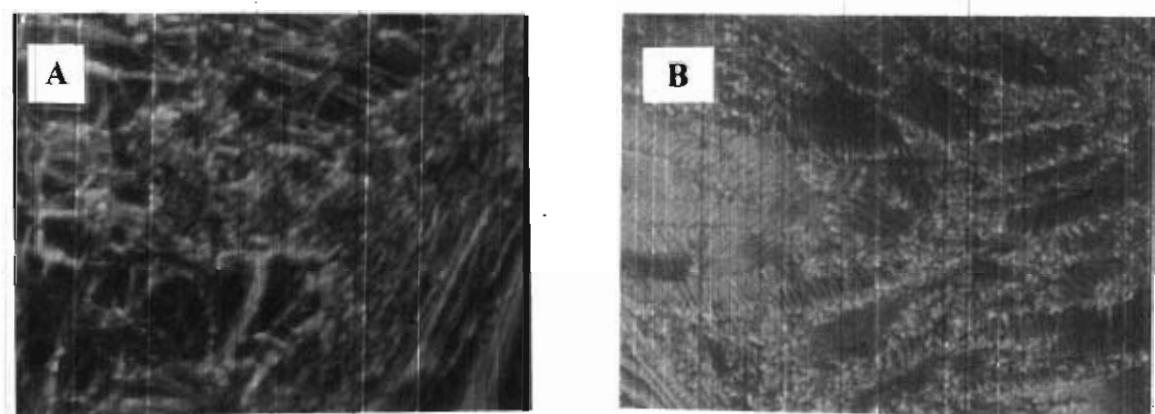


Figure 4.9. Optical micrographs of 5b: (A) oily streak of cholesteric phase and (B) focal conic texture of smectic phase.

and cooling cycles. This can be explained on the basis of the thermal stability of these compounds. The TGA curve of **3b** for example, is shown in Figure 4.10. From this figure it is clear that the decomposition temperature of **3b** is close to that of its isotropization temperature. After each heating cycle a small amount of the compound undergoes decomposition and the decomposed products change the phase transition temperature of these materials. The DSC trace of compound **3b**, after repeated heating and cooling cycles, is shown in Figure 4.11. The decomposition temperatures of other compounds are also close to the isotropization temperature and show similar DSC pattern. The phase transition temperatures of the first heating and cooling cycle as well as the decomposition temperatures of these compounds measured by TGA are summarized in Table 4.1.

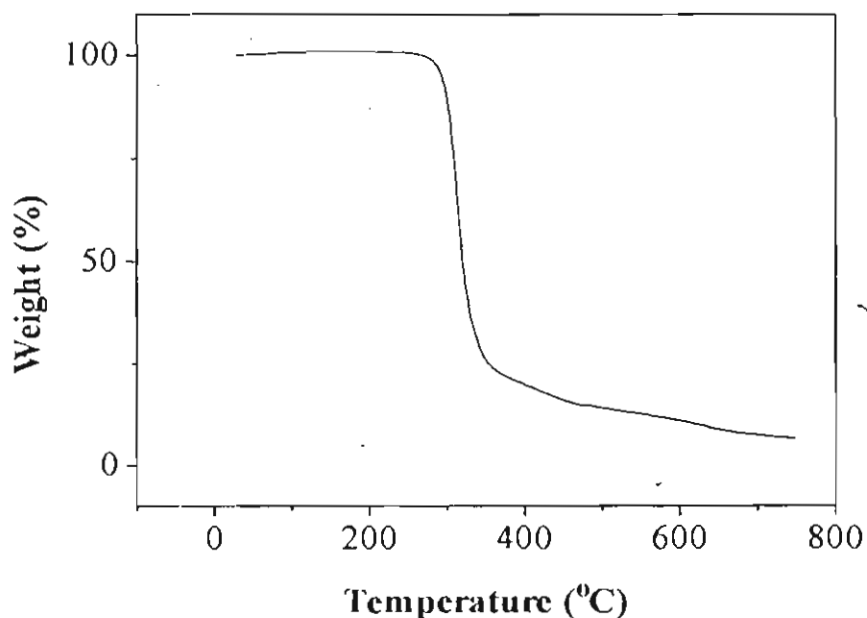


Figure 4.10. TGA curve of 3b under nitrogen atmosphere.

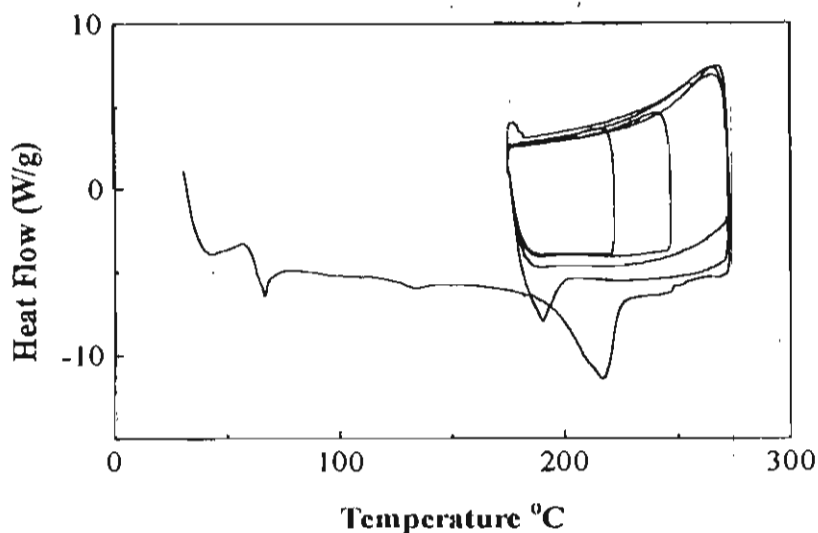


Figure 4.11. DSC trace of 3b showing several heating and cooling cycles.

Table 4.1. Phase transition properties of 3a-d and 5a,b examined by DSC and POM techniques

Compound	Decomposition temp. (TGA)	DSC ^a T_h (°C)	POM ^b (°C)
3a	270	172, 240	K 170 Ch 221 I I 220 S _A 120 K
3b	273	208, 265	K 202 Ch 266 I I 242 S _A 186 K
3c	110	205	K 196 Ch 231 I
3d	271	138	K 140 Ch 254 I I 248 S _A 150 K
5a	268	220	K 216 Ch 264 I I 179 S _A 171 K
5b	271	135	K 137 Ch 250 I I 247 S _A 163 K

^aFirst heating cycle; T_h =transition temperatures on heating,

^bK=crystalline; S_A=monotropic smectic A; Ch=cholesteric and I=isotropic phase.

4.3.2. Nonlinear Optical Studies

Nonlinear optical properties of compounds **3a-d** and **5a,b** were measured by both electric field poling and hyper-Rayleigh scattering techniques. Electric field poling was performed in thin films consisting of 5 wt % of the compound in PMMA (mw 20,000). Alignment of the chromophore was achieved by applying a high dc voltage (~ 3000 V) across the film, which was kept at a temperature above the glass transition temperature (T_g) of the polymer. Because of the anisotropic nature of liquid crystals, application of electric field generates a torque within the molecule, which can give rise to a reorientation of the director. Polar azo groups present in the molecule also tend to align in the electric field. Due to the ease with which both the cholesterol group and chromophore moiety can align in the electric field, the electric field poling was performed at a lower field. The d_{33} values of these compounds were obtained relative to quartz plate (0.5 mm thickness, $l_c = 20.6 \mu\text{m}$, $d_{33} = 0.5 \text{ pm/V}$). The results are summarized in Table 4.2.

Table 4.2. Observed NLO coefficients of the cholesterol derivatives

Compound	DM (azo compd.) (Debye units)	β (azo compd.) (10^{-30} esu)	d_{33} (pm/V)	β_{HRS} ($\times 10^{-30}$ esu)
3a	0.43	1.11	3.87	22
3b	7.05	7.15	3.48	86
3c	2.01	9.41	4.84	42
3d	0.20	1.00	3.10	36
5a	7.03	10.79	7.74	96
5b	3.26	1.14	1.35	41

The dipole moment and β values of the corresponding azo compounds calculated theoretically^{79, 80} are also given for comparison. NLO coefficient of these compounds increases with increasing dipole moment. The maximum value is obtained for compound **5a**, where the donor (OC_2H_4) and acceptor (NO_2) combination tend to maximize the dipole moment and subsequently the NLO properties among this class of compounds. The d_{33} value of this compound (7.74 pm/V) is comparable to that of quartz. There is a good correlation between the NLO coefficient determined experimentally with the dipole moment (Figure 4.12). The NLO coefficient increases with increasing dipole moment. The low d_{33} value of **5b** is attributed to

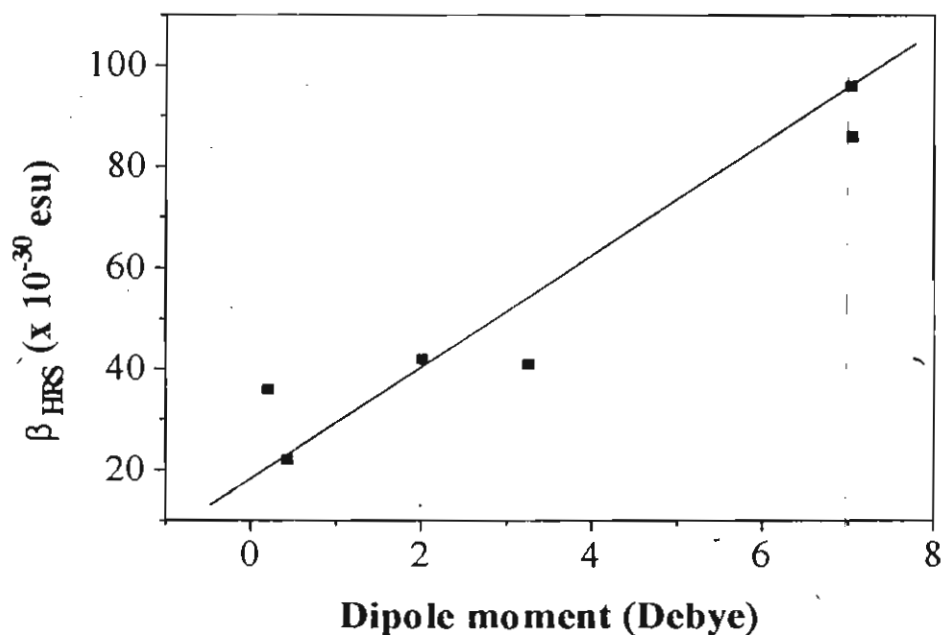


Figure 4.12. Correlation between dipole moment of the azo moiety and β_{IRS} values of the corresponding cholesterol derivatives.

the greater flexibility of chromophore moiety due to the presence of butyl group at one end and the ethoxy group at the other. Even though the greater flexibility favors the proper alignment of the molecules in the applied electric field, it also enhances a faster reorientation to the initial state after the removal of the field. The β values of these azobenzene linked cholesterol derivatives are slightly higher than those of azobenzene derivatives reported⁸¹ and theoretically calculated using the MOPAC program.^{79,80}

4.3.3. Photoinduced Pitch Change of Liquid Crystalline Films

Thin films consisting of the cholesterol derivative was prepared by dissolving 10 mol percentage of compounds **3a-d** and **5a,b** in a cholesteric mixture consisting of cholesteryl oleyl carbonate (COC), cholesteryl chloride (CC) and cholesteryl nonanoate (CN) in the ratio 55:130:210 respectively, in each case, by weight. Thin layers of mixtures were sandwiched between glass plates previously rubbed with 0.25 μm of diamond paste. Mylar spacers of 0.8 mm thickness were placed between these plates. Transparent films with planar textures were obtained when the eutectic mixtures were sheared between the glass plates, in each case. These mixtures showed characteristic visible reflection colours of cholesteric pitch and are stable between the temperature range of 20 °C to 73 °C. All the measurements were performed within the temperature range where the cholesteric mesophase was stable.

The change in helical pitch upon irradiation of the film using 355 nm light was monitored by following the reflectance band as well as the absorbance of the *cis*-isomer. When a eutectic mixture of COC, CC and CN containing 10 mol percent of **3a**, for example was irradiated at 355 nm, there was a decrease in

intensity of absorption at 355 nm whereas the *trans* form absorbs and a concomitant increase in intensity at 450 nm which is the region where the *cis* form absorbs (Figure 4.13). This indicates that the conversions are brought about by the *trans-cis* photoisomerization of the azobenzene moiety as shown in Scheme 4.3. These changes were accompanied by a red-shift of the reflectance band suggesting an enhancement of the pitch of the cholesteric mixture. Figure 4.14 shows the shift of reflectance band as a function of irradiation time for this mixture. The maximum change namely 50 nm shift was reached after about 200 seconds irradiation. Similar results were obtained for eutectic mixtures containing 3d and 5b. In all these studies the maximum change in reflectance band was observed within about 100-200 seconds of irradiation. Table 4.3 shows the maximum

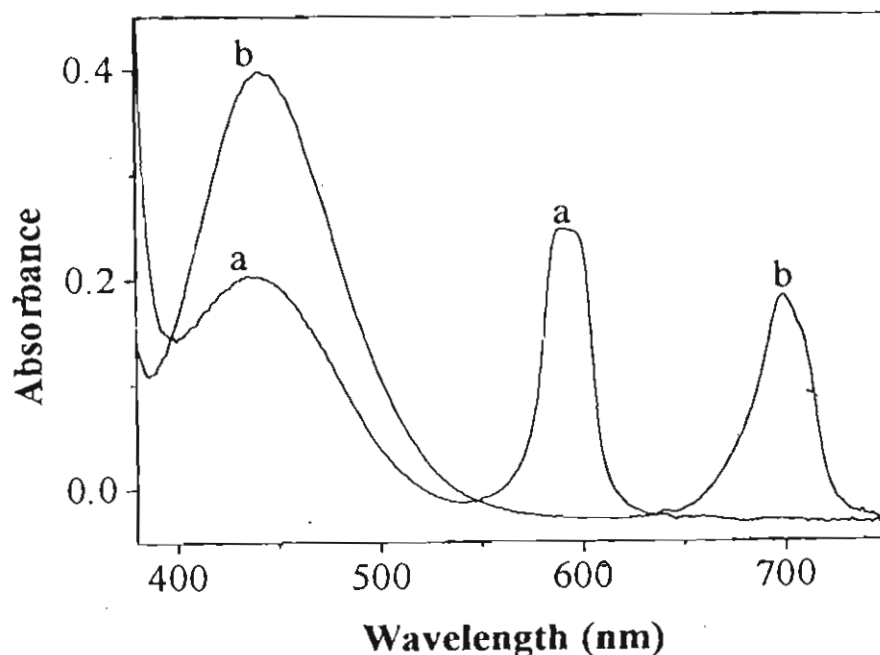
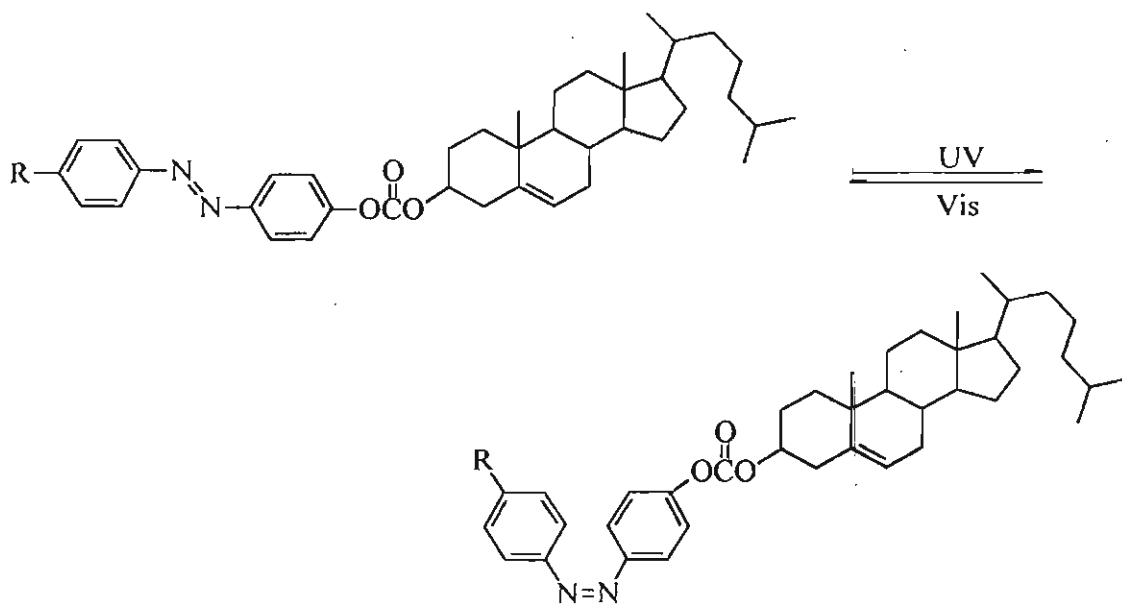


Figure 4.13. Absorption spectra of eutectic mixture of 3a. (a) before irradiation and (b) after irradiation.



Scheme 4.3

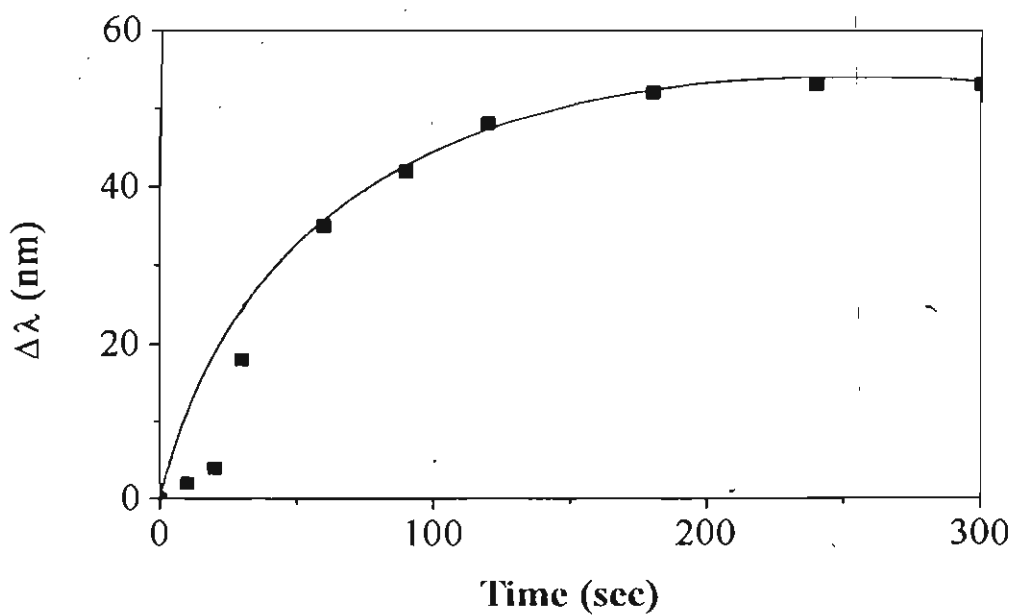


Figure 4.14. Change of reflectance band ($\Delta\lambda$) of eutectic mixture of 3a on irradiation at 60 °C.

Table 4.3. Maximum change of reflectance band of eutectic mixtures of 3a-d and 5a,b upon irradiation for 5 min at 60 °C

Compound	$\Delta\lambda$ nm
3a	63
3b	5
3c	23
3d	59
5a	4
5b	103

shift in λ_{\max} of reflectance band on irradiation for these mixtures. The best change, namely 103 nm shift was observed for the eutectic mixture containing **5b**. These changes can also be perceived visually as a colour change from green to red, on irradiation, as shown in Figure 4.15.

The thermal *cis-trans* isomerization, which occurs over very long periods, depending on the temperature of the film is accompanied by a return of the reflectance band to its original value. Figure 4.16 shows these changes for the eutectic mixture of **3a**, after irradiating the film for 5 min at 60 °C.



Figure 4.15. Visual change of reflectance on irradiation of a thin film made from a cholesteric mixture consisting of cholesteryl oleyl carbonate, cholesteryl chloride, cholesteryl nonanoate and compound 3a in the ratio 55:130:210:15 by weight. The initials of Photochemistry Research Unit (PRU) have been imaged on the film using a photomask. The irradiated portions are coloured red whereas the unirradiated portions are coloured green (λ_{\max} of irradiation, 355 nm).

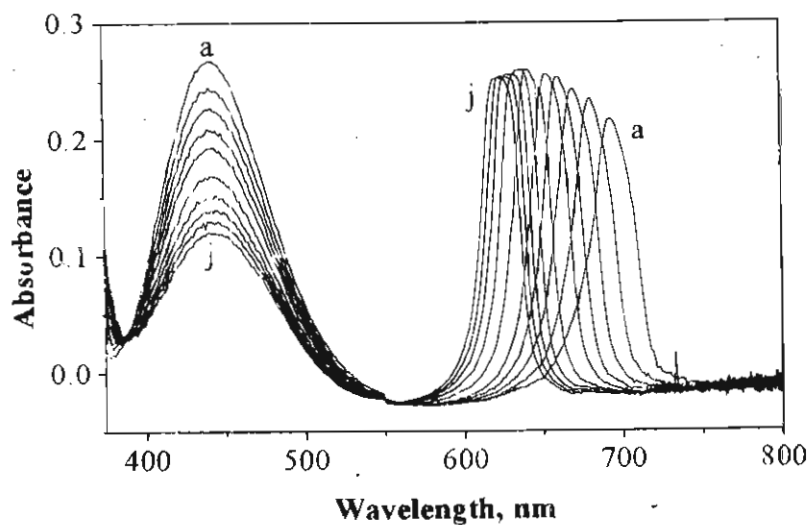


Figure 4.16. Change of cholesteric pitch of eutectic mixture of 3a, at different time intervals after irradiation at 60 °C for 5 min. a) 0 min, b) 15 min, c) 30 min, d) 45 min, e) 60 min, f) 90 min, g) 120 min, h) 150 min, i) 80 min, j) 220 min.

Eutectic mixture of compounds **3d** and **5b** also exhibit similar properties. Figure 4.17 illustrates the reverse *cis-trans* thermal transition of films containing eutectic mixture of **5b**, after irradiation at 60 °C for 300 seconds. Other compounds in the series did not show much shift which may be due to the fast reverse transition (*cis-trans*), after photoirradiation.

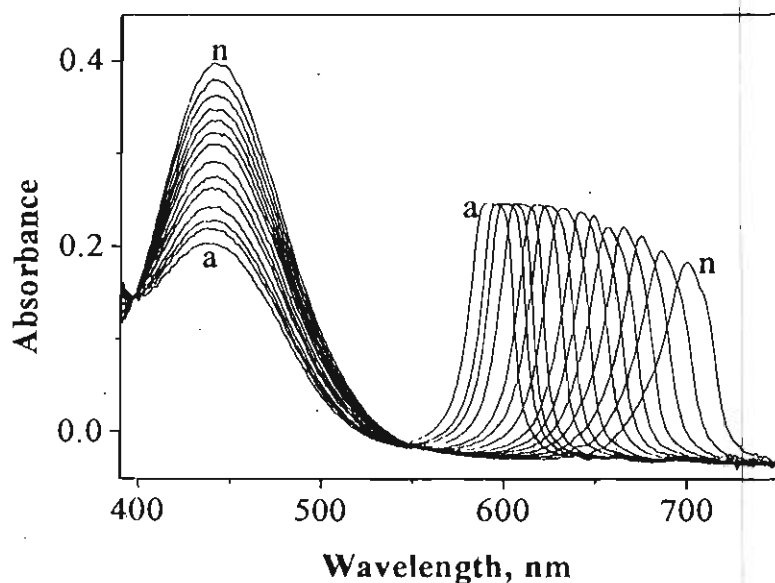


Figure 4.17. Change of cholesteric pitch of eutectic mixture of **5b**, at different time intervals after irradiation at 60 °C for 5 min. a) 0 min, b) 5 min, c) 10 min, d) 15 min, e) 20 min, f) 25 min, g) 30 min, h) 40 min, i) 50 min, j) 60 min, k) 80 min, l) 100 min, m) 120 min, n) 200 min.

The *cis-trans* isomerization, that occurs in the dark follows first order kinetics as shown in Figure 4.18 for **3a**. The rate constant for these processes were calculated using the rate equation of the first order kinetics (equation 4.6),

$$k = \frac{2.303}{t} \log \frac{A_{\infty} - A_0}{A_{\infty} - A_t} \quad 4.6$$

where, k is the rate constant of reaction, A_0 and A_t are the initial absorbance and at time t , respectively, and A_{∞} is the final value of absorbance. The rate constant for the reverse transition (*cis-trans*) at different temperatures for **3a** are shown in Table 4.4. From the plot of $\log k$ versus temperature (K), the activation energy of the process can be calculated using the Arrhenius equation (equation 4.7),

$$k = \exp(-\Delta E/RT) \quad 4.7$$

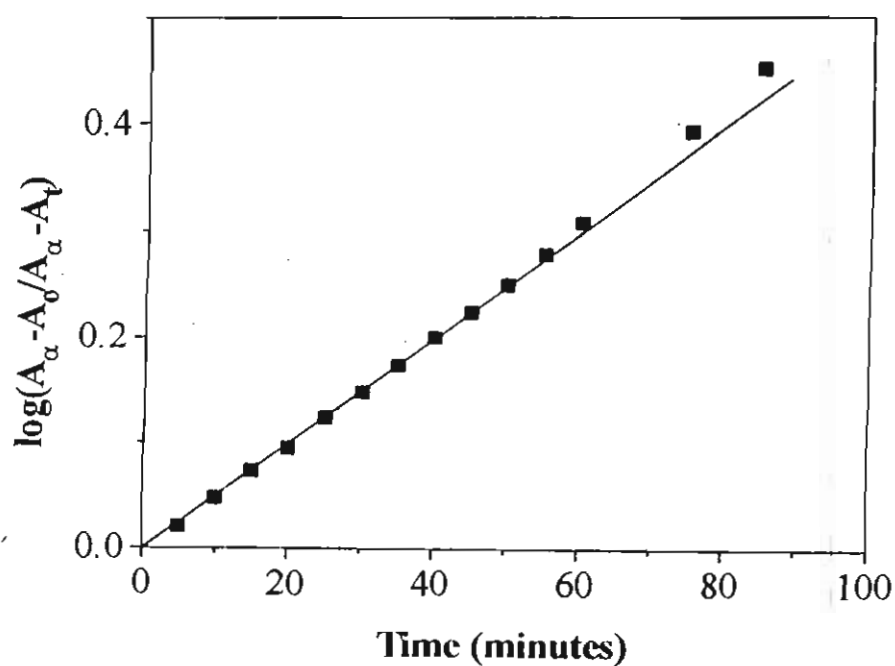


Figure 4.18. Kinetic plot of **3a** cutectic mixture, showing the rate of formation of *trans* isomer after irradiation at 60 °C.

Table 4.4. Rate of *cis-trans* isomerization of a eutectic mixture of 3a at different temperatures

T (K)	k (sec ⁻¹)
316	4.10 x 10 ⁻³
323	4.50 x 10 ⁻³
333	1.50 x 10 ⁻²
343	2.83 x 10 ⁻²
353	1.75 x 10 ⁻¹

where, ΔE is the activation energy of the process and is found to be 92.71 kJmol⁻¹. The reported activation energy of photoisomerization of azobenzene in *n*-heptane is 94.05 kJmol⁻¹.⁸¹ This shows that even though the bulk viscosity of the liquid crystal matrix is greater than that of *n*-heptane, the micro viscosity around the azo moiety is the same in both these cases.

Most photochromic molecules can change their molecular shape upon photoirradiation, and this property has been used extensively to control the orientation of LCs by light.⁸³⁻⁸⁶ For instance, the *trans*-form of azobenzene derivatives is rod-like, which stabilizes the LC phase, whereas the *cis* form is bent and destabilizes the LC phase when it is present. Therefore the *trans-cis* photoisomerization of azobenzenes in LC phase can cause disorganization of the phase structure. This leads to a change in the pitch length and consequently, a change in the reflectance wavelength according to equation 4.1: The reversible change of the selective reflectivity on photoirradiation of cholesteric LCs doped with azobenzene was reported by Sackmann in 1971.⁸⁷ Ogura *et al.* in 1982 reported the photo-

chemical phase transition of smectic LC doped with photochromic azobenzene derivatives.⁸⁸

Azobenzenes exist in two isomeric forms, the E (*trans*) and the Z (*cis*) form which can be recognized by the difference in their UV absorption spectra.⁸⁹ Hartley was the first to establish the influence of light on the configuration of the N=N double bond.⁹⁰ Photoirradiation of the mixture with UV light caused the *trans-cis* isomerization of azobenzene derivatives, lowering the smectic-to-nematic transition temperature (T_{sn}) of the mixture, and induced the phase transition to the nematic state at the exposed area. In this way, the image is stored in the mixture, which is then kept very stable by transforming the nematic phase to the smectic phase by photoirradiation with a visible light. In all these reports, azobenzene derivatives were doped on to cholesteric mixture and the colour change was obtained on photoisomerization of the azo moiety. In this report, however, azobenzene derivatives are covalently attached to the cholesterol frame. These systems showed greater change of reflectance band (more than 100 nm) whereas in the previous reports it is only of the order of 50 nm.⁸⁷

4.4. Experimental Section

Melting points are uncorrected and were recorded on a Mel-temp-II melting point apparatus. IR spectra were recorded on a Perkin Elmer Model 882 IR spectrometer. NMR spectra were recorded on a JEOL 90 MHz NMR spectrometer with tetramethylsilane as internal standard. Phase transitions were observed under Nikon HFX 35A Optiphot polarized light microscope equipped with Linkam THMS 600 heating and freezing stage connected to Linkam TP92 temperature programmer. DSC scans were performed using Du Pont DSC 2010 Differential

Scanning Calorimeter attached to Thermal Analyst 2100 data station under air. The heating rate was 20 °C/min in all cases. Nonlinear optical studies were carried out as described in Chapter 3.

Steady state photolyses were carried out on an ORIEL optical bench. Monochromatic light wave was obtained by using band pass filters. Eutectic mixtures of the cholesterol derivatives **3a-d** and **5a,b** were prepared by melting 10 mol percentage of the corresponding compound in cholesteric mixture consisting of cholesteryl oleyl carbonate (COC), cholesteryl chloride (CC) and cholesteryl nonanoate (CN) in the ratio 55:130:210, respectively, by weight. The temperature of the film was kept constant by circulating water through the film holder, at the desired temperature. The reflection and absorption studies were carried out using Shimadzu UV 2100 and GBC UV spectrophotometers.

4.4.1. Materials

Reagent grade reactants and solvents were used as received from chemical suppliers. Extremely dry solvents were prepared as per reported procedures. Spectroscopic grade solvents were used for all measurements. Cholesteryl oleyl carbonate and cholesteryl nonanoate were purchased from Aldrich Chemical Co. USA and used without further purification. Cholesteryl chloride, purchased from Aldrich Chemical Co. USA was further purified by column chromatography, using hexane as eluent.

General procedure for the synthesis of cholesteryl derivative of azobenzenes

Equimolar amounts of azobenzene and pyridine were dissolved in benzene and to it was added a solution of an equivalent amount of cholesteryl chloroformate in benzene. The contents were refluxed for 1 h, the precipitated salt was

removed by filtration and the benzene solution of the product was purified by column chromatography over silica gel. Elution with benzene gave the pure products as reddish yellow solids. The products were further purified by recrystallization from a mixture (1:1) of benzene and petroleum ether.

Cholesteryl azophenyl carbonate (3a)

This compound was prepared from cholesteryl chloroformate (2.28 g, 5.07 mmol) and 4-hydroxyazobenzene (1 g, 5.07 mmol). The product was purified by column chromatography to give 2.81 g (91%) of the title compound, which melted at 221 °C, after recrystallization from a mixture (1:1) of benzene and petroleum ether.

IR ν_{\max} (KBr): 2942, 2900, 2876 (CH), 1768 (C=O), 1590 (C=C) cm^{-1} ; UV λ_{\max} (CHCl_3): 333 nm (ϵ 17900 $\text{M}^{-1}\text{cm}^{-1}$); ^1H NMR (CDCl_3): δ 0.60-3.20 (44 H, m, cholesteric), 4.4-4.6 (1 H, m, OCH), 5.3-5.6 (1 H, m, vinylic), 6.70-6.90 (2 H, d, aromatic), 7.20-7.50 (2 H, d, aromatic), 7.80-8.10 (4 H, d, aromatic); ^{13}C NMR (CDCl_3): δ 11.81, 18.67, 19.18, 21.00, 22.52, 22.76, 23.83, 24.22, 27.65, 27.92, 28.16, 31.80, 35.74, 36.16, 36.48, 36.78, 37.89, 39.47, 39.68, 40.15, 42.24, 49.94, 56.15, 56.59, 78.79, 111.40, 121.31, 123.16, 124.95, 139.06, 139.36, 143.56, 150.75, 151.74, 152.36, 152.57. Exact mol wt calcd for $\text{C}_{40}\text{H}_{55}\text{N}_2\text{O}_3$ (MH^+) 611.4213; found 611.4196 (FAB, high resolution mass spectroscopy).

Cholesteryl 4-nitrozophenyl carbonate (3b)

Treatment of cholesteryl chloroformate (560 mg, 1.25 mmol) and 4-nitro-4'-hydroxyazobenzene (305 mg, 1.25 mmol) gave a crude product, which was

further purified by chromatography. Recrystallization from a mixture (1:1) of benzene and petroleum ether gave 458 mg (56%) of a pure sample of **3b**, mp 266 °C.

IR ν_{\max} (KBr): 2957, 2897, 2871 (CH), 1751 (C=O), 1594 (C=C) cm^{-1} ; UV λ_{\max} (CHCl_3): 343 nm (ϵ 11500 $\text{M}^{-1}\text{cm}^{-1}$); ^1H NMR (CDCl_3): δ 0.60-2.60 (43 H, m, cholesteryl), 4.2-4.7 (1 H, m, OCH), 5.3-5.6 (1 H, m, vinylic), 7.30-7.50 (2 H, d, aromatic), 7.90-8.20 (4 H, m, aromatic), 8.30-8.50 (2 H, m, aromatic); ^{13}C NMR (CDCl_3): δ 11.81, 18.67, 19.21, 21.00, 22.52, 22.76, 23.83, 24.22, 27.62, 27.95, 28.16, 31.83, 35.74, 36.16, 36.51, 36.81, 37.89, 39.50, 39.68, 42.27, 49.97, 56.15, 56.65, 79.27, 121.81, 122.77, 123.30, 123.39, 124.68, 128.26, 138.97, 139.42, 148.75, 149.86, 152.27, 154.06, 155.53. Exact mol wt calcd for $\text{C}_{40}\text{H}_{54}\text{N}_3\text{O}_5$ (MH^+) 656.4063; found 656.4051 (FAB, high resolution mass spectroscopy).

Cholesteryl 4-N,N-dimethylaminoazophenyl carbonate (**3c**)

Compound **3c** was synthesized from cholesteryl chloroformate (500 mg, 1.2 mmol) and 4-N,N-dimethylamino-4'-hydroxyazobenzene (270 mg, 1.12 mmol). The product was recrystallized from a mixture (1:1) of benzene and petroleum ether to afford 620 mg (85%) of the title compound, mp 231 °C.

IR ν_{\max} (KBr): 2952, 2872 (CH), 1766 (C=O), 1524 (C=C) cm^{-1} ; UV λ_{\max} (CHCl_3): 413 nm (ϵ 16350 $\text{M}^{-1}\text{cm}^{-1}$); ^1H NMR (CDCl_3): δ 0.70-2.60 (44 H, m, aliphatic), 4.3-4.7 (1 H, m, OCH), 5.3-5.6 (1 H, m, vinylic), 7.30-7.70 (4 H, m, aromatic), 7.80-8.20 (4 H, m, aromatic); ^{13}C NMR (CDCl_3): δ 11.81, 18.70, 19.21, 21.00, 22.55, 22.79, 23.83, 24.22, 27.59, 27.95, 28.16, 31.80, 35.74, 36.19, 36.48, 36.78, 37.89, 39.50, 39.68, 42.27, 49.94, 56.15, 56.62, 79.00, 121.54, 122.86, 123.19, 123.99, 128.97, 130.97, 139.00, 150.16, 152.42, 152.51, 153.02.

Exact mol wt calcd for $C_{42}H_{55}N_2O_3$ (MH^+) 654.4635; found 654.4603 (FAB, high resolution mass spectroscopy).

Cholesteryl 4-butylazophenylcarbonate (3d)

Treatment of cholesteryl chloroformate (3 g, 6.7 mmol) with azobenzene derivative **1d** (1.75 g, 6.7 mmol) gave the crude product which was further purified by column chromatography. Recrystallization from a mixture (1:1) of benzene and petroleum ether gave 4.2 g (94%) of the title compound, which melted at 254 °C.

IR ν_{max} (KBr): 3070, 2927, 2884 (CH), 1711 (C=O), 1607, 1598 (C=C) cm^{-1} ; UV λ_{max} ($CHCl_3$): 338 nm (ϵ 22200 $M^{-1}cm^{-1}$); 1H NMR ($CDCl_3$): δ 0.5-2.6 (52 H, m, aliphatic), 4.4-4.6 (1 H, m, OCH), 5.4 (1 H, m, vinylic), 7.1-7.4 (4 H, m, aromatic), 7.8-8.1 (4 H, m, aromatic); ^{13}C NMR ($CDCl_3$): δ 11.78, 13.87, 18.67, 19.18, 20.97, 22.28, 22.52, 22.76, 23.86, 27.56, 27.92, 31.77, 33.29, 35.53, 35.74, 36.16, 36.45, 36.78, 37.89, 39.47, 42.21, 49.88, 56.12, 56.56, 78.91, 121.45, 122.86, 123.16, 123.84, 128.94, 138.97, 146.43, 150.22, 150.75, 152.39, 152.75. Exact mol wt calcd for $C_{44}H_{63}N_2O_3$ (MH^+) 667.4839; found 667.4849 (FAB, high resolution mass spectroscopy).

Cholesteryl 4-nitro-4'-ethoxyazophenyl carbonate (5a)

Compound **5a** was prepared from cholesteryl chloroformate (1.65 g, 3.65 mmol) and 4-nitro-4'-ethoxyazobenzene (1 g, 3.65 mmol). The product was purified by column chromatography to give 2.42 g (96%) of the title compound,

which melted at 264 °C, after recrystallization from a mixture (1:1) of benzene and petroleum ether.

IR ν_{\max} (KBr): 2950, 2873 (CH), 1770 (C=O), 1613 (C=C) cm^{-1} ; UV λ_{\max} (CHCl_3): 340 nm (ϵ 28300 $\text{M}^{-1}\text{cm}^{-1}$); ^1H NMR (CDCl_3): δ 0.50-2.80 (47 H, m, aliphatic), 4.35-4.70 (1 H, m, OCH), 5.2-5.6 (1 H, vinylic), 7.2-7.6 (2 H, d, aromatic), 7.8-8.1 (4 H, d, aromatic), 8.2-8.5 (2 H, d, aromatic); ^{13}C NMR (CDCl_3): δ 11.84, 18.70, 19.24, 21.06, 22.55, 22.79, 23.83, 24.25, 27.62, 27.98, 28.19, 31.86, 35.77, 36.19, 36.54, 36.84, 37.89, 39.50, 39.71, 42.30, 50.00, 56.18, 56.68, 79.30, 121.84, 123.42, 124.68, 139.00, 148.78, 149.89, 152.27, 154.09, 155.56. Analysis calcd for $\text{C}_{42}\text{H}_{57}\text{N}_3\text{O}_6$: C, 72.07, H, 8.21, N, 6.00; found C, 72.51, H, 8.19, N, 6.14.

Cholesteryl 4-butylazo (4-ethoxyphenyl)carbonate (5b)

Treatment of cholesteryl chloroformate (3 g, 6.68 mmol) with the azobenzene derivative **4b** (2 g, 6.68 mmol) gave a crude product which was further purified by column chromatography. Recrystallization from a mixture (1:1) of benzene and petroleum ether gave 4.15 g (87%) of a pure sample of **5b**, which melted at 250 °C.

IR ν_{\max} (KBr): 2938, 2868 (C-H), 1768 (C=O), 1588, 1544 cm^{-1} ; UV λ_{\max} (CHCl_3): 335 nm (ϵ 21500 $\text{M}^{-1}\text{cm}^{-1}$); ^1H NMR (CDCl_3): δ 0.7-2.8 (56 H, m, aliphatic) 4.4-4.7 (1 H, m, OCH), 5.3-5.5 (1 H, m, vinylic), 7.1-7.4 (4 H, m, aromatic), 7.7-8.1 (4 H, m, aromatic); ^{13}C NMR (CDCl_3): δ 11.57, 13.69, 18.49, 18.97, 20.82, 22.10, 22.34, 22.58, 23.69, 24.01, 27.38, 27.74, 27.98, 31.59, 33.11, 35.32, 35.56, 35.98, 36.25, 36.57, 37.68, 39.29, 42.03, 49.70, 55.94, 56.35, 78.80, 121.25, 122.68, 122.95, 123.63, 128.73, 138.76, 146.22, 150.01, 150.54, 152.18,

152.57. Analysis calcd for $C_{46}H_{66}N_2O_4$: C, 77.69, H, 9.35, N, 3.94; found C, 79.13, H, 9.22, N, 4.57.

4.5. References

1. Friedel, G. *Ann. Physique*, **1922**, *18*, 273.
2. Leadbetter, A. J. in *Thermotropic Liquid Crystals*; Gray, G. W. Ed., Wiley, Chichester (1987). Chapter 1.
3. Pershan, P. S. *Structure of Liquid Crystal Phases*, World Scientific, Singapore, 1988.
4. Reinitzer, F. *Monatsh.* **1888**, *9*, 421.
5. Oseen, C. W. *Trans. Faraday Soc.* **1933**, *29*, 883.
6. Saupe, A. *Angew. Chem. Int. Ed. Engl.* **1968**, *7*, 97.
7. Fergason, J. L. *Mol. Cryst.* **1966**, *1*, 293.
8. de Vries, H. L. *Acta. Cryst.* **1951**, *4*, 219.
9. Stegemeyer, H.; Mainusch, K. J. *Chem. Phys. Lett.* **1970**, *6*, 5.
10. Berreman, D. W.; Scheffer, T. J. *Phys. Rev. Lett.* **1970**, *25*, 557.
11. Dreher, R.; Meier, G. *Phys. Rev. A.* **1973**, *8*, 1616.
12. Saupe, A.; Meier, G. *Phys. Rev. A.* **1983**, *27*, 2196.
13. Reinitzer, F. *Monatsh Chem.* **1888**, *9*, 421.
14. Lehmann, O. *Physikal. Chem.* **1889**, *4*, 462.
15. Fergason, J. L. *Appl. Opt.* **1968**, *7*, 1729.
16. Haas, W.; Adams, J. *Appl. Opt.* **1968**, *7*, 1203.
17. Heilmeyer, G. H.; Goldmacher, J. E. *Appl. Phys. Lett.* **1968**, *13*, 132.
18. Fergason, J. L. *Scientific American* **1964**, *211*, 77.
19. Fergason, J. L. *Mol. Cryst.* **1966**, *1*, 309.

20. Haas, W.; Adams, J.; Wysocki, J. *Mol. Cryst. Liq. Cryst.* **1969**, *7*, 371.
21. Haas, W. E. Nelson, K. F.; Adams, J. E.; Dir, G. A. *J. Electrochem. Soc.* **1974**, *121*, 1667.
22. Keating, P. N. *Mol. Cryst. Liq. Cryst.* **1969**, *8*, 315.
23. Ferguson, J. L.; Goldberg, N. N.; Nadalin, R. J. *Mol. Cryst.* **1966**, *1*, 309.
24. Ferguson, J. L. *Scientific American* **1964**, *211*, 77.
25. Selawry, O. S.; Selawry, H. S.; Holland, J. F. *Mol. Cryst.* **1966**, *1*, 495.
26. Woodmansce, W. E. *Appl. Optics* **1968**, *7*, 1721.
27. Hansen, J.; Ferguson, J. L.; Okaya, A. *Appl. Optics* **1964**, *3*, 987.
28. Keilmann, F. *Appl. Optics* **1970**, *9*, 1319.
29. Ennulat, R. D.; Ferguson, J. L. *Mol. Cryst. Liq. Cryst.* **1971**, *13*, 149.
30. Iizuka, K. *Electronics Lett.* **1969**, *5*, 26.
31. Pollmann, P.; Stegemeyer, H. *Chem. Phys. Lett.* **1973**, *20*, 87.
32. Chandrasekhar, S.; Ratna, B. R. *Mol. Cryst. Liq. Cryst.* **1976**, *35*, 109.
33. Keyes, P. H.; Weston, H. T.; Daniels, W. B. *Phys. Rev. Lett.* **1973**, *31*, 628.
34. Shashidhar, R.; Chandrasekhar, S. *J. de Physique* **1975**, *36*, C1-49.
35. Adams, J. E.; Haas, W. E. L. *Mol. Cryst. Liq. Cryst.* **1971**, *15*, 27.
36. Adams, J. E.; Haas, W. E. L.; Wysocki, J. *J. Phys. Rev. Lett.* **1969**, *22*, 92.
37. Nakagiri, T.; Kodama, H.; Kobayashi, K. K. *Phys. Rev. Lett.* **1971**, *27*, 564.
38. Buckingham, A. D.; Ceaser, G. P.; Dunn, M. B. *Chem. Phys. Lett.* **1969**, *3*, 540.
39. Saeva, F. D. *Mol. Cryst. Liq. Cryst.* **1973**, *23*, 171.
40. Ozaki, M.; Myokin, K.; Uto, S.; Moritake, H.; Yashino, K.; Patel, J. S. *Jpn. J. Appl. Phys.* **1995**, *34*, m6628.
41. Freund, I.; Rentzepis, P. M. *Phys. Rev. Lett.* **1967**, *18*, 393.
42. Sionnest, P. G.; Shiung, H.; Shen, Y. R. *Phys. Rev. Lett.* **1986**, *57*, 2963.

43. Ikeda, T.; Tsutsumi, O. *Science*, **1995**, *268*, 1873.
44. Levine, B. F.; Bethea, C. G. *J. Chem. Phys.* **1975**, *63*, 2666.
45. Risser, S.; Klemm, S.; Allender, D. W.; Lee, M. A. *Mol. Cryst. Liq. Cryst.* **1987**, *150B*, 631.
46. Beratan, D. N.; Onuchie, J. N.; Perry, J. W. *J. Chem. Phys.* **1987**, *91*, 2696.
47. Prost, J.; Lalanne, J. R. *Phys. Rev. A.* **1973**, *8*, 2090.
48. Wong, G. K.; Shen, Y. R. *Phys. Rev. Lett.* **1973**, *30*, 895.
49. Rao, D. V. G. N.; Jayaraman, S. *Appl. Phys. Lett.* **1973**, *23*, 539.
50. Palffy-Muhoray, M.; Balzarini, D. A. *Can. J. Phys.* **1981**, *59*, 515.
51. Horn, R. G. *J. Physique* **1978**, *39*, 105.
52. Odulov, S. G.; Reznikov, Y. A.; Soskin, M. A.; Khizhnyak, A. I. *Sov. Phys. JETP* **1983**, *58*, 1154.
53. Singer, K. D.; Kuzyk, M. G.; Sohn, J. E. *J. Opt. Soc. Am. B.* **1987**, *4*, 968.
54. Arakelian, S. M.; Grigorian, G. L.; Nersisyan, S. Ts.; Nshayan, M. A.; Chilingaryan, Y. S. *Sov. Phys. JETP Lett.* **1978**, *28*, 186.
55. Arakelian, S. M.; Lyakhov, G. A.; Chilingaryan, Y. S. *Sov. Phys. Usp.* **1980**, *23*, 245.
56. Barnik, M. I.; Blinov, L. M.; Drozhkin, A. M.; Shtyov, N. M. *Mol. Cryst. Liq. Cryst.* **1983**, *98*, 1.
57. Pershan, P. S. *Phys. Rev.* **1963**, *130*, 919.
58. Zhong-can, O.-Y.; Yu-zhang, X. *Phys. Rev. A.* **1985**, *32*, 1189.
59. Vtyurin, A. N.; Yermakov, V. P.; Ostrovsky, B. I.; Shavanov, V. F. *Krystallografiya* **1981**, *26*, 546.
60. Barnik, M. I.; Blinov, L. M.; Shtykov, N. M. *Sov. Phys. JETP* **1984**, *59*, 980.

51. Sprunt, S.; Naciri, J.; Ratna, B. R.; Shashidhar, R.; Bihari, B.; Kumar, J.; Tripathy, S. K. *Appl. Phys. Lett.* **1995**, *66*, 1443.
62. Kobayashi, K.; Watanabe, T.; Uto, S.; Ozaki, M.; Yoshino, K.; Svensson, M.; Helgec, B.; Skarp, K. *Jpn. J. Appl. Phys.* **1996**, *35*, L104.
63. Durand, .; Lee, C. H. *Mol. Cryst.* **1968**, *5*, 171.
64. Freund, I.; Rentzepis, P. M. *Phys. Rev. Lett.* **1967**, *18*, 393.
65. Ozaki, M.; Myojin, K.; Uto, S.; Moritake, H.; Yoshino, K.; Patel, J. S. *Jpn. J. Appl. Phys.* **1995**, *34*, L628.
66. Meyer, R. B. *Phys. Rev. Lett.* **1969**, *22*, 918.
67. Manfred, E.; Wendorff, J. H. *Macromol. Chem. Rapid. Commun.* **1987**, *8*, 59.
68. Albrt, I.D.L.; Morley, J. O.; Pugh, D. *J. Phys. Chem.* **1995**, *99*, 8204.
69. Gao, L. H.; Wang, K. Z.; Huang, C. H.; Zhae, I. S.; Xia, J. M.; Li, K.; Xu, M. *Chem. Mater.* **1995**, *7*, 1047.
70. Sekkat, Z.; Knoll, W. *J. Opt. Soc. Am. B.* **1995**, *12*, 1855,
71. Cross, E. M.; White, K. M.; Moshretzadeh, R. S.; Francis, C. V. *Macromolecules* **1995**, *28*, 2526.
72. Feringa, B. L.; Jager, W. F. de Lauge, B. *Tetrahedron*, **1993**, *49*, 8267.
73. Murata, K.; Aoki, M.; Suzuki, T.; Harada, T.; Kawabata, H.; Koniori, T.; Oshetom F.; Ueda, K.; Shinkai, S. *J. Am. Chem. Soc.* **1994**, *116*, 6664.
74. Murata, K.; Aoki, M.; Nishi, T.; Ikeda, A.; Shinkai, S. *J. Chem. Soc. Chem. Commun.* **1991**, 1715.
75. Tokuhisa, H.; Kimura, K.; Yokoyama, M.; Shinkai, S. *J. Chem. Soc. Faraday Trans.* **1995**, *91*, 1237.
76. Man, H.-T.; Yoon, H. N. *Adv. Mater.* **1992**, *4*, 159.
77. Clays, K.; Persoons, A. *Rev. Sci. Instr.* **1992**, *63*, 3285.

78. Demus, D.; Richter, L. *Textures of Liquid Crystals*, VEB Beutcher Verlag für Grundstoffindustrie, 1980.
79. Dewar, M. S. J.; Zoebisch, E. G.; Healy, E. F.; Stewart, J. *J. Am. Chem. Soc.* 1985, 107, 3902.
80. QCMP program 137 Version 6.12, Department of Chemistry, Indiana University, Bloomington, IN 47405.
81. Moylan, C. R.; Twieg, R. J.; Lee, V. Y.; Swanson, S. A.; Betterion, K. M.; Miller, R. D. *J. Am. Chem. Soc.* 1993, 115, 12599.
82. Brown, E. V.; Grahneman, G. R. *J. Am. Chem. Soc.* 1975, 97, 621.
83. Ogura, K.; Hirabayashi, H. Uejima, A.; Nakamura, K. *Jpn. J. Appl. Phys.* 1982, 21, 969.
84. Eich, M.; Wondorff, J. H. *Makromol. Chem. Rapid Commun.* 1987, 8, 467.
85. Kurihara, S.; Ikeda, T.; Sasaki, T.; Kim, H.-B.; Tazuke, S. *J. Chem. Soc. Chem. Commun.* 1990, 1751.
86. Ikeda, T.; Sasaki, T.; Kim, H.-B. *J. Phys. Chem.* 1991, 95, 509.
87. Sackman, E. *J. Am. Chem. Soc.* 1971, 93, 7088.
88. Ogura, K.; Hirabayashi, H. Uejima, A.; Nakamura, K. *Jpn. J. Appl. Phys.* 1982, 21, 969.
89. *Trans* $\lambda_{\max} = 300$ nm, *cis* $\lambda_{\max} > 380$ nm, strongly depending on substitution pattern.
90. Hartley, G. S. *Nature* 1937, 140, 281.

APPENDIX 1. X-ray Crystal Data of Compounds Listed in Chapter 2.
Table A2.1. Summary of crystal data and intensity parameters for 14a (C₂₀H₁₈N₃O) and 15c (C₁₅H₁₄N₂OS₂)

	14a	15c
Empirical formula	C ₂₀ H ₁₈ N ₃ O	C ₁₅ H ₁₄ N ₂ OS ₂
Colour; habit	Yellow, irregular	Colourless, irregular
Crystal size (mm)	0.40 x 0.30 x 0.20	0.5 x 0.4 x 0.2
Crystal system	Tetragonal	Monoclinic
Space group	P4 ₃ 2 ₁ 2	P2 ₁ /c
Unit cell dimensions		
a	9.87690 (10) Å	10.598
b	9.87690 (10) Å	7.5746
c	35.3642 (2) Å	19.053
α	90°	90°
β	90°	103.026°
γ	90°	90°
Volume	3449.89 (5) Å ³	1490.1 (4) Å ³
Z	8	4
Formula weight	316.37	302.40
Density (calc., mg/m ³)	1.218	1.348
Absorption coefficient (mm ⁻¹)	0.077	0.354
F (000)	1336	632
Diffractometer used	Siemens CCD	Siemens P4
Radiation	MoKα (λ = 0.71073 Å)	MoKα (λ = 0.71073 Å)
Temperature (K)	223 (2)	295 (2)
Monochromator	Highly oriented graphite crystal	Same as in 14a

θ range for data collection	2.14 to 27°	1.97 to 28.00°
Limiting indices	$-8 \leq h \leq 9, 0 \leq k \leq 13, 0 \leq l \leq 47$	$-1 \leq h \leq 13, -1 \leq k \leq 10, -25 \leq l \leq 24$
Background measurement	Stationary crystal and stationary counter at beginning and end of scan, each for 25.0% of total scan time	
Refinement method	Full-matrix least-squares on F^2	Same as 14a
Reflections collected	73530	4727
Independent reflections	3773 ($R_{int} = 0.10$)	3579 ($R_{int} = 0.0229$)
Absorption correction	none	None
Final R indices [$I > 2\sigma(I)$]	$R1 = 0.0504,$ $wR2 = 0.1030$	$R1 = 0.0495,$ $wR2 = 0.0944$
R indices (all data)	$R1 = 0.0784,$ $wR2 = 0.1175$	$R1 = 0.0981,$ $wR2 = 0.1136$
Goodness-of-fit on F^2	1.043	1.015
Largest difference peak	0.133 eÅ ⁻³	0.236 eÅ ⁻³
Largest difference hole	-0.127 eÅ ⁻³	-0.197 eÅ ⁻³

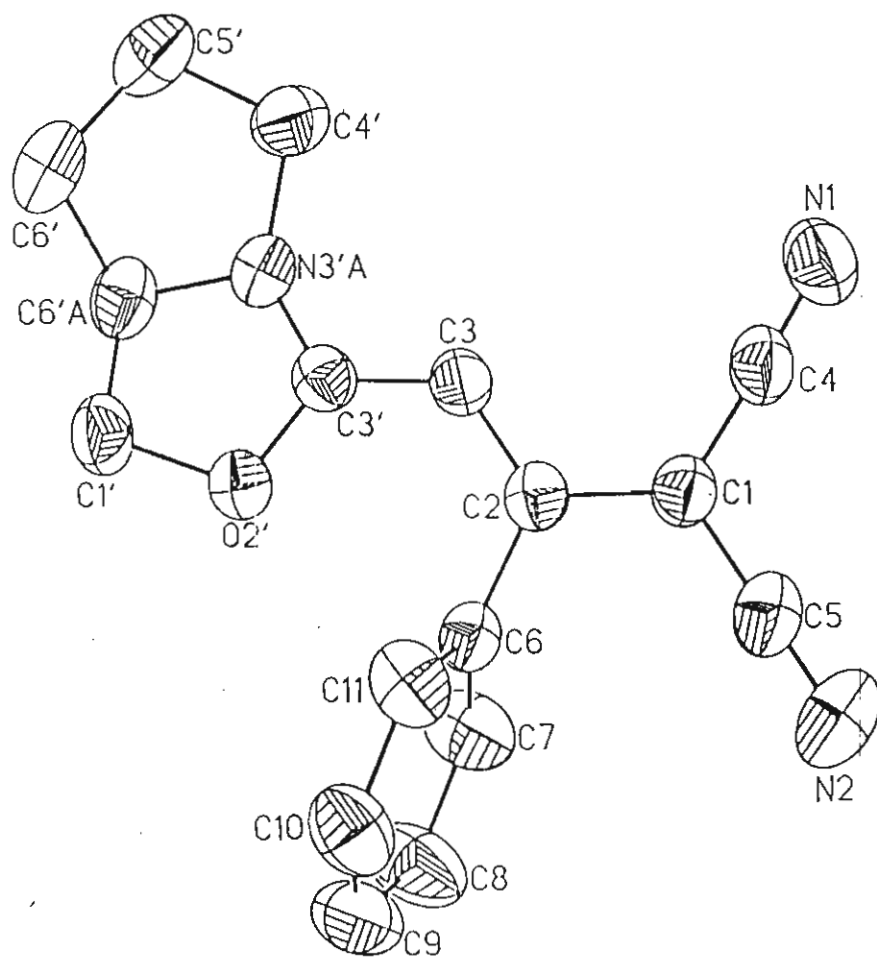


**Figure A.2.1. Projection view drawing of the structure of 14a.
The thermal ellipsoids are drawn at 50 % probability.**

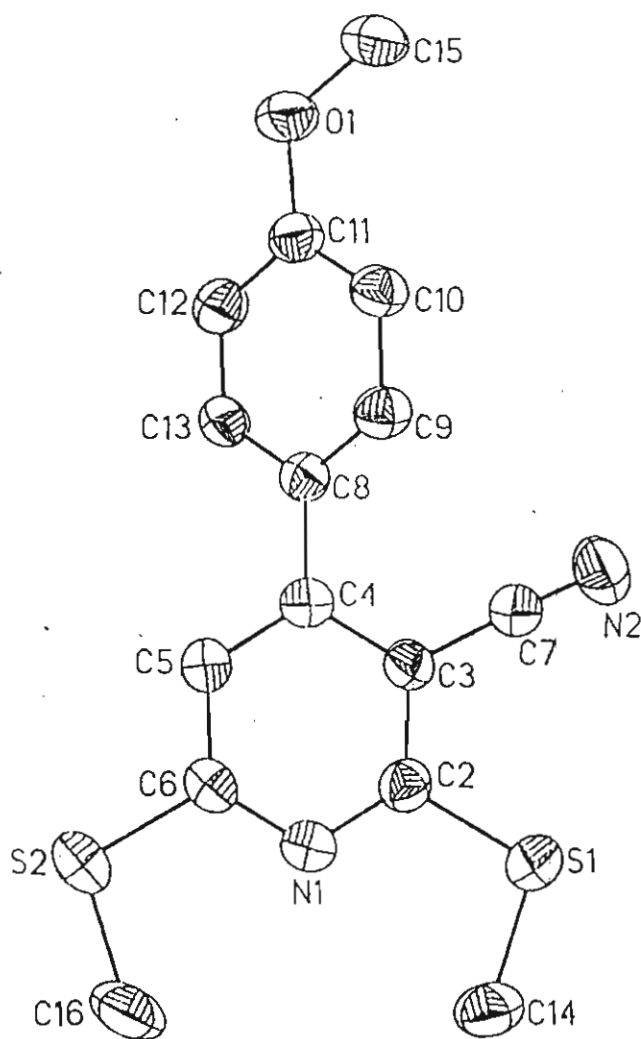


**Figure A.2.2. Projection view drawing of the structure of 15c.
the thermal ellipsoids are drawn at 50 % probability**

Table A2.1A. Selected Bond distances (Å) and Bond Angles (deg) of 14a**Bond Distances (14a)**

O (2') - C (3')	1.338 (2)	O (2') - C (1')	1.471 (2)
N (1) - C (4)	1.146 (3)	N (2) - C (5)	1.151 (3)
N (3'A) - C (3')	1.330 (2)	N (3'A) - C (4')	1.462 (3)
N (3'A) - C(6'A)	1.469 (2)	C (1') - C (6'A)	1.510 (3)
C(1) - C (2)	1.401 (3)	C (1) - C (5)	1.422 (3)
C (1) - C (4)	1.429 (3)	C (2) - C (3)	1.393 (3)
C (2) - C (6)	1.494 (3)	C (3') - C (3)	1.390 (3)
C (4') - C (5')	1.529 (3)	C (5') - C (6')	1.527 (3)
C (6'A) - C (6')	1.520 (3)	C (6) - C (7)	1.380 (3)
C (6) - C (11)	1.381 (3)	C (7) - C (8)	1.382 (3)
C (8) - C (9)	1.372 (4)	C (9) - C (10)	1.363 (3)
C (10) - C (11)	1.381 (3)	C (1S) - C (2S)#1	1.367 (4)
C (1S) - C (2S)	1.367 (4)	C (2S) - C (3S)	1.371 (5)
C (3S) - C (4S)	1.351 (4)	C (4S) - C (3S)#1	1.351 (4)

Bond Angles (14a)

C (3') - O (2') - C (1')	107.6 (2)	C (3') - N (3'A) - C (4')	129.1 (2)
C (3') - N (3'A) - C (6'A)	111.9 (2)	C (4') - N (3'A) - C (6'A)	113.0 (2)
O (2') - C (1') - C (6'A)	105.2 (2)	C (2) - C (1) - C (5)	121.8 (2)
O (2) - C (1) - C (4)	121.6 (2)	C (5) - C (1) - C (4)	116.5 (2)
C (3) - C (2) - C (1)	122.0 (2)	C (3) - C (2) - C (6)	122.5 (2)
C (1) - C (2) - C (6)	115.6 (2)	N (3'A) - C (3') - O (2')	111.3 (2)
N (3'A) - C (3') - C (3)	124.4 (2)	O (2') - C (3') - C (3)	124.1 (2)
C (3') - C (3) - C (2)	127.0 (2)	N (3'A) - C (4') - C (5')	102.4 (2)
N (1) - C (4) - C (1)	179.0 (2)	C (6') - C (5') - C (4')	104.6 (2)
N (2) - C (5) - C (1)	179.3 (2)	N (3'A) - C (6'A) - C (1')	100.8 (2)
N (3'A) - C (6'A) - C (6')	101.9 (2)	C (1') - C (6'A) - C (6')	121.6 (2)
C (6'A) - C (6') - C (5')	102.0 (2)	C (7) - C (6) - C (11)	118.2 (2)
C (7) - C (6) - C (2)	120.6 (2)	C (11) - C (6) - C (2)	121.1 (2)
C (6) - C (7) - C (8)	120.9 (2)	C (9) - C (8) - C (7)	119.7 (2)
C (10) - C (9) - C (8)	120.3 (2)	C (9) - C (10) - C (11)	119.9 (2)
C (6) - C (11) - C (10)	121.0 (2)	C (2S)#1 - C (1S) - C (2S)	119.6 (5)
C (1S) - C (2S) - C (3S)	119.5 (3)	C (4S) - C (3S) - C (2S)	121.1 (3)
C (3S)#1 - C (4S) - C (3S)	119.2 (5)		

Symmetry transformations used to generate equivalent atoms; #1 y, x, -z,

Table A2.1B. Selected Bond distances (Å) and Bond Angles (deg) of 15c
Bond Distances (15c)

S (1) - C (2)	1.756 (2)	S (1) - C (14)	1.788 (3)
S (2) - C (6)	1.748 (2)	S (2) - C (16)	1.786 (3)
O (1) - C (11)	1.367 (2)	O (1) - C (15)	1.426 (3)
N (1) - C (2)	1.335 (3)	N (1) - C (6)	1.339 (3)
N (2) - C (7)	1.140 (3)	C (2) - C (3)	1.403 (3)
C (3) - C (4)	1.405 (3)	C (3) - C (7)	1.440 (3)
C (4) - C (5)	1.388 (3)	C (4) - C (8)	1.486 (3)
C (5) - C (6)	1.395 (3)	C (8) - C (9)	1.392 (3)
C (8) - C (13)	1.396 (3)	C (9) - C (10)	1.381 (3)
C (10) - C (11)	1.383 (3)	C (11) - C (12)	1.391 (3)
C (12) - C (13)	1.379 (3)		

Bond Angles (15c)

C (2) – S (1) – C (14)	102.34 (12)	C (6) – S (2) – C (16)	102.99 (13)
C (11) – O (1) – C (15)	117.5 (2)	C (2) – N (1) – C (6)	117.1 (2)
N (1) – C(2) – C (3)	123.3 (2)	N (1) – C (2) – S (1)	118.1 (2)
C (3) – C(2) – S (1)	118.6 (2)	C (2) – C (3) – C (4)	119.2 (2)
C (2) – C(3) – C (7)	118.3 (2)	C (4) – C (3) – C (7)	122.5 (2)
C (5) – C(4) – C (3)	117.2 (2)	C (5) – C (4) – C (8)	120.7 (2)
C (3) – C(4) – C (8)	122.1 (2)	C (4) – C (5) – C (6)	119.4 (2)
N (1) – C(6) – C (5)	123.8 (2)	N (1) – C (6) – S (2)	118.5 (2)
C (5) – C(6) – S (2)	117.6 (2)	N (2) – C(7) – C (3)	178.3 (2)
C (9) – C(8) – C (13)	117.8 (2)	C (9) – C(8) – C (4)	121.4 (2)
C (13) – C(8) – C (4)	120.8 (2)	C (10) – C(9) – C (8)	121.7 (2)
C (9) – C(10) – C (11)	119.7 (2)	O (1) – C(11) – C (10)	124.4 (2)
O (1) – C(11) – C (12)	116.0 (2)	C (10) – C(11) – C (12)	119.6 (2)
C (13) – C(12) – C (11)	120.3 (2)	C (12) – C(13) – C (8)	120.9 (2)